ASYMPTOTIC ANALYSIS OF THE NARROW ESCAPE AND BERG-PURCELL PROBLEMS ON GENERAL THREE-DIMENSIONAL DOMAINS WITH REACTIVE BOUNDARY PATCHES

ALAN E. LINDSAY*, ANDREW J. BERNOFF†, DENIS S. GREBENKOV‡, JEREMY G. HOSKINS§, AND MICHAEL J. WARD¶

Abstract. We present an asymptotic analysis of two diffusive capture problems in general smooth closed three-dimensional geometries with multiple small reactive boundary patches of arbitrary shapes. (i) The narrow escape problem seeks to determine the escape rate of Brownian particles from an enclosed region through small boundary windows. (ii) The related Berg-Purcell (or narrow entrance) problem seeks to resolve the capture rate for signaling molecules diffusing outside the cell and entering through localized reactions at membrane-bound receptors. We obtain matched asymptotic solutions of these two problems and thus address the long-standing challenge of describing the role that curvature and local reactivities play in modulating diffusive capture rates. Our explicit expansions quantify local effects on diffusive capture through the sizes, shapes, and reactivities of the patches together with the principal curvatures of the manifold at each patch. In turn, we examine global effects on diffusive capture such as the spatial configuration of patches on the manifold, as enclooded by the associated surface Neumann Green's function and its regular part. The accuracy of our asymptotic formulas is validated against a full numerical solution for an ellipsoidal domain. Overall, our results yield new insights on how geometry and stochasticity combine to shape the dynamics of various biological processes.

Key words. Narrow escape problem, Berg-Purcell, Diffusion, Asymptotic expansions.

1. Introduction. The event where a diffusing particle hits a threshold or arrives at a small reaction site is a key milestone in the completion of numerous biological phenomena. Examples include the binding of the T-cell receptor to a ligand on an opposing cell, the entry of a virus into a cell or the trafficking of intra-cellular molecules through nuclear pore complexes [5, 11, 12, 26, 45, 51, 52, 54, 55, 60, 64].

An ongoing and challenging avenue of research is to describe how the interaction of diffusive processes with complex geometries affects the timescale of such processes incling shielding, confinement and boundary induced motion. The interaction of diffusive particles with curved manifolds is of great importance in understanding cellular functions where morphology plays a significant role [1, 15, 22, 53].

In this paper, we describe the solution by matched asymptotic analysis of two related problems in diffusive transport, the *Narrow Escape Problem* (NEP) [14, 17, 34, 38, 54, 56] and the *Berg-Purcell (BP) problem* [6, 33, 40, 44]. Before introducing the precise mathematical formulation of these problems and our main results, we outline the geometric setting which is common to both.

Let $\mathcal{M} \subset \mathbb{R}^3$ be a three-dimensional simply-connected bounded domain, whose smooth reflecting boundary $\partial\mathcal{M}$ hosts the union $\partial\mathcal{M}_a = \cup_{i=1}^{N} \partial\mathcal{M}_i$ of N small partially reactive patches $\partial\mathcal{M}_i$. Each boundary patch $\partial\mathcal{M}_i$ has a length-scale L_i, and a

*University of Notre Dame, Notre Dame, IN, 46556, USA. Email: a.lindsay@nd.edu (corresponding author),

†Department of Mathematics, Harvey Mudd College, Claremont, CA, 91711, USA. Email: bernoff@g.hmc.edu,

‡Laboratoire de Physique de la Matiére Condensée, CNRS – Ecole Polytechnique, Institut Polytechnique de Paris, 91120 Palaiseau, France. Email: denis.grebenkov@polytechnique.edu,

§Department of Statistics, University of Chicago, USA and NSF-Simons National Institute for Theory and Mathematics in Biology, Chicago, IL. Email: jeremyhoskins@uchicago.edu

¶Department of Mathematics, University of British Columbia, Vancouver, B.C., Canada, V6T 1Z2. Email: ward@math.ubc.ca

constant reactivity $\mathcal{B}_i > 0$. More specifically, we denote $2L_i$ to be the diameter of the orthogonal projection of the patch $\partial\Omega_i$ when mapped onto the tangent plane. The geometry of each patch is assumed to be simply-connected with a smooth boundary, but with an otherwise arbitrary shape. Within this setting, the NEP is posed on the interior of $\mathcal{M}$ while the BP problem is solved in the exterior region $\mathbb{R}^3 \setminus \mathcal{M}$. Owing to differences that arise from this geometric consideration, we outline the two problems separately.

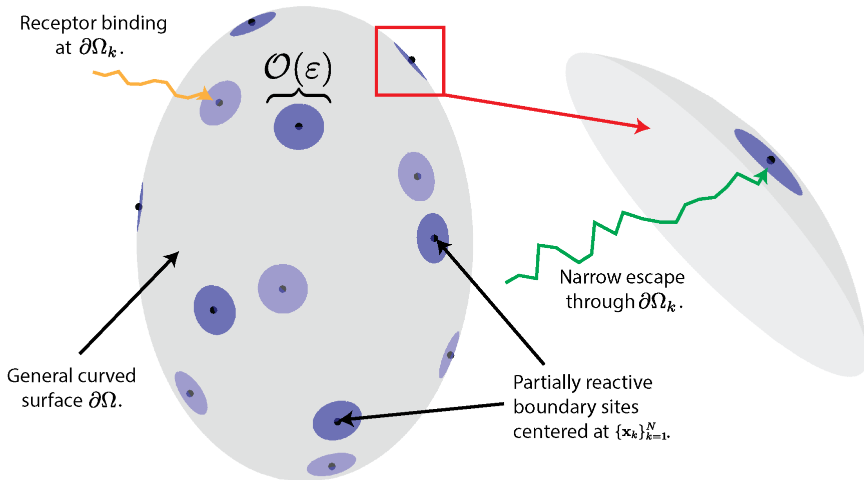

FIG. 1.1. *Three-dimensional diffusion interior ($\mathbf{x} \in \Omega$) and exterior ($\mathbf{x} \in \mathbb{R}^3 \setminus \Omega$) to a general closed and smooth curved surface $\partial\Omega$. The Berg-Purcell problem (1.1) solves the exterior diffusion problem and seeks the capture rate of ligands on a cell surface with localized reaction receptors $\{\partial\Omega_k\}_{k=1}^N$. The narrow escape problem (1.6) solves the interior diffusion problem and seeks the escape rate of diffusing molecules in Ω through small boundary windows $\{\partial\Omega_k\}_{k=1}^N$. The non-overlapping reactive patches are centered at points $\{\mathbf{x}_k\}_{k=1}^N$ with spatial extent $\varepsilon \ll 1$.*

The Berg-Purcell (BP) problem: A foundational model of diffusion-mediated signaling, introduced by Howard Berg and Edward Purcell [6], posits that interactions between cells and the extra-cellular medium is negotiated through binding of ligands to membrane-bound surface receptors. In this context, the steady-state concentration $\mathcal{U}$ of diffusing ligands satisfies the mixed Neumann-Robin boundary value problem (BVP)

$$\Delta_{\mathbf{X}}\mathcal{U} = 0\,, \quad \mathbf{X} \in \mathbb{R}^3\backslash\mathcal{M}\,, \tag{1.1a}$$

$$D\partial_n\mathcal{U} + \mathcal{B}_i\mathcal{U} = 0\,, \quad \mathbf{X} \in \partial\mathcal{M}_i\,, \quad i = 1,\ldots,N\,, \tag{1.1b}$$

$$\partial_n\mathcal{U} = 0\,, \quad \mathbf{X} \in \partial\mathcal{M}_r = \partial\mathcal{M}\backslash \cup_{i=1}^N \partial\mathcal{M}_i\,, \tag{1.1c}$$

$$\mathcal{U} \sim \mathcal{U}_{\text{inf}}\left(1 - \frac{\mathcal{C}_{\text{T}}}{|\mathbf{X}|} + \mathcal{O}(|\mathbf{X}|^{-2})\right)\,, \quad \text{as} \quad |\mathbf{X}| \to \infty\,, \tag{1.1d}$$

where $D > 0$ is the constant diffusivity, $\mathcal{U}_{\text{inf}}$ is the constant concentration imposed at infinity, $\Delta_{\mathbf{X}}$ is the Laplacian in the dimensional coordinate $\mathbf{X}$, and ∂_n is the outward normal derivative to $\partial\mathcal{M}$, directed into $\mathcal{M}$. We emphasize that the original work [6] dealt with perfectly reactive patches ($\mathcal{B}_i = \infty$), in which case the Robin condition (1.1b) is reduced to the Dirichlet condition $\mathcal{U} = 0$; various physical and probabilistic interpretations of the Robin boundary condition (1.1b) are discussed in [25, 26]. The monopole coefficient $\mathcal{C}_{\mathrm{T}}$ in the far-field (1.1d) is referred to as the *capacitance* of the heterogeneous partially reactive boundary $\partial\mathcal{M}$. The key quantity of interest is the combined flux through the whole cell surface, given by

$$J \equiv -D \int_{\partial\mathcal{M}} \partial_n \mathcal{U}\, dS = 4\pi D\, \mathcal{U}_{\mathrm{inf}} \mathcal{C}_{\mathrm{T}} \,. \tag{1.2}$$

In arriving at (1.2), we have used the divergence theorem to relate the total flux J to the far field behavior (1.1d). Our analysis will provide an asymptotic expansion for the total flux J in the small patch diameter limit.

To analyze (1.1), we introduce the dimensionless variables

$$\mathbf{x} = \frac{\mathbf{X}}{R_\star}, \quad L = \max_i \{L_i\}, \quad \varepsilon = \frac{L}{R_\star}, \quad a_i = \frac{L_i}{L}, \quad b_i = \frac{L\mathcal{B}_i}{D}, \quad u = \frac{\mathcal{U}}{\mathcal{U}_{\mathrm{inf}}}, \quad C_{\mathrm{T}} = \frac{\mathcal{C}_{\mathrm{T}}}{R_\star}, \tag{1.3}$$

where $R_\star$ is a length-scale for $\mathcal{M}$. We also consider the rescaled domain $\Omega = R_\star^{-1}\mathcal{M}$ and the rescaled patches $\partial\Omega_i^\varepsilon = R_\star^{-1}\partial\mathcal{M}_i$ of small $\mathcal{O}(\varepsilon)$ diameter, which are assumed to satisfy $\partial\Omega_i^\varepsilon \to \mathbf{x}_i \in \partial\Omega$ as $\varepsilon \to 0$. Moreover, we assume that the patches are well-separated in the sense that $|\mathbf{x}_i - \mathbf{x}_j| = \mathcal{O}(1)$ for all $i \neq j$ as $\varepsilon \to 0$. In the region exterior to Ω, (1.1) becomes

$$\Delta_{\mathbf{x}} u = 0 \,, \quad \mathbf{x} \in \mathbb{R}^3 \setminus \Omega \,, \tag{1.4a}$$

$$\varepsilon \partial_n u + b_i u = 0 \,, \quad \mathbf{x} \in \partial\Omega_i^\varepsilon \,, \quad i = 1, \ldots, N \,, \tag{1.4b}$$

$$\partial_n u = 0 \,, \quad \mathbf{x} \in \partial\Omega_r = \partial\Omega \setminus \cup_{i=1}^N \partial\Omega_i^\varepsilon \,, \tag{1.4c}$$

$$u \sim 1 - \frac{C_{\mathrm{T}}}{|\mathbf{x}|} + \mathcal{O}(|\mathbf{x}|^{-2}) \,, \quad \text{as} \quad |\mathbf{x}| \to \infty \,, \tag{1.4d}$$

where $\Delta_{\mathbf{x}}$ is the Laplacian in $\mathbf{x}$, and ∂_n is the outward normal derivative, directed into Ω. The relevant biophysical question is to understand the dependence of $J_i \equiv J_i(\mathbf{x}_1, \ldots, \mathbf{x}_N)$ on the geometry Ω together with the trapping configuration as described by the locations $\{\mathbf{x}_1, \ldots, \mathbf{x}_N\} \in \partial\Omega$ of the centers of the patches, their relative sizes, shapes, and reactivities $\{b_1, \ldots, b_N\}$ (see Fig. 1.1). The distribution of fluxes across the reactive sites plays an important role in cellular mechanisms of source detection [7, 9, 21, 40, 43].

In §2 we will analyze the BP problem (1.4) in the small patch limit $\varepsilon \to 0$ by using the method of matched asymptotic expansions. Our analysis provides a three-term asymptotic expansion for the capacitance C_{T}, which is valid for a general smooth and closed domain Ω. The result extends previous works [10, 40, 41] where perfectly absorbing circular patches ($b_i = \infty$) on the boundary of a sphere were considered. It also extends upon the results of [31] where a three-term expansion for C_{T} was derived for a spherical domain with partially reactive boundary patches of arbitrary shape. Our result C_{T} for an arbitrary bounded 3-D domain is given by (2.46) and depends on the exterior surface Neumann Green's function, which will be computed numerically, together with some local geometric properties of the domain boundary $\partial\Omega$ near the patch locations. An important case of biological interest is N identical perfectly absorbing circular patches of radius ε. In this scenario, our main result for $\varepsilon \to 0$, as given in Proposition 1, simplifies to

$$\frac{1}{C_T} \sim \frac{\pi}{\varepsilon N} \left[1 - \frac{\varepsilon \overline{\mathcal{H}}}{N\pi} \log(4\varepsilon) + \frac{4\varepsilon}{N} \left(p_e(\mathbf{x}_1, \ldots, \mathbf{x}_N) + \frac{3\overline{\mathcal{H}}}{8\pi} \right) + \mathcal{O}(\varepsilon^2 \log \varepsilon) \right] . \tag{1.5a}$$

Here

$$\overline{\mathcal{H}} \equiv \sum_{i=1}^{N} \mathcal{H}_i, \tag{1.5b}$$

where $\mathcal{H}_i$ is the mean curvature of the surface at $\mathbf{x} = \mathbf{x}_i$, defined in terms of the two principal curvatures $\kappa_1(\mathbf{x})$ and $\kappa_2(\mathbf{x})$ at $\mathbf{x} = \mathbf{x}_i$ by $\mathcal{H}_i = \frac{1}{2}\left[\kappa_1(\mathbf{x}_i) + \kappa_2(\mathbf{x}_i)\right]$, with sign convention that $\mathcal{H}_i = -1$ if Ω is the unit sphere. In (1.5a), the inter-patch interaction energy $p_e(\mathbf{x}_1, \ldots, \mathbf{x}_N)$ is defined in terms of the exterior surface Neumann Green's function G_e and its regular part R_e (see (2.18a) and (2.18b) below) by

$$p_e(\mathbf{x}_1, \ldots, \mathbf{x}_N) = \sum_{i=1}^{N} \left[R_e(\mathbf{x}_i) + \sum_{\substack{j=1 \\ j \neq i}}^{N} G_e(\mathbf{x}_j; \mathbf{x}_i) \right]. \tag{1.5c}$$

The Narrow Escape Problem (NEP): By using a similar asymptotic framework, we will also analyze the *mean first-reaction time* (MFRT) for diffusing ligands inside $\mathcal{M}$ to react on a collection of small well-separated partially reactive patches situated on an otherwise reflecting boundary. Adopting the same notation as (1.4), the MFRT $\mathcal{U}(\mathbf{X})$ for a Brownian particle starting at $\mathbf{X} \in \mathcal{M}$ satisfies the mixed Neumann-Robin problem

$$-D\Delta_{\mathbf{X}}\mathcal{U} = 1\,, \quad \mathbf{X} \in \mathcal{M}\,, \tag{1.6a}$$

$$D\partial_n \mathcal{U} + \mathcal{B}_i \mathcal{U} = 0\,, \quad \mathbf{X} \in \partial\mathcal{M}_i\,, \quad i = 1, \ldots, N\,, \tag{1.6b}$$

$$\partial_n \mathcal{U} = 0\,, \quad \mathbf{X} \in \partial\mathcal{M}_r = \partial\mathcal{M} \setminus \cup_{i=1}^{N} \partial\mathcal{M}_i\,, \tag{1.6c}$$

where ∂_n now denotes the normal derivative directed outward to $\mathcal{M}$. A central quantity to describe is the global (or volume-averaged) MFRT,

$$\overline{U} \equiv \frac{1}{|\mathcal{M}|} \int_{\mathcal{M}} U(\mathbf{X})\, d\mathbf{X}\,, \tag{1.7}$$

which corresponds to the average MFRT with respect to a uniform distribution of initial points $\mathbf{X} \in \mathcal{M}$. Here $|\mathcal{M}|$ denotes the volume of $\mathcal{M}$. We non-dimensionalize the MFRT problem (1.6) by introducing the dimensionless variables defined by

$$\mathbf{x} = \frac{\mathbf{X}}{R_\star}\,, \quad L = \max_i\{L_i\}\,, \quad \varepsilon = \frac{L}{R_\star}\,, \quad a_i = \frac{L_i}{L}\,, \quad b_i = \frac{L\mathcal{B}_i}{D}\,, \quad u(\mathbf{x}) = \frac{D}{R_\star^2} U(\mathbf{x}R_\star)\,. \tag{1.8}$$

In terms of (1.8), the dimensionless MFRT $u(\mathbf{x})$ with partially reactive patches and dimensionless reactivities $b_i > 0$ satisfies

$$\Delta_{\mathbf{x}} u = -1\,, \quad \mathbf{x} \in \Omega\,, \tag{1.9a}$$

$$\varepsilon\partial_n u + b_i u = 0\,, \quad \mathbf{x} \in \partial\Omega_i^\varepsilon\,, \quad i = 1, \ldots, N\,, \tag{1.9b}$$

$$\partial_n u = 0\,, \quad \mathbf{x} \in \partial\Omega_r = \partial\Omega \setminus \cup_{i=1}^{N} \partial\Omega_i^\varepsilon\,, \tag{1.9c}$$

with the same notation and assumptions on the patches as for (1.4). For a uniform distribution of initial points $\mathbf{x} \in \Omega$, the dimensionless global MFRT is

$$\overline{u} \equiv \frac{1}{|\Omega|} \int_{\Omega} u(\mathbf{x})\, d\mathbf{x}\,. \tag{1.10}$$

By using the method of matched asymptotic expansions, we will derive in §3 a three-term asymptotic expansion for $\overline{u}$ in the limit $\varepsilon \to 0$, which is valid for a general smooth and closed domain Ω. Our analysis extends that of [20] and [29] for perfectly absorbing and for partially reactive patches, respectively, on the boundary of a spherical domain. It also extends the work of [47] for a single perfectly absorbing boundary patch by describing the interaction of N non-overlapping partially reactive patches. Finally, it extends to higher order the two-term asymptotic result of [22] for perfectly absorbing circular patches on the boundary of non-spherical domains.

For the important case of N identical perfectly absorbing circular patches with common radius ε, our main result for (1.10) given in Proposition 2 simplifies to

$$\overline{u} \sim \frac{|\Omega|}{4N\varepsilon}\left[1 - \frac{\varepsilon\overline{\mathcal{H}}}{N\pi}\log 4\varepsilon + \frac{4\varepsilon}{N}\left(p_s(\mathbf{x}_1,\ldots,\mathbf{x}_N) + \frac{3\overline{\mathcal{H}}}{8\pi}\right) + \mathcal{O}(\varepsilon^2\log\varepsilon)\right]. \tag{1.11}$$

In (1.11), the quantities $\overline{\mathcal{H}}$ and $p_s(\mathbf{x}_1,\ldots,\mathbf{x}_N)$ take the form outlined in (1.5c), but with values drawn from the interior surface Neumann Green's function G_s and its regular part R_s satisfying (3.2) and (3.3). In (1.11), the sign convention is now $\mathcal{H}_i = 1$ if Ω is the unit sphere.

Our asymptotic analysis of (1.4) and (1.9) relies heavily on a careful resolution of the singularity behavior of the surface Neumann Green's function with Dirac source located on the curved boundary. While some previous works on resolving this behavior were given in [42, 47, 50, 57, 58], our local analysis in Appendix B of this singularity behavior is characterized in terms of the local tangential-normal coordinate system near each patch (see Appendix A). This local coordinate system recapitulates the weak path-dependent singularity structure uncovered using a microlocal analysis approach in [47], but in terms of coordinates that are especially convenient for our asymptotic analysis. In comparison to the analysis in [50] and [58], which yielded the first two terms of the singularity behavior only on the surface, our analysis resolves the first three terms of this singularity behavior, and is valid in a small neighborhood of the singular point, i.e. both on and off the surface.

The outline of the paper is the following. In §2 we analyze the BP problem (1.4) in the limit $\varepsilon \to 0$. Our result provides explicit formulas for the capacitance C_T (1.4d) in terms of the reactivities and spatial configuration of boundary patches. In §3, we apply this asymptotic analysis to the NEP defined in (1.9). Again our result takes the form of an explicit asymptotic expansion for the mean exit time of a Brownian particle through multiple boundary windows. Numerical validation of our results are given in §4 and we show that the derived expansion has the errors predicted by the asymptotic theory. We also demonstrate that our asymptotic framework is able to accurately describe the effects that non-constant surface curvature has on the capture statistics of Brownian particles to small reactive sites. In §5 we conclude by discussing some future research directions which emanate from this work.

2. Asymptotic analysis of the Berg-Purcell problem. We now use the method of matched asymptotic expansions to derive a three-term asymptotic expansion for (1.4) in the small-patch limit $\varepsilon \to 0$. The analysis is valid for arbitrary reactivities and arbitrary patch shapes on the domain boundary.

For our analysis, it is convenient to introduce U by

$$u = -C_{\mathrm{T}} U\,, \tag{2.1}$$

so that from (1.4) we find that U satisfies

$$\Delta_{\mathbf{x}} U = 0\,, \quad \mathbf{x} \in \mathbb{R}^3 \backslash \Omega\,, \tag{2.2a}$$

$$\varepsilon \partial_n U + b_i U = 0\,, \quad \mathbf{x} \in \partial\Omega_i^{\varepsilon}\,, \quad i = 1, \ldots, N\,, \tag{2.2b}$$

$$\partial_n U = 0\,, \quad \mathbf{x} \in \partial\Omega_r = \partial\Omega \backslash \cup_{i=1}^{N} \partial\Omega_i^{\varepsilon}\,, \tag{2.2c}$$

$$U \sim -\frac{1}{C_{\mathrm{T}}} + \frac{1}{|\mathbf{x}|} + \frac{\mathbf{p}_T \cdot \mathbf{x}}{C_{\mathrm{T}} |\mathbf{x}|^3} + \cdots\,, \quad \text{as} \quad |\mathbf{x}| \to \infty\,. \tag{2.2d}$$

In (2.2d), $\mathbf{p}_T$ is the dipole vector. Equivalently, we can write the far-field condition (2.2d) as a flux condition over the boundary $\partial\Omega_\sigma$ of a large sphere of radius σ centered at $\mathbf{x} = 0$, in the form

$$\lim_{\sigma \to \infty} \int_{\partial\Omega_\sigma} \partial_r U|_{r=\sigma}\, dS = -4\pi\,. \tag{2.2e}$$

In the outer region away from the boundary patches we expand the outer solution for (2.2) as

$$U \sim \varepsilon^{-1} U_0 + U_1 + \varepsilon \log(\varepsilon)\, U_2 + \varepsilon U_3 + \ldots\,, \tag{2.3}$$

where U_0 is a constant to be determined. The correction terms U_k for $k \geq 1$ satisfy

$$\begin{aligned} &\Delta_{\mathbf{x}} U_k = 0\,, \quad \mathbf{x} \in \mathbb{R}^3 \backslash \Omega\,; \qquad \partial_n U_k = 0\,, \quad \mathbf{x} \in \partial\Omega \backslash \{\mathbf{x}_1, \ldots, \mathbf{x}_N\}\,, \\ &\lim_{\sigma \to \infty} \int_{\partial\Omega_\sigma} \partial_n U_k|_{r=\sigma}\, dS = -4\pi \delta_{k1}\,, \end{aligned} \tag{2.4}$$

where δ_{k1} is the Kronecker symbol. Singularity behaviors for U_k as $\mathbf{x} \to \mathbf{x}_i$, for each $i = 1, \ldots, N$, will be derived by asymptotic matching to the local or inner solutions near each patch.

Near each boundary patch centered at $\mathbf{x} = \mathbf{x}_i \in \partial\Omega$, in (A.2) of Appendix A we introduce a local tangential-normal coordinate system $(t_1, t_2, d)^T$, where $d = \mathrm{dist}(\mathbf{x}, \partial\Omega) \geq 0$, and where t_1 and t_2 are aligned with the two principal directions through $\mathbf{x}_i \in \partial\Omega$ associated with the two principal curvatures κ_{1i} and κ_{2i}, respectively. We define the $\varepsilon-$localized coordinates by $\xi_1 \equiv t_1/\varepsilon$, $\xi_2 \equiv t_2/\varepsilon$, and $\eta \equiv d/\varepsilon$, and label the inner solution near each $\mathbf{x}_i$ as $V_i(\mathbf{y})$, where $\mathbf{y} \equiv (\xi_1, \xi_2, \eta)^T$.

We then expand the inner solution near each patch as

$$V \sim \varepsilon^{-1} V_{0i} + \log(\varepsilon)\, V_{1i} + V_{2i} + \ldots\,. \tag{2.5}$$

Upon substituting (2.5) into the local transformation (A.6) of the Laplacian derived in Appendix A, we obtain that V_{ki} for $k = 0, 1$ satisfies

$$\Delta_{\mathbf{y}} V_{ki} = 0\,, \quad \mathbf{y} \in \mathbb{R}_+^3\,, \tag{2.6a}$$

$$-\partial_\eta V_{ki} + b_i V_{ki} = 0\,, \quad \eta = 0\,, \, (\xi_1, \xi_2) \in \Gamma_i\,, \tag{2.6b}$$

$$\partial_\eta V_{ki} = 0\,, \quad \eta = 0\,, \, (\xi_1, \xi_2) \notin \Gamma_i\,, \tag{2.6c}$$

where $\Delta_{\mathbf{y}} \equiv \partial_{\xi_1 \xi_1} + \partial_{\xi_2 \xi_2} + \partial_{\eta\eta}$, with the behavior at infinity being fixed below via asymptotic matching conditions. Here $\Gamma_i \asymp \varepsilon^{-1} \partial\Omega_i^{\varepsilon}$ is the flattened compactly-supported partially reactive patch on the horizontal plane $\eta = 0$, obtained from the $\varepsilon-$localized tangential-normal coordinate system (e.g., if $\partial\Omega_i^{\varepsilon}$ is a small spherical cap of radius εa_i, then Γ_i is the disk of radius a_i; in other words, Γ_i represents a rescaled flattened shape of the patch in the limit $\varepsilon \to 0$). In addition, we find that V_{2i} satisfies

$$\Delta_{\mathbf{y}} V_{2i} = 2\mathcal{H}_i \left(\eta V_{0i,\eta\eta} + V_{0i,\eta}\right) - 2\mathcal{Q}_i \eta \left(V_{0i,\xi_1\xi_1} - V_{0i,\xi_2\xi_2}\right) , \quad \mathbf{y} \in \mathbb{R}^3_+ , \tag{2.7a}$$

$$-\partial_\eta V_{2i} + b_i V_{2i} = 0 , \quad \eta = 0 , \, (\xi_1, \xi_2) \in \Gamma_i , \tag{2.7b}$$

$$\partial_\eta V_{2i} = 0 , \quad \eta = 0 , \, (\xi_1, \xi_2) \notin \Gamma_i . \tag{2.7c}$$

Here $\mathcal{H}_i$ and $\mathcal{Q}_i$ are the mean curvature and curvature difference of $\partial\Omega$ at $\mathbf{x}_i$, given

$$\mathcal{H}_i \equiv \frac{1}{2}(\kappa_{1i} + \kappa_{2i}) , \qquad \mathcal{Q}_i \equiv \frac{1}{2}(\kappa_{1i} - \kappa_{2i}) , \tag{2.8}$$

with $\mathcal{H}_i < 0$ if $\partial\Omega$ is convex at $\mathbf{x}_i$ as seen from a point $\mathbf{x} \in \mathbb{R}^3 \setminus \Omega$. In (2.6) and (2.7), we label the upper half-space by

$$\mathbb{R}^3_+ \equiv \{\mathbf{y} = (\xi_1, \xi_2, \eta)^T \mid \eta > 0 , \, -\infty < \xi_1, \xi_2 < \infty\} . \tag{2.9}$$

Upon imposing the leading-order matching condition $V_{0i} \sim U_0$ as $|\mathbf{y}| \to \infty$, the solution to (2.6) for $k = 0$ is

$$V_{0i} = U_0 \left(1 - w_i\right) , \tag{2.10}$$

where $w_i(\mathbf{y}; b_i)$ is the solution to

$$\Delta_{\mathbf{y}} w_i = 0 , \quad \mathbf{y} \in \mathbb{R}^3_+ , \tag{2.11a}$$

$$-\partial_\eta w_i + b_i w_i = b_i , \quad \eta = 0 , \, (\xi_1, \xi_2) \in \Gamma_i , \tag{2.11b}$$

$$\partial_\eta w_i = 0 , \quad \eta = 0 , \, (\xi_1, \xi_2) \notin \Gamma_i , \tag{2.11c}$$

$$w_i \sim \frac{C_i(b_i)}{|\mathbf{y}|} + \frac{\mathbf{p}_i(b_i)\cdot\mathbf{y}}{|\mathbf{y}|^3} + \cdots , \quad \text{as} \quad |\mathbf{y}| \to \infty , \tag{2.11d}$$

where $|\mathbf{y}| = (\xi_1^2+\xi_2^2+\eta^2)^{1/2}$. In (2.11d), $C_i(b_i)$ is referred to as the *reactive capacitance* of Γ_i (cf. [29],[31]). From the divergence theorem, it satisfies the identity

$$C_i(b_i) = \frac{1}{\pi} \int_{\Gamma_i} q_i(\xi_1, \xi_2; b_i) \, d\xi_1 d\xi_2 , \quad \text{where} \quad q_i(\xi_1, \xi_2; b_i) \equiv -\frac{1}{2} \partial_\eta w_i|_{\eta=0} . \tag{2.12}$$

We refer to q_i as the *charge density* in analogy with electrostatics. We remark that $C_i(b_i)$ is invariant under rotation of a given patch shape Γ_i. As a result, in computing $C_i(b_i)$ it is not necessary to align the coordinate axes of Γ_i along the two principal directions. The dipole vector $\mathbf{p}_i = \mathbf{p}_i(b_i)$ in (2.11d) must have the form $\mathbf{p}_i = (p_{1i}, p_{2i}, 0)^T$ to ensure that the far-field behavior (2.11d) satisfies (2.11c).

In [29] (see also [31]), the reactive capacitance for a circular patch was computed numerically in terms of a Steklov eigenfunction expansion. The form of this expansion was the motivation for constructing a heuristic approximation for C_i, which is rather accurate over the full range $0 < b_i < \infty$ (see [29] and §4.2). Moreover, this analysis of [29] and [31] was extended in [28] to numerically compute $C_i(b_i)$ for patches of arbitrary shape and to derive monotonicity principles for C_i. For circular patches, the following lemma was established in [31] (see also [29]):

Lemma 2.1. *(Lemma 3.1 of [29]) When Γ_i is the disk $0 \le s \le a_i$, where $s^2 \equiv \xi_1^2 + \xi_2^2$, we have $w_i = w_i(s, \eta; b_i)$ and*

$$C_i(b_i) = 2 \int_0^{a_i} q_i(s; b_i) s \, ds , \qquad q_i(s; b_i) = -\frac{1}{2} w_{i,\eta}|_{\eta=0} , \tag{2.13}$$

where w_i is the solution to (2.11). The asymptotics of C_i are

$$C_i(b_i) \sim C_i(\infty) + \mathcal{O}\left(\frac{\log b_i}{b_i}\right), \quad \textit{as} \quad b_i \to \infty, \quad \textit{with} \quad C_i(\infty) = \frac{2a_i}{\pi}, \tag{2.14a}$$

$$C_i(b_i) \sim a_i\left[c_1(b_i a_i) - c_2(b_i a_i)^2 + c_3(b_i a_i)^3 + \mathcal{O}((b_i a_i)^4)\right], \quad \textit{as} \quad b_i \to 0, \tag{2.14b}$$

where $c_1 = 0.5$, $c_2 = 4/(3\pi) \approx 0.4244$ and $c_3 \approx 0.3651$. Moreover, for $b_i \to \infty$, $q_i \sim q_i(s;\infty) = \pi^{-1}\left(a_i^2 - s^2\right)^{-1/2}$ on $0 \le s < a_i$.

We now proceed with the asymptotic analysis. The matching condition is that the local behavior of the outer expansion (2.3) as $\mathbf{x} \to \mathbf{x}_i$ must agree with the far-field behavior of the inner expansion (2.5), so that for each $i = 1, \ldots, N$ we must have

$$\begin{aligned} &\frac{U_0}{\varepsilon} + U_1 + \varepsilon \log(\varepsilon)\, U_2 + \varepsilon U_3 + \ldots \\ &\qquad\qquad \sim \frac{U_0}{\varepsilon}\left(1 - \frac{C_i}{|\mathbf{y}|} - \frac{\mathbf{p}_i \cdot \mathbf{y}}{|\mathbf{y}|^3}\right) + \log(\varepsilon) V_{1i} + V_{2i} + \ldots . \end{aligned} \tag{2.15}$$

By using $|\mathbf{y}| \sim \varepsilon^{-1}|\mathbf{x} - \mathbf{x}_i|$ from (A.9) of Appendix A, this matching condition provides the singular behavior for U_1 as $\mathbf{x} \to \mathbf{x}_i$. In this way, we conclude that U_1 satisfies

$$\Delta_{\mathbf{x}} U_1 = 0, \quad \mathbf{x} \in \mathbb{R}^3 \backslash \Omega; \qquad \partial_n U_1 = 0, \quad \mathbf{x} \in \partial\Omega \backslash \{\mathbf{x}_1, \ldots, \mathbf{x}_N\}, \tag{2.16a}$$

$$U_1 \sim -\frac{U_0 C_i}{|\mathbf{x} - \mathbf{x}_i|}, \quad \text{as} \quad \mathbf{x} \to \mathbf{x}_i \in \partial\Omega, \quad i = 1, \ldots, N, \tag{2.16b}$$

$$\lim_{\sigma \to \infty} \int_{\partial\Omega_\sigma} \partial_r U_1|_{r=\sigma}\, dS = -4\pi. \tag{2.16c}$$

From the divergence theorem, the solvability condition for (2.16) determines U_0 as

$$U_0 = -\frac{2}{\overline{C}}, \qquad \text{where} \qquad \overline{C} \equiv \sum_{i=1}^{N} C_i(b_i). \tag{2.17}$$

To determine U_1, we introduce the surface Neumann Green's function $G_e(\mathbf{x}; \mathbf{x}_i)$ for the exterior problem, which is the unique solution to

$$\begin{aligned} &\Delta_{\mathbf{x}} G_e = 0, \quad \mathbf{x} \in \mathbb{R}^3 \backslash \Omega; \qquad \partial_n G_e = \delta(\mathbf{x} - \mathbf{x}_i), \quad \mathbf{x} \in \partial\Omega, \\ &G_e \sim \frac{1}{4\pi|\mathbf{x}|}, \quad \text{as} \quad |\mathbf{x}| \to \infty, \end{aligned} \tag{2.18a}$$

where $\mathbf{x}_i \in \partial\Omega$ and ∂_n is the outward normal derivative to $\mathbb{R}^3 \backslash \Omega$, which points into Ω. In Appendix B we show that the local singularity behavior of G_e is

$$G_e(\mathbf{x}; \mathbf{x}_i) = \frac{1}{2\pi|\mathbf{x} - \mathbf{x}_i|} - \frac{\mathcal{H}_i}{4\pi} \log\left(|\mathbf{x} - \mathbf{x}_i| + d\right) + e(\mathbf{x}; \mathbf{x}_i) + R_e(\mathbf{x}_i) + o(1), \quad \text{as} \quad \mathbf{x} \to \mathbf{x}_i. \tag{2.18b}$$

Here $\mathcal{H}_i$ is the mean curvature of $\partial\Omega$ at $\mathbf{x} = \mathbf{x}_i$ (with $\mathcal{H}_i = -1$ if Ω is the unit sphere), $d = \text{dist}(\mathbf{x}, \partial\Omega) > 0$, while the term $e(\mathbf{x}; \mathbf{x}_i)$ given in (B.29) is proportional to the curvature difference and depends on the specific path of approach to $\mathbf{x} = \mathbf{x}_i \in \partial\Omega$. In contrast, $R_e(\mathbf{x}_i)$ is a *globally determined quantity*, referred to as the *regular part* of G_e, which depends on the domain shape and on $\mathbf{x}_i$. When Ω is the unit sphere, the explicit analytical solution to (2.18a) and the corresponding regular part R_e are given in (B.30). For the case of prolate spheroids, a series solution for G_e and R_e has been derived in [42], while for more general domains a numerical method is also available [42].

The solution to (2.16) is represented in terms of G_e as

$$U_1 = \overline{U}_1 - 2\pi U_0 \sum_{j=1}^{N} C_j G_e(\mathbf{x};\mathbf{x}_j)\,, \tag{2.19}$$

where $\overline{U}_1$ is an unknown constant, which must be expanded as (cf. [20], [44], [29])

$$\overline{U}_1 = \overline{U}_{10}\log(\varepsilon) + \overline{U}_{11}\,, \tag{2.20}$$

where $\overline{U}_{10}$ and $\overline{U}_{11}$ are constants, independent of ε, to be determined. The term $\overline{U}_{10}\log(\varepsilon)$ is a "switchback term" (cf. [39]) and simply corresponds to inserting a constant term between U_0/ε and U_1 in the outer expansion (2.3).

In order to determine the local behavior of U_1 as $\mathbf{x}\to\mathbf{x}_i$, in Appendix B we establish the refined asymptotic behavior of the surface Neumann Green's function G_e as $\mathbf{x}\to\mathbf{x}_i$, written in terms of the local tangential-normal coordinate system. In terms of the ε-localized boundary-fitted coordinates it is given in (B.28). In this way, by using (B.28) and (2.20) in (2.19), we obtain as $\mathbf{x}\to\mathbf{x}_i$ that

$$\begin{aligned} U_1 \sim -\frac{U_0 C_i}{\varepsilon|\mathbf{y}|} + \left(\frac{\mathcal{H}_i U_0 C_i}{2} + \overline{U}_{10}\right)\log\varepsilon + \frac{\mathcal{H}_i U_0 C_i}{2}\left(\log\left(\eta+|\mathbf{y}|\right) - \frac{\eta(\xi_1^2+\xi_2^2)}{|\mathbf{y}|^3}\right) \\ - \frac{\mathcal{Q}_i U_0 C_i}{4}\left(\frac{2\eta}{|\mathbf{y}|^3} + \frac{1}{\left(\eta+|\mathbf{y}|\right)^2}\right)(\xi_1^2-\xi_2^2) + \overline{U}_{11} + U_0\beta_{ei}\,. \end{aligned} \tag{2.21}$$

Here the constant β_{ei} is the i-th component of a matrix-vector product defined by

$$\beta_{ei} \equiv -2\pi\left(\mathcal{G}_e\mathbf{C}\right)_i\,, \tag{2.22}$$

where $\mathbf{C}\equiv(C_1,\ldots,C_N)^T$ and $\mathcal{G}_e$ is the Green's matrix defined by

$$\mathcal{G}_e \equiv \begin{pmatrix} R_{e1} & G_{e12} & \cdots & G_{e1N} \\ G_{e21} & R_{e2} & \cdots & G_{e2N} \\ \vdots & \vdots & \ddots & \vdots \\ G_{eN1} & \cdots & G_{eN,N-1} & R_{eN} \end{pmatrix}, \quad R_{ei}\equiv R_e(\mathbf{x}_i)\,, \quad G_{eij}\equiv G_e(\mathbf{x}_i;\mathbf{x}_j)\,. \tag{2.23}$$

Upon substituting (2.21) into the matching condition (2.15), we observe that the $\mathcal{O}(\log\varepsilon)$ term in (2.21) specifies the far-field limiting behavior $V_{1i}\sim\overline{U}_{10}+\mathcal{H}_i U_0 C_i/2$ as $|\mathbf{y}|\to\infty$, where V_{1i} satisfies the inner problem (2.6) with $k=1$. In terms of w_i of (2.11), we conclude that

$$V_{1i} = \left(\frac{\mathcal{H}_i U_0 C_i}{2} + \overline{U}_{10}\right)(1-w_i)\,, \tag{2.24}$$

which has the far-field behavior

$$V_{1i} \sim \left(\frac{\mathcal{H}_i U_0 C_i}{2} + \overline{U}_{10}\right)\left(1 - \frac{C_i}{|\mathbf{y}|} + \cdots\right), \quad \text{as} \quad |\mathbf{y}|\to\infty\,. \tag{2.25}$$

Upon substituting (2.25) into the matching condition (2.15), we obtain the singularity behavior for the correction U_2 in the outer expansion (2.3). In this way, we conclude that U_2 satisfies

$$\Delta_{\mathbf{x}} U_2 = 0\,, \quad \mathbf{x} \in \mathbb{R}^3 \backslash \Omega\,; \qquad \partial_n U_2 = 0\,, \quad \mathbf{x} \in \partial\Omega \backslash \{\mathbf{x}_1, \ldots, \mathbf{x}_N\}\,, \tag{2.26a}$$

$$U_2 \sim -\left(\frac{\mathcal{H}_i U_0 C_i}{2} + \overline{U}_{10}\right) \frac{C_i}{|\mathbf{x}-\mathbf{x}_i|}\,, \quad \text{as} \quad \mathbf{x} \to \mathbf{x}_i \in \partial\Omega\,, \quad i = 1, \ldots, N\,, \tag{2.26b}$$

$$\lim_{\sigma\to\infty} \int_{\partial\Omega_\sigma} \partial_r U_2|_{r=\sigma}\, dS = 0\,. \tag{2.26c}$$

By using the divergence theorem, we readily find that (2.26) is solvable only when $\sum_{j=1}^N C_j \left[\overline{U}_{10} + \mathcal{H}_j U_0 C_j/2\right] = 0$, which determines $\overline{U}_{10}$ as

$$\frac{\overline{U}_{10}}{U_0} = -\frac{1}{2\overline{C}} \left(\sum_{j=1}^N \mathcal{H}_j C_j^2\right)\,, \quad \text{where} \quad \overline{C} = \sum_{j=1}^N C_j\,. \tag{2.27}$$

With $\overline{U}_{10}$ determined in this way, the solution to (2.26) is given in terms of the surface Neumann Green's function and an additional unknown constant $\overline{U}_2$ as

$$U_2 = \overline{U}_2 - 2\pi \sum_{j=1}^N C_j \left(\frac{\mathcal{H}_j U_0 C_j}{2} + \overline{U}_{10}\right) G_e(\mathbf{x}; \mathbf{x}_j)\,. \tag{2.28}$$

Next, we match the $\mathcal{O}(1)$ terms in (2.21) when substituted into the matching condition (2.15). In this way, we find that V_{2i} satisfies (2.7) with the far-field behavior

(2.29)
$$\begin{aligned} V_{2i} \sim V_{2i\infty} \equiv \beta_{ei} U_0 + \overline{U}_{11} + \frac{\mathcal{H}_i U_0 C_i}{2} \left(\log(\eta + |\mathbf{y}|) - \frac{\eta(\xi_1^2 + \xi_2^2)}{|\mathbf{y}|^3}\right)\,, \\ - \frac{\mathcal{Q}_i U_0 C_i}{4} \left[\frac{2\eta}{|\mathbf{y}|^3} + \frac{1}{(\eta + |\mathbf{y}|)^2}\right] (\xi_1^2 - \xi_2^2)\,, \quad \text{as} \quad |\mathbf{y}| \to \infty\,. \end{aligned}$$

To analyze (2.29), it is convenient to decompose V_{2i} as

$$V_{2i} = \left(\beta_{ei} U_0 + \overline{U}_{11}\right)(1 - w_i) + \mathcal{H}_i U_0 \Phi_{i+} + \mathcal{Q}_i U_0 \Phi_{i-}\,, \tag{2.30}$$

while substituting $V_{0i} = U_0(1 - w_i)$ into the right-hand side of (2.7). In this way, we obtain that Φ_{i+} satisfies

$$\Delta_{\mathbf{y}} \Phi_{i+} = -2\left(\eta w_{i,\eta\eta} + w_{i,\eta}\right)\,, \quad \mathbf{y} \in \mathbb{R}_+^3\,, \tag{2.31a}$$

$$-\partial_\eta \Phi_{i+} + b_i \Phi_{i+} = 0\,, \quad \eta = 0\,,\ (\xi_1, \xi_2) \in \Gamma_i\,, \tag{2.31b}$$

$$\partial_\eta \Phi_{i+} = 0\,, \quad \eta = 0\,,\ (\xi_1, \xi_2) \notin \Gamma_i\,, \tag{2.31c}$$

$$\Phi_{i+} \sim \frac{C_i}{2}\left(\log(\eta + |\mathbf{y}|) - \frac{\eta(\xi_1^2 + \xi_2^2)}{|\mathbf{y}|^3}\right)\,, \quad \text{as} \quad |\mathbf{y}| \to \infty\,, \tag{2.31d}$$

while Φ_{i-} is the solution to

$$\Delta_{\mathbf{y}} \Phi_{i-} = \mathcal{N}_{-}(\mathbf{y}) \equiv 2\eta \left(w_{i,\xi_1\xi_1} - w_{i,\xi_2\xi_2} \right) , \quad \mathbf{y} \in \mathbb{R}^3_+ , \tag{2.32a}$$

$$-\partial_\eta \Phi_{i-} + b_i \Phi_{i-} = 0 , \quad \eta = 0 , \, (\xi_1, \xi_2) \in \Gamma_i , \tag{2.32b}$$

$$\partial_\eta \Phi_{i-} = 0 , \quad \eta = 0 , \, (\xi_1, \xi_2) \notin \Gamma_i , \tag{2.32c}$$

$$\Phi_{i-} \sim -\frac{C_i}{4} \left[\frac{2\eta}{|\mathbf{y}|^3} + \frac{1}{(\eta + |\mathbf{y}|)^2} \right] (\xi_1^2 - \xi_2^2) , \quad \text{as} \quad |\mathbf{y}| \to \infty . \tag{2.32d}$$

In Appendix C of [29] (see also [31]), with derivation summarized below in Appendix C, it was shown that the solution to (2.31) has the refined far-field behavior

$$\Phi_{i+} \sim \frac{C_i}{2} \left(\log(\eta + |\mathbf{y}|) - \frac{\eta(\xi_1^2 + \xi_2^2)}{|\mathbf{y}|^3} \right) + \frac{E_{i+}}{|\mathbf{y}|} , \quad \text{as} \quad |\mathbf{y}| \to \infty . \tag{2.33}$$

The properties of the monopole coefficient $E_{i+} = E_{i+}(b_i)$, as derived in [29] and also summarized in Appendix C (see also [31]), are given in the next lemma.

LEMMA 2.2. *For an arbitrary patch shape Γ_i, we have*

$$E_{i+}(b_i) = -\frac{1}{2\pi^2} \int\limits_{\Gamma_i} \int\limits_{\Gamma_i} q_i(\mathbf{y}; b_i) \, q_i(\mathbf{y}'; b_i) \, \log |\mathbf{y} - \mathbf{y}'| \, d\mathbf{y} \, d\mathbf{y}' , \tag{2.34}$$

where we have labeled $\mathbf{y} = (\xi_1, \xi_2)^T$ and $\mathbf{y}' = (\xi_1', \xi_2')^T$. As $b_i \to 0$, we have $q_i \sim b_i/2$ so that to leading order

$$E_{i+}(b_i) \sim -\frac{b_i^2}{8\pi^2} \left(\int\limits_{\Gamma_i} \int\limits_{\Gamma_i} \log |\mathbf{y} - \mathbf{y}'| \, d\mathbf{y} \, d\mathbf{y}' \right) . \tag{2.35}$$

The coefficient E_{i+} is invariant under rotations and so does not depend on the orientation of the patch with respect to the principal directions. When Γ_i is the disk $s^2 \equiv \xi_1^2 + \xi_2^2 \leq a_i^2$, for which $q_i = q_i(s; b_i)$ in (2.12) is radially symmetric, we have

$$E_{i+} = E_{i+}(b_i) = -\frac{\log a_i}{2} [C_i(b_i)]^2 + 2 \int_0^{a_i} \frac{1}{s} \left(\int_0^s t q_i(t; b_i) \, dt \right)^2 ds , \tag{2.36}$$

where $C_i(b_i)$ is given by Lemma 2.1. For the disk, the asymptotic behavior of E_{i+} is

$$E_{i+} \sim E_{i+}(\infty) \equiv -\frac{2a_i^2}{\pi^2} \left(\log a_i + \log 4 - \frac{3}{2} \right) , \quad \textit{as} \quad b_i \to \infty , \tag{2.37a}$$

$$E_{i+} \sim \frac{b_i^2 a_i^4}{8} \left(\frac{1}{4} - \log a_i \right) , \quad \textit{as} \quad b_i \to 0 . \tag{2.37b}$$

The new problem (2.32), which incorporates curvature anisotropy due to differences in the two principal curvatures for non-circular patches, is analyzed in Appendix D. There it is shown that, in terms of an additional monopole coefficient $E_{i-} = E_{i-}(b_i)$, Φ_{i-} has the refined far-field asymptotic behavior

$$\Phi_{i-} \sim -\frac{C_i}{4} \left[\frac{2\eta}{|\mathbf{y}|^3} + \frac{1}{(\eta + |\mathbf{y}|)^2} \right] (\xi_1^2 - \xi_2^2) + \frac{E_{i-}}{|\mathbf{y}|} . \tag{2.38}$$

As derived in Appendix D, this new monopole coefficient is characterized as follows:

Lemma 2.3. *For an arbitrary patch shape* Γ_i*, we have*

$$E_{i-}(b_i) = \frac{1}{4\pi^2}\int_{\Gamma_i} q_i(\mathbf{y};b_i)\mathcal{J}_i(\mathbf{y};b_i)\,d\mathbf{y}\,, \quad \text{with} \quad q_i(\mathbf{y};b_i) = -\frac{1}{2}w_{i,\eta}|_{\eta=0}\,, \tag{2.39a}$$

where $\mathcal{J}_i$ *is defined by*

$$\mathcal{J}_i(\mathbf{y};b_i) \equiv \int_{\Gamma_i} \frac{(\xi_1'-\xi_1)^2-(\xi_2'-\xi_2)^2}{|\mathbf{y}'-\mathbf{y}|}\, q_i(\mathbf{y}';b_i)\,d\mathbf{y}'\,. \tag{2.39b}$$

As $b_i\to 0$*, we have* $q_i\sim b_i/2$ *so that to leading order*

$$E_{i-}(b_i) \sim \frac{b_i^2}{16\pi^2}\int_{\Gamma_i}\int_{\Gamma_i} \frac{(\xi_1'-\xi_1)^2-(\xi_2'-\xi_2)^2}{|\mathbf{y}'-\mathbf{y}|}d\mathbf{y}\,d\mathbf{y}'\,. \tag{2.40}$$

In (2.39) and (2.40), we have labeled $\mathbf{y}=(\xi_1,\xi_2)^T$ *and* $\mathbf{y}'=(\xi_1',\xi_2')^T$*. The coefficient* E_{i-} *is not invariant under rotations of* Γ_i*, and so it depends on the orientation of the patch with respect to the two principal directions. When* Γ_i *is a disk, then* $E_{i-}\equiv 0$ *for all* $b_i>0$*.*

To show that $E_{i-}\equiv 0$ when Γ_i is a disk of radius a_i, we first observe for a disk that q_i is radially symmetric so that $q_i = q_i\left(|\mathbf{y}'|;b_i\right)$. It then readily follows that $\mathcal{J}_i$ in (2.39b) has the symmetry property (written in component form) $\mathcal{J}_i(\xi_1,\xi_2;b_i) = -\mathcal{J}_i(\xi_2,\xi_1;b_i)$. As a result, since the integrand in (2.39a) is an odd function with respect to reflection about the line $\xi_1=\xi_2$ that partitions the disk Γ_i into equal halves, it follows from symmetry that $E_{i-}\equiv 0$ for all $b_i>0$.

With the properties of $E_{i\pm}$ established above, we now proceed with the asymptotic analysis. To determine the refined far-field behavior of V_{2i} we substitute the far-field behaviors (2.33), (2.38), and $w_i\sim C_i/|\mathbf{y}|$ as $|\mathbf{y}|\to\infty$ into our decomposition (2.30). We conclude that

$$V_{2i} \sim V_{2i\infty} + \frac{E_iU_0}{|\mathbf{y}|} - \frac{C_i\left(U_0\beta_{ei}+\overline{U}_{11}\right)}{|\mathbf{y}|}\,, \qquad \text{as} \quad |\mathbf{y}|\to\infty\,, \tag{2.41}$$

where $V_{2i\infty}$ was defined in (2.29) and E_i is defined in terms of $E_{i\pm}$ by

$$E_i \equiv \mathcal{H}_iE_{i+} + \mathcal{Q}_iE_{i-}\,, \tag{2.42}$$

where $\mathcal{H}_i$ and $\mathcal{Q}_i$ were defined in (2.8).

Upon substituting (2.41) into the matching condition (2.15), we observe that the two monopole terms in (2.41) determine one component of the required singularity behavior for the outer correction U_3 in (2.3). The remaining part of the singularity condition arises from the dipole term $\mathbf{p}_i$ in (2.11d), which is written in outer variables using $\mathbf{y}\sim\mathbf{Q}_i(\mathbf{x}-\mathbf{x}_i)/\varepsilon$ from (A.8), where $\mathbf{Q}_i$ is a suitable orthogonal matrix. In this way, we conclude from (2.4), (2.15) and (2.41) that U_3 must satisfy

$$\Delta_{\mathbf{x}}U_3 = 0\,, \quad \mathbf{x}\in\mathbb{R}^3\backslash\Omega\,; \qquad \partial_nU_3=0\,, \quad \mathbf{x}\in\partial\Omega\backslash\{\mathbf{x}_1,\ldots,\mathbf{x}_N\}\,, \tag{2.43a}$$

$$U_3 \sim \frac{\left[U_0E_i - \left(\beta_{ei}U_0+\overline{U}_{11}\right)C_i\right]}{|\mathbf{x}-\mathbf{x}_i|} - U_0\frac{\mathbf{p}_i{\cdot}\mathbf{Q}_i(\mathbf{x}-\mathbf{x}_i)}{|\mathbf{x}-\mathbf{x}_i|^3}\,,$$
$$\text{as} \quad \mathbf{x}\to\mathbf{x}_i\in\partial\Omega\,, \quad i=1,\ldots,N\,, \tag{2.43b}$$

$$\lim_{\sigma\to\infty}\int_{\partial\Omega_\sigma}\partial_rU_3|_{r=\sigma}\,dS = 0\,. \tag{2.43c}$$

From the divergence theorem, we conclude that (2.43) has a solution if and only if $\overline{U}_{11}$ satisfies

$$\frac{\overline{U}_{11}}{U_0} = \frac{1}{\overline{C}} \left(\sum_{j=1}^{N} E_j - \sum_{j=1}^{N} \beta_{ej} C_j \right) . \tag{2.44}$$

We remark that the contribution from the dipole term vanishes identically by symmetry since $\mathbf{p}_i$ has the form $\mathbf{p}_i = (p_{1i}, p_{2i}, 0)^T$. Finally, by using (2.22) for β_{ei}, and recalling (2.42) for E_i, we determine $\overline{U}_{11}$ as

$$\frac{\overline{U}_{11}}{U_0} = \frac{2\pi}{\overline{C}} \mathbf{C}^T \mathcal{G}_e \mathbf{C} + \frac{\overline{E}}{\overline{C}} , \quad \text{where} \quad \overline{E} \equiv \sum_{j=1}^{N} E_j = \sum_{j=1}^{N} \left(\mathcal{H}_j E_{j+} + \mathcal{Q}_j E_{j-} \right) . \tag{2.45}$$

Finally, to identify the capacitance C_{T} in (2.2d), we must take the limit as $|\mathbf{x}| \to \infty$ of our outer asymptotic expansion (2.3) and compare it with the required limiting behavior in (2.2d). By comparing the $\mathcal{O}(1)$ terms in the resulting expression we obtain the following main result for C_{T}:

Proposition 1. *As $\varepsilon \to 0$, the dimensionless capacitance C_{T} for (2.2) in the presence of N well-separated partially reactive Robin patches, centered at $\mathbf{x}_i$ and with local reactivities b_i for $i = 1, \ldots, N$, has the three-term asymptotic expansion*

$$\frac{1}{C_{\mathrm{T}}} \sim \frac{|U_0|}{\varepsilon} \left[1 + \varepsilon \frac{\overline{U}_{10}}{U_0} \log(\varepsilon) + \varepsilon \frac{\overline{U}_{11}}{U_0} + \mathcal{O}\left(\varepsilon^2 \log \varepsilon\right) \right] , \tag{2.46a}$$

where

$$|U_0| = \frac{2}{\overline{C}} , \qquad \frac{\overline{U}_{10}}{U_0} = -\frac{1}{2\overline{C}} \sum_{j=1}^{N} \mathcal{H}_j C_j^2 ,$$
$$\frac{\overline{U}_{11}}{U_0} = \frac{2\pi}{\overline{C}} \mathbf{C}^T \mathcal{G}_e \mathbf{C} + \frac{\overline{E}}{\overline{C}} , \qquad \overline{E} = \sum_{j=1}^{N} \left(\mathcal{H}_j E_{j+} + \mathcal{Q}_j E_{j-} \right) , \tag{2.46b}$$

with $\mathcal{H}_j = (\kappa_{1j} + \kappa_{2j})/2$, $\mathcal{Q}_j = (\kappa_{1j} - \kappa_{2j})/2$, and $\overline{C} = \sum_{j=1}^{N} C_j$. Here E_{j+} and E_{j-} are characterized in Lemmas 2.2 and 2.3, respectively. The Green's matrix $\mathcal{G}_e$ in (2.46b) is given by (2.23) in terms of the surface Neumann Green's function of (2.18a). In terms of the dimensional capacitance $\mathcal{C}_{\mathrm{T}}$, defined in (1.1d), we use (1.3) to obtain for a domain of diameter $2R_\star$ and with a collection of partially reactive boundary patches of maximum diameter $2L$, that

$$\mathcal{C}_{\mathrm{T}} = R_\star C_{\mathrm{T}} , \tag{2.47}$$

which determines the dimensional flux to all the surface receptors as (see (1.2))

$$J \equiv 4\pi D \,\mathcal{U}_{\mathrm{inf}} \mathcal{C}_{\mathrm{T}} . \tag{2.48}$$

In evaluating C_{T} from (2.46) for the dimensional problem, we use $C_i = C_i\left(L\mathcal{B}_i/D\right)$ and $E_{i\pm} = E_{i\pm}\left(L\mathcal{B}_i/D\right)$, while calculating the Green's matrix $\mathcal{G}_e$ at $\mathbf{x}_i = \mathbf{X}_i/R_\star$.

When Ω is the unit sphere, we have $\mathcal{H}_i = -1$ and $\mathcal{Q}_i = 0$ for all $i = 1, \ldots, N$, and so our main result (2.46) reduces to that derived in Proposition 1 of [31].

For N identical locally circular, and perfectly absorbing, patches of radius ε on a smooth boundary, our main result (2.46) can be simplified to that given in (1.5) by setting $C_i = 2/\pi$, $E_{i-} = 0$, and $E_{i+} = -2(\log 4 - 3/2)/\pi^2$ for $i = 1, \ldots, N$.

We emphasize that the term $\mathcal{Q}_i E_{i-}$ appearing in (2.46b) will in general be non-vanishing *only* when the patch has a non-circular shape and is centered at a point on the boundary where the two principal curvatures are different.

3. The Mean First-Reaction Time. In this section we use a very similar asymptotic approach to analyze (1.9) and to derive a three-term expansion for the global MFRT $\overline{u}$ in (1.10).

In the outer region, we expand the outer solution as in (2.3) where U_0 is a constant to be determined, and where the correction terms U_k for $k \geq 1$ satisfy

$$\Delta_{\mathbf{x}} U_k = -\delta_{k1}\,, \quad \mathbf{x} \in \Omega\,; \qquad \partial_n U_k = 0\,, \quad \mathbf{x} \in \partial\Omega \backslash \{\mathbf{x}_1, \ldots, \mathbf{x}_N\}\,, \tag{3.1}$$

where δ_{k1} is the Kronecker symbol. Singularity behaviors for U_k as $\mathbf{x} \to \mathbf{x}_i$, for $i = 1, \ldots, N$, will be derived by asymptotic matching to the inner (local) solutions near each patch. The outer corrections U_k for $k \geq 1$ are now represented in terms of the surface Neumann Green's function $G_s(\mathbf{x}; \mathbf{x}_i)$ for the interior problem, which is the unique solution to

$$\Delta_{\mathbf{x}} G_s = \frac{1}{|\Omega|}\,, \quad \mathbf{x} \in \Omega\,; \qquad \partial_n G_s = \delta(\mathbf{x} - \mathbf{x}_i)\,, \quad \mathbf{x} \in \partial\Omega\,; \qquad \int_\Omega G_s \, d\mathbf{x} = 0\,, \tag{3.2}$$

with $\mathbf{x}_i \in \partial\Omega$. As shown in Appendix B the local singularity behavior of G_s is

$$G_s(\mathbf{x}; \mathbf{x}_i) = \frac{1}{2\pi|\mathbf{x} - \mathbf{x}_i|} - \frac{\mathcal{H}_i}{4\pi} \log\left(|\mathbf{x} - \mathbf{x}_i| + d\right) + e(\mathbf{x}; \mathbf{x}_i) + R_s(\mathbf{x}_i) + o(1)\,, \quad \text{as} \quad \mathbf{x} \to \mathbf{x}_i\,, \tag{3.3}$$

where $d = \text{dist}(\mathbf{x}, \partial\Omega)$. For this interior problem we note the sign convention that if the boundary at $\mathbf{x} = \mathbf{x}_i \in \partial\Omega$ is locally convex as seen from $\mathbf{x} \in \Omega$, then $\mathcal{H}_i > 0$. When Ω is the unit sphere, $\mathcal{H}_i = 1$, and the exact solution to (3.2) is given in (B.31).

Since the asymptotic analysis of the inner solution near each patch is identical to that for the exterior problem studied in §2, we can readily determine the appropriate singularity behavior for U_k as $\mathbf{x} \to \mathbf{x}_i$ for (3.1) by simply appealing to the results in §2.

In particular, in analogy with (2.16), we obtain that U_1 satisfies

$$\Delta_{\mathbf{x}} U_1 = -1\,, \quad \mathbf{x} \in \Omega\,; \qquad \partial_n U_1 = 0\,, \quad \mathbf{x} \in \partial\Omega \backslash \{\mathbf{x}_1, \ldots, \mathbf{x}_N\}\,, \tag{3.4a}$$

$$U_1 \sim -\frac{U_0 C_i}{|\mathbf{x} - \mathbf{x}_i|}\,, \quad \text{as} \quad \mathbf{x} \to \mathbf{x}_i \in \partial\Omega\,, \quad i = 1, \ldots, N\,. \tag{3.4b}$$

From the divergence theorem, the solvability condition for (3.4) determines U_0 as

$$U_0 = \frac{|\Omega|}{2\pi \overline{C}}\,, \quad \text{where} \quad \overline{C} \equiv \sum_{j=1}^N C_j\,. \tag{3.5}$$

In terms of constants $\overline{U}_{10}$ and $\overline{U}_{11}$ to be determined, the solution to (3.4) is

$$U_1 = \overline{U}_1 - 2\pi U_0 \sum_{j=1}^N C_j G_s(\mathbf{x}; \mathbf{x}_j)\,, \quad \text{where} \quad \overline{U}_1 = \overline{U}_{10} \log(\varepsilon) + \overline{U}_{11}\,. \tag{3.6}$$

In analogy with (2.26), we obtain that U_2 satisfies

$$\Delta_{\mathbf{x}} U_2 = 0\,, \quad \mathbf{x} \in \Omega\,; \qquad \partial_n U_2 = 0\,, \quad \mathbf{x} \in \partial\Omega \backslash \{\mathbf{x}_1, \ldots, \mathbf{x}_N\}\,, \tag{3.7a}$$

$$U_2 \sim -\left(\frac{\mathcal{H}_i U_0 C_i}{2} + \overline{U}_{10} \right) \frac{C_i}{|\mathbf{x} - \mathbf{x}_i|}\,, \quad \text{as} \quad \mathbf{x} \to \mathbf{x}_i \in \partial\Omega\,, \quad i = 1, \ldots, N\,. \tag{3.7b}$$

By using the divergence theorem, the solvability condition for (3.7) determines $\overline{U}_{10}$ as

$$\frac{\overline{U}_{10}}{U_0} = -\frac{1}{2\overline{C}} \left(\sum_{j=1}^{N} \mathcal{H}_j C_j^2 \right)\,, \quad \text{where} \quad \overline{C} \equiv \sum_{j=1}^{N} C_j\,. \tag{3.8}$$

The solution to (3.7) is then represented in terms of an unknown constant $\overline{U}_2$ as

$$U_2 = \overline{U}_2 - 2\pi \sum_{j=1}^{N} C_j \left(\frac{\mathcal{H}_j U_0 C_j}{2} + \overline{U}_{10} \right) G_s(\mathbf{x}; \mathbf{x}_j)\,. \tag{3.9}$$

Finally, in analogy with (2.43), we obtain that U_3 satisfies

$$\Delta_{\mathbf{x}} U_3 = 0\,, \quad \mathbf{x} \in \Omega\,; \qquad \partial_n U_3 = 0\,, \quad \mathbf{x} \in \partial\Omega \backslash \{\mathbf{x}_1, \ldots, \mathbf{x}_N\}\,, \tag{3.10a}$$

$$U_3 \sim \frac{\left[U_0 E_i - \left(\beta_{si} U_0 + \overline{U}_{11} \right) C_i \right]}{|\mathbf{x} - \mathbf{x}_i|} - U_0 \frac{\mathbf{p}_i \cdot \mathbf{Q}_i (\mathbf{x} - \mathbf{x}_i)}{|\mathbf{x} - \mathbf{x}_i|^3}\,, \quad \text{as} \quad \mathbf{x} \to \mathbf{x}_i \in \partial\Omega\,, \quad i = 1, \ldots, N\,, \tag{3.10b}$$

where E_i was defined in (2.42) and $\mathbf{Q}_i$ is the rotation matrix between Cartesian and local coordinates (see (A.2a)). In (3.10b), β_{si} is defined by the matrix-vector product

$$\beta_{si} = -2\pi \left(\mathcal{G}_s \mathbf{C} \right)_i\,, \tag{3.11}$$

where $\mathbf{C} = (C_1, \ldots, C_N)^T$ and

$$\mathcal{G}_s \equiv \begin{pmatrix} R_{s1} & G_{s12} & \cdots & G_{s1N} \\ G_{s21} & R_{s2} & \cdots & G_{s2N} \\ \vdots & \vdots & \ddots & \vdots \\ G_{sN1} & \cdots & G_{sN,N-1} & R_{sN} \end{pmatrix}\,, \quad R_{si} \equiv R_s(\mathbf{x}_i)\,, \quad G_{sij} \equiv G_s(\mathbf{x}_i; \mathbf{x}_j)\,. \tag{3.12}$$

From the divergence theorem, (3.10) has a solution only when $\overline{U}_{11}$ satisfies

$$\frac{\overline{U}_{11}}{U_0} = \frac{1}{\overline{C}} \left(\sum_{j=1}^{N} E_j - \sum_{j=1}^{N} \beta_{sj} C_j \right)\,. \tag{3.13}$$

By using (3.11) for β_{si}, and recalling (2.42) for E_i, we conclude that

$$\frac{\overline{U}_{11}}{U_0} = \frac{2\pi}{\overline{C}} \mathbf{C}^T \mathcal{G}_s \mathbf{C} + \frac{\overline{E}}{\overline{C}}\,, \quad \text{where} \quad \overline{E} \equiv \sum_{j=1}^{N} E_j = \sum_{j=1}^{N} \left(\mathcal{H}_j E_{j+} + \mathcal{Q}_j E_{j-} \right)\,. \tag{3.14}$$

We summarize our main result for the dimensionless MFRT $u(\mathbf{x})$ and the global MFRT $\overline{u}$ in the small-patch limit in the following formal proposition. We also provide the corresponding dimensional result based on the scalings (1.8).

Proposition 2. *As $\varepsilon \to 0$, the asymptotic solution to (1.9) is given in the outer region $|\mathbf{x}-\mathbf{x}_i| \gg \mathcal{O}(\varepsilon)$ for $i=1,\dots,N$ by*

(3.15)
$$u(\mathbf{x}) \sim \frac{U_0}{\varepsilon}\left[1+\varepsilon\log(\varepsilon)\frac{\overline{U}_{10}}{U_0}+\varepsilon\left(\frac{\overline{U}_{11}}{U_0}-2\pi\sum_{j=1}^{N}C_jG_s(\mathbf{x};\mathbf{x}_j)\right)\right.$$
$$\left.+\varepsilon^2\log(\varepsilon)\left(\frac{\overline{U}_2}{U_0}-2\pi\sum_{j=1}^{N}C_j\left(\frac{\mathcal{H}_jC_j}{2}+\frac{\overline{U}_{10}}{U_0}\right)G_s(\mathbf{x};\mathbf{x}_j)\right)+\mathcal{O}(\varepsilon^2)\right],$$

up to an unknown constant $\overline{U}_2$. The global MFRT $\overline{u}$, defined by (1.10), satisfies

$$\overline{u} \sim \frac{U_0}{\varepsilon}\left[1+\varepsilon\log(\varepsilon)\frac{\overline{U}_{10}}{U_0}+\varepsilon\frac{\overline{U}_{11}}{U_0}+\mathcal{O}\left(\varepsilon^2\log\varepsilon\right)\right]. \tag{3.16}$$

In (3.15) and (3.16), U_0, $\overline{U}_{10}$ and $\overline{U}_{11}$ are determined in terms of $\mathbf{C}=(C_1,\dots,C_N)^T$, $\overline{C}=\sum_{j=1}^N C_j$, $\overline{E}=\sum_{j=1}^N E_j$, and the Green's matrix $\mathcal{G}_s$, defined in (3.12), by

$$U_0=\frac{|\Omega|}{2\pi\overline{C}}, \qquad \frac{\overline{U}_{10}}{U_0}=-\frac{1}{2\overline{C}}\sum_{j=1}^{N}\mathcal{H}_jC_j^2, \qquad \frac{\overline{U}_{11}}{U_0}=\frac{2\pi}{\overline{C}}\mathbf{C}^T\mathcal{G}_s\mathbf{C}+\frac{\overline{E}}{\overline{C}}. \tag{3.17}$$

Here $\mathcal{H}_i$ is the mean curvature of $\partial\Omega$ at $\mathbf{x}=\mathbf{x}_i$, and E_j is defined in (3.14). In terms of the dimensional variables, we use (1.8) to conclude for a domain with length-scale $R_\star$, which has a well-separated collection of partially reactive Robin patches of length-scale L, that

$$\overline{U} \sim \frac{R_\star^2}{D}\overline{u}. \tag{3.18}$$

Here in calculating $\overline{u}$ in (3.16) we set $C_i=C_i\left(L\mathcal{B}_i/D\right)$ and $E_{i\pm}=E_{i\pm}\left(L\mathcal{B}_i/D\right)$ in (3.17), while evaluating the Green's matrix $\mathcal{G}_s$ at $\mathbf{x}_i=\mathbf{X}_i/R_\star$.

Although determining the constant $\overline{U}_2$ in (3.15) from a higher-order analysis is intractable analytically, our analysis does provide the spatial dependence of the MFRT, up to this unknown constant.

When Ω is the unit sphere, for which $\mathcal{H}_i=1$ and $\mathcal{Q}_i=0$ for $i=1,\dots,N$, (3.16) reduces to the result derived in Proposition 1 of [29]. This previous result of [29] extended that derived in [20] for the case of perfectly reactive circular patches on the boundary of the sphere.

For N identical locally circular patches of a common radius ε on a smooth boundary that are all perfectly absorbing, (3.15) reduces to the result given in (1.11) upon setting $C_i=2/\pi$, $E_{i-}=0$ and $E_{i+}=-2(\log 4-3/2)/\pi^2$ for $i=1,\dots,N$. In particular, for one such circular patch centered at $\mathbf{x}_1$ on the boundary, (1.11) can be written as

$$\overline{u} \sim \frac{|\Omega|}{4\varepsilon}\left[1-\frac{\varepsilon\mathcal{H}_1}{\pi}\log(4\varepsilon)+\varepsilon\left(4R_s(\mathbf{x}_1)+\frac{3\mathcal{H}_1}{2\pi}\right)+\mathcal{O}(\varepsilon^2\log\varepsilon)\right]. \tag{3.19}$$

This result for the global MFRT is equivalent to that derived in Theorem 1.2 of [47]. For one circular perfectly absorbing patch of radius ε on the boundary of the unit sphere we substitute the known values $\mathcal{H}_1 = 1$, $R_s(\mathbf{x}_1) = \frac{1}{4\pi}\log 2 - \frac{9}{20\pi}$ (see (B.31b) of Appendix B.1) for any $\mathbf{x}_1 \in \partial\Omega$. With $|\Omega| = 4\pi/3$ this reduces (3.19) to

$$\overline{u} = \frac{|\Omega|}{4\varepsilon}\left(1 - \frac{\varepsilon}{\pi}\log(2\varepsilon) - \frac{3\varepsilon}{10\pi}\right), \tag{3.20}$$

which agrees with the single patch result previously derived in Eq. (2.45) of [20]. We remark that the leading-order term of this expansion was discovered by Lord Rayleigh [4], whereas the logarithmic correction was first given in [58], but with an incorrect numerical prefactor.

Another limiting case of our main result corresponds to a perfectly absorbing elliptical-shaped patch Γ_1 of semi-axes εa_1 and εa_2 that are aligned with the directions of principal curvatures. By adapting the approach in [61], for this special case in Lemma E.1 of Appendix E we give explicit analytical formulas for the reactive capacitance $C_1 = C_1(\infty)$, the charge density $q_1(\mathbf{y};\infty)$, and the monopole coefficients $E_{1+} = E_{1+}(\infty)$ and $E_{1-} = E_{1-}(\infty)$. For this special case, (3.16) can be written as

$$\overline{u} \sim \frac{|\Omega|}{4\pi}\left[\frac{2}{C_1\varepsilon} - \mathcal{H}_1\log\varepsilon + 4\pi R_s(\mathbf{x}_1) + 2\left(\mathcal{H}_1\frac{E_{1+}}{C_1^2} + \mathcal{Q}_1\frac{E_{1-}}{C_1^2}\right) + \mathcal{O}(\varepsilon\log\varepsilon)\right], \tag{3.21a}$$

where C_1, E_{1+}/C_1^2 and E_{1-}/C_1^2 are given in (E.12), (E.10) and (E.11), respectively. The resulting expression for the global MFRT for one perfectly absorbing elliptical-shaped patch is equivalent to that derived in Eq. (1.3) of Theorem 1.3 of [47]. Moreover, in Lemma E.1 we derive the new result that the ratios $E_{1\pm}/C_1^2$ in (3.21a) can be explicitly written in terms of the semi-axes of the ellipse as

$$\frac{E_{1+}}{C_1^2} = -\frac{1}{2}\log\left(\frac{a_1+a_2}{2}\right) - \log 2 + \frac{3}{4}, \qquad \frac{E_{1-}}{C_1^2} = \frac{a_1-a_2}{4(a_1+a_2)}. \tag{3.21b}$$

3.1. Principal Eigenvalue of the Laplacian. By using the result in (3.16) and (3.17) for the MFRT $\overline{u}$, we now briefly outline the derivation of the asymptotic result for the principal eigenvalue λ_0 of the Laplacian for

$$\Delta_{\mathbf{x}}\phi + \lambda\phi = 0, \quad \mathbf{x}\in\Omega; \qquad \int_\Omega \phi^2\, d\mathbf{x} = 1, \tag{3.22a}$$

$$\varepsilon\partial_n\phi + b_i\phi = 0, \quad \mathbf{x}\in\partial\Omega_i^\varepsilon, \quad i = 1,\dots,N, \tag{3.22b}$$

$$\partial_n\phi = 0, \quad \mathbf{x}\in\partial\Omega_r = \partial\Omega\setminus\cup_{i=1}^N\partial\Omega_i^\varepsilon. \tag{3.22c}$$

In Sec. 4.5 of [29] a three-term expansion of λ_0 was derived for (3.22) when Ω is a sphere, which extended the previous result in [20] that was limited to perfectly reactive circular patches on the boundary of the sphere.

To derive the corresponding result for λ_0 for a general domain, we simply proceed as in Sec. 4.5 of [29] to relate λ_0 to $\overline{u}$, through an eigenfunction expansion of u in terms of the eigenpairs of (3.22), which yields that

$$\lambda_0 \sim \frac{1+\mathcal{O}(\varepsilon^2)}{\overline{u} - \mathcal{O}(\varepsilon^2)}. \tag{3.23}$$

Upon substituting the expansion (3.16) for $\overline{u}$ in (3.23) we observe that we can neglect the $\mathcal{O}(\varepsilon^2)$ terms in (3.23), to obtain

$$\lambda_0 \sim \frac{\varepsilon}{U_0}\left(1 + \varepsilon\log\varepsilon\frac{\overline{U}_{10}}{U_0} + \varepsilon\frac{\overline{U}_{11}}{U_0} + \mathcal{O}(\varepsilon^2\log\varepsilon)\right)^{-1}. \tag{3.24}$$

Then, by using $(1+y)^{-1} \sim 1 - y + \mathcal{O}(y^2)$ for $|y| \ll 1$ together with (3.17) we obtain that the principal eigenvalue λ_0 of (3.22) has the three-term asymptotics

$$\lambda_0|\Omega| \sim 2\pi\varepsilon\overline{C} + \pi\varepsilon^2 \log\varepsilon \sum_{j=1}^{N} \mathcal{H}_j C_j^2 - 2\pi\varepsilon^2 \left(2\pi \mathbf{C}^T \mathcal{G}_s \mathbf{C} + \overline{E}\right) + \mathcal{O}(\varepsilon^3 \log^2 \varepsilon)\,, \tag{3.25}$$

where $\overline{C} = \sum_{j=1}^{N} C_j$, $\overline{E} = \sum_{j=1}^{N} (\mathcal{H}_j E_{j+} + \mathcal{Q}_j E_{j-})$, while $\mathcal{G}_s$ is the surface Neumann Green's matrix defined in (3.12). When Ω is the unit sphere, where $\mathcal{H}_j = 1$ and $\mathcal{Q}_j = 0$ for $j = 1, \ldots, N$, (3.25) is equivalent to that derived in [29] upon noting the different definition of the common diagonal elements of the Green's matrix that was compensated for by the modified logarithmic gauge $\log(\varepsilon/2)$.

4. Numerical validation and optimization results. In this section, we describe our methods for the boundary integral solution of the Berg-Purcell (1.4) and narrow escape problems (1.9). Using these numerical methods, we validate the main results in Propositions 1 and 2, and demonstrate that these expansions exhibit the predicted error as $\varepsilon \to 0$. Through some simple examples, we explore how geometry and patch configurations combine to modulate the key quantities of capacitance and GMFRT.

4.1. Boundary integral method. Previous numerical methods relied on the Neumann-to-Dirichlet map to represent the solution of (1.4) and (1.9) followed by spectral expansion of the surface potential and flux on each patch [8, 35], as well as other spectral methods [24] and Monte Carlo simulations [31, 49]. In our numerical treatment, we use a standard boundary integral equation approach to solve both the Berg-Purcell problem (1.4) and narrow escape problem (1.9). In order to make the presentation as self-contained as possible, we briefly sketch the procedure. We first describe the approach for solving (1.4) before outlining the modifications required for (1.9). In the following we will always take $\partial\Omega$ to be smooth and $\mathbf{n}$ to denote its outward pointing normal (note that this is the opposite of the convention used in (1.4) but is more standard in the boundary integral literature).

We begin by introducing the ansatz,

$$u(\mathbf{x}) = 1 + \int_{\partial\Omega} \frac{1}{4\pi|\mathbf{x}-\mathbf{y}|}\sigma(\mathbf{y})\, ds(\mathbf{y}), \quad \mathbf{x} \in \mathbb{R}^3 \setminus \Omega\,, \tag{4.1}$$

where σ is a yet to be determined boundary density. Noting that $\Delta_{\mathbf{x}}[4\pi|\mathbf{x}-\mathbf{y}|]^{-1} = -\delta(\mathbf{x}-\mathbf{y})$, it follows immediately that the $u(\mathbf{x})$ defined in (4.1) trivially satisfies (1.4a) and (1.4d), provided $\sigma \in L^1(\partial\Omega)$. All that remains is to satisfy the boundary conditions on $\partial\Omega$. To that end, we note that for $\sigma \in L^2(\partial\Omega)$ the normal trace of the integral exists in an $L^2(\partial\Omega)$ sense [36], and

$$\int_{\partial\Omega} \left| \mathbf{n}(\mathbf{x}) \cdot \nabla_{\mathbf{x}} \mathcal{S}[\sigma](\mathbf{x} \pm h\mathbf{n}(\mathbf{x})) - S'[\sigma](\mathbf{x}) \pm \frac{1}{2}\sigma(\mathbf{x}) \right|^2 ds(\mathbf{x}) \to 0\,, \tag{4.2}$$

as $h \to 0^+$, where we have defined

$$\mathcal{S}[\sigma](\mathbf{x}) \equiv \int_{\partial\Omega} \frac{1}{4\pi|\mathbf{x}-\mathbf{y}|}\sigma(\mathbf{y})\, ds(\mathbf{y})\,, \quad \mathbf{x} \notin \partial\Omega\,,$$

and

$$S'[\sigma](\mathbf{x}) \equiv \int_{\partial\Omega} \frac{(\mathbf{x}-\mathbf{y}) \cdot \mathbf{n}(\mathbf{x})}{4\pi|\mathbf{x}-\mathbf{y}|^3}\sigma(\mathbf{y})\, ds(\mathbf{y})\,, \quad \mathbf{x} \in \partial\Omega\,.$$

We also let S denote the trace of $\mathcal{S}$, i.e. $S[\sigma](\mathbf{x}) = \lim_{h\to 0} \mathcal{S}[\sigma](\mathbf{x}+h\mathbf{n}(\mathbf{x}))$ for $\mathbf{x} \in \partial\Omega$.

Inserting our ansatz into the boundary conditions (1.4b-1.4c) yields the following integral equation

$$\frac{1}{2}\sigma(\mathbf{x}) - S'[\sigma](\mathbf{x}) + \sum_{i=1}^{N} \frac{b_i}{\varepsilon}\chi_{\partial\Omega_i^\varepsilon}(\mathbf{x})S[\sigma](\mathbf{x}) = -\sum_{i=1}^{N} \frac{b_i}{\varepsilon}\chi_{\partial\Omega_i^\varepsilon}(\mathbf{x})\,, \quad \mathbf{x} \in \partial\Omega\,, \tag{4.3}$$

where $\chi_{\partial\Omega_i^\varepsilon}$ denotes the indicator function of $\partial\Omega_i^\varepsilon$. Standard arguments [37] give that S and S' are compact from $L^2(\partial\Omega)$ to itself which in turn implies that the above equation is a Fredholm second-kind integral equation. Uniqueness of (4.3) follows by standard arguments, see [37], for example. For the given right-hand side, standard bootstrapping arguments give that σ is C^∞ away from the boundaries of the patches $\partial\Omega_i^\varepsilon$. Near the patch boundaries σ is discontinuous, and the leading singular behavior beyond the jump scales like $d\log d$, where d is the distance to the patch boundary.

Conveniently, we note that the capacitance C_{T} can be computed directly from σ as

$$C_{\mathrm{T}} = -\frac{1}{4\pi}\int_{\partial\Omega} \sigma(\mathbf{x})\,\mathrm{d}\mathbf{x}\,.$$

We discretize (4.3) using the package `fmm3dbie` [3], which uses the collocation scheme described in [32]. Since σ is discontinuous across the patch boundaries, we require meshes with patch boundaries coinciding with edges of mesh elements. We construct such meshes as follows. We first compute a first-order triangular mesh using `distmesh` [48], modified to constrain a ring of vertices to lie on each patch boundary, so that every patch boundary is approximated by a closed polygon of mesh edges. Each triangle is then upgraded to a curvilinear mesh element by placing Vioreanu–Rokhlin nodes [63, 65] on the flat triangle and projecting them onto $\partial\Omega$ by a Newton iteration along the gradient of the level-set function defining Ω. For triangles with an edge or vertex on a patch boundary, the chart is blended with a parameterization of the bounding circle, so that curvilinear mesh element boundaries lie on the patch boundaries to the full order of the interpolation. Finally, mesh elements may be graded dyadically toward the patch boundaries to resolve singularities in the density.

Solving (1.9) proceeds in an almost identical way, replacing the ansatz (4.1) with

$$u(\mathbf{x}) = -\frac{|\mathbf{x}|^2}{6} + \mathcal{S}[\sigma](\mathbf{x})\,, \quad \mathbf{x} \in \Omega\,.$$

The volume integral (1.10) can be reduced to a boundary integral using integration by parts. For further details, see [16, 42].

Numerical experiments suggest our method is able to resolve the solutions of (1.4) and (1.9) with numerous well separated small patches. With modest grading, we obtain relative errors in the density of at most 10^{-4} which is sufficient for verification of the asymptotic results.

4.2. Calculation of capacitance and monopole constants. For validation of the asymptotic expansions in the case of circular patches, we need to calculate the capacitance C and monopole coefficient E_+. For a disk-shaped patch Γ of radius a with reactivity b, the capacitance is given by [31, Eqn. (2.6)],

$$C(b) = a\mathcal{C}(ab)\,, \quad \text{where} \quad \mathcal{C}(z) = \frac{z}{2\pi}\sum_{k=0}^{\infty} \frac{\mu_k d_k^2}{\mu_k + z}\,. \tag{4.4}$$

In the formulation (4.4), the pairs (μ_k, d_k) are determined by the exterior Steklov eigenvalue problem for the unit disk $\Gamma = \{(y_1, y_2) \in \mathbb{R}^2 \mid y_1^2 + y_2^2 \leq 1\}$. This is defined [31, Eqn. B1] by

$$\Delta\Psi_k = 0, \quad \mathbf{y} \in \mathbb{R}^3_+; \tag{4.5a}$$

$$\partial_n \Psi_k = \mu_k \Psi_k, \quad y_3 = 0, \ (y_1, y_2) \in \Gamma; \tag{4.5b}$$

$$\partial_n \Psi_k = 0, \quad y_3 = 0, \quad (y_1, y_2) \notin \Gamma; \tag{4.5c}$$

$$\Psi_k(\mathbf{y}) = \mathcal{O}(1/|\mathbf{y}|), \quad \text{as} \quad |\mathbf{y}| \to \infty. \tag{4.5d}$$

This problem (see [29]) admits infinitely many nontrivial solutions $\{\mu_k, \Psi_k\}_{k=0}^{\infty}$ such that the eigenvalues form an ordered sequence

$$0 = \mu_0 < \mu_1 \leq \mu_2 \leq \ldots$$

while the restriction of the eigenfunctions $\Psi_k|_\Gamma$ form a complete orthonormal basis $L^2(\Gamma)$ (see [2, 13] for more details). The complementary values d_k are defined by

$$d_k = \int_\Gamma \Psi_k(\mathbf{y}) d\mathbf{y}.$$

Algorithms to numerically compute the parameters μ_k and d_k were provided in [27, 31]. Extensions to patches of general shape were developed in [28].

The monopole coefficient E_+ was determined in [31, Appendix E] to be

$$E_+(\kappa) = -\frac{C^2}{2} \log a + a^2 \mathcal{E}(a\kappa), \tag{4.6a}$$

where the function $\mathcal{E}(z)$ is defined by

$$\mathcal{E}(z) = 2 \int_0^1 \frac{1}{r} \left(\int_0^r r' a q(ar'; z/a) dr' \right)^2 dr \,, \tag{4.6b}$$

where $q(\mathbf{y}; \kappa)$ is the charge density defined in (2.12). By representing the charge density $q(\mathbf{y}; \kappa)$ in terms of the Steklov problem (4.5), the calculation of (4.6b) is reduced to quadrature.

4.3. Convergence of the MFRT for prolate spheroids. To validate the asymptotic analysis, we consider a prolate spherical geometry with boundary given by

$$\partial\Omega = \left\{ (x, y, z) \in \mathbb{R}^3 \;\middle|\; \frac{x^2 + y^2}{a_e^2} + \frac{z^2}{c_e^2} = 1 \right\}, \tag{4.7}$$

where $c_e > a_e > 0$. The prolate spheroidal coordinate system for $\mathbf{x} = (x, y, z)^T$ is

$$x = f\sqrt{(\zeta^2 - 1)(1 - \chi^2)} \cos\phi \,, \quad y = f\sqrt{(\zeta^2 - 1)(1 - \chi^2)} \sin\phi \,, \quad z = f\, \zeta\, \chi \,, \tag{4.8}$$

where $f = \sqrt{c_e^2 - a_e^2}$ is half the inter-focal distance. Here $\zeta \in [1, \infty)$ is the radial variable, $\chi \in [-1, 1]$ is the elevation coordinate and $\phi \in [0, 2\pi)$ is the azimuthal variable. The surface of the prolate spheroid is defined by points $\mathbf{x} = (\chi, \phi, \zeta_b)$ where $\zeta_b = c_e/f$. In our experiments below we fill fix $a_e = 1$ and $c_e = \sqrt{2}$ so that $f = 1$ and $\zeta_b = \sqrt{2}$.

To apply (3.19) for the prolate spheroid case, we note that the mean curvature of this surface at the point (χ, ϕ, ζ_b) is

$$\mathcal{H} = \frac{\zeta_b(2\zeta_b^2 - \chi^2 - 1)}{2(\zeta_b^2 - 1)^{\frac{1}{2}}(\zeta_b^2 - \chi^2)^{\frac{3}{2}}}\,. \tag{4.9}$$

The evaluation of the regular part $R_s(\mathbf{x}_1)$ satisfying (3.3) is performed numerically using the methods described in [42]. The values of $\mathcal{H}$ and R_s as the elevation coordinate $\chi \in [-1, 1]$ is varied are shown in Fig. 4.1(a).

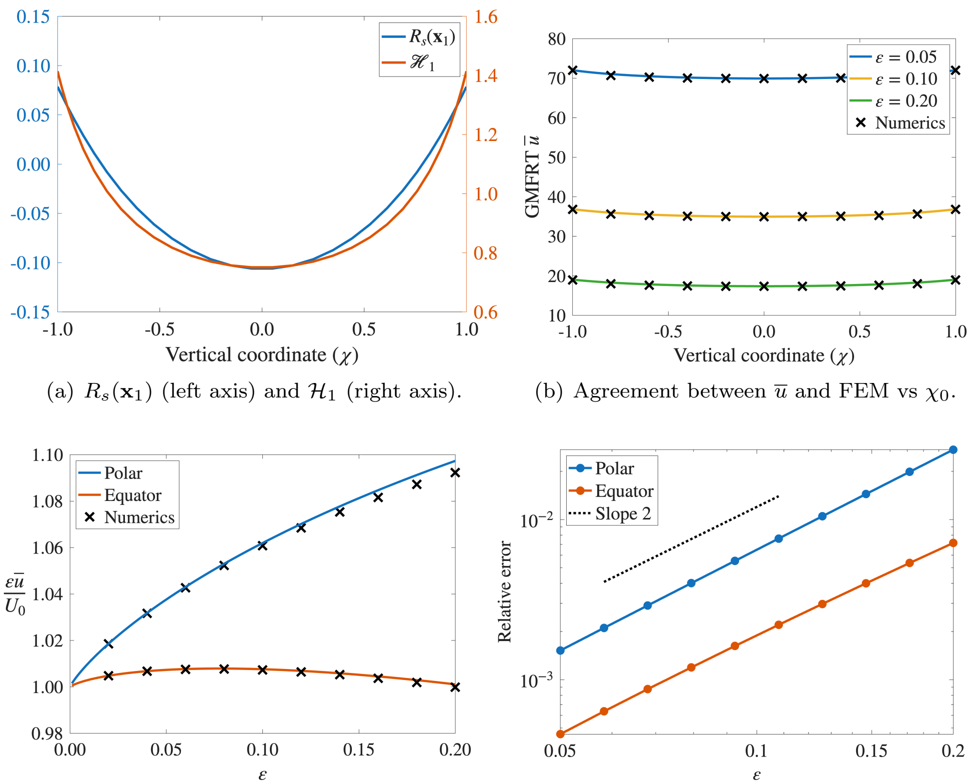

(a) $R_s(\mathbf{x}_1)$ (left axis) and $\mathcal{H}_1$ (right axis).

(b) Agreement between $\overline{u}$ and FEM vs χ_0.

(c) Rescaled GMFRT $\varepsilon\overline{u}/U_0$ for a single polar and equator patch vs. ε.

(d) Relative error in $\overline{u}$ against ε.

Fig. 4.1. *Validation of the GMFRT calculation for a single perfectly absorbing circular patch centered at $\mathbf{x}_1 = (\chi, \phi, \zeta_b)$. Panel (a): The regular part $R_s(\mathbf{x}_1)$ and $\mathcal{H}_1$ versus χ. Panel (b): Comparison of asymptotics (3.19) and the numerical solution (FEM) as the patch center moves from the south pole ($\chi = -1$) to the north pole ($\chi = 1$) for various values of ε. Panel (c): Comparison between numerical solution and asymptotics for a single patch centered at the north pole and the equator. Panel (d): Convergence of the relative errors (4.10) between the asymptotic approximation and numerical solution as $\varepsilon \to 0$ with line of slope 2 overlaid.*

One of our primary observations from Fig. 4.1(b)-4.1(c) is that the GMFRT $\overline{u}$ is minimized when the boundary patch is placed at the equator. This location corresponds to the global minimum of both $R_s(\mathbf{x}_1)$ and $\mathcal{H}_1$ as seen in Fig. 4.1(a) and, as predicted by our asymptotic result (3.19), should correspond to the location where $\overline{u}$ is minimized when $\varepsilon \ll 1$. This expected behavior is confirmed in Fig. 4.1(b) where we show, for several values of ε, that the minimizer occurs for a patch centered at the equator. Conversely, the global MFRT $\overline{u}$ is maximized when the single patch is centered at a pole as shown in Fig. 4.1(c). In Fig. 4.1(d), we calculate the relative error

$$\mathcal{E}_{\text{rel}} = \left| \frac{\overline{u}_{\text{num}} - \overline{u}_{\text{asy}}}{\overline{u}_{\text{num}}} \right| , \tag{4.10}$$

where $\overline{u}_{\text{num}}$ is the GMFRT from the numerical solution (see §4.1) and $\overline{u}_{\text{asy}}$ is the asymptotic result (3.19). This result is consistent with the predicted behavior of the relative error $\mathcal{O}(\varepsilon^2 \log \varepsilon)$ as $\varepsilon \to 0$.

4.4. Validation of the Berg-Purcell problem. In this subsection we consider several special cases of our result in Proposition 1 for the Berg-Purcell problem. We again use the prolate spheroid described by (4.7).

A single perfectly absorbing patch. We first consider perfectly absorbing circular patches of a common radius ε so that $C_i = 2/\pi$ and $E_{i+} = -2\big(\log 4 - \frac{3}{2}\big)\pi^2$. In this case, (2.46) for C_T was given previously in (1.5). For a single patch ($N = 1$), (1.5) becomes

$$\frac{1}{C_T} \sim \frac{\pi}{\varepsilon} \left[1 - \frac{\varepsilon \mathcal{H}_1}{\pi} \log(4\varepsilon) + 4\varepsilon \left(R_e(\mathbf{x}_1) + \frac{3\mathcal{H}_1}{8\pi} \right) + \mathcal{O}(\varepsilon^2 \log \varepsilon) \right] , \tag{4.11}$$

where the regular part of the exterior surface Neumann Green's function $R_e(\mathbf{x}_1)$ was defined in (2.18b). This expression shows how C_T depends on local geometric factors through the mean curvature $\mathcal{H}_1$ and the global contribution $R_e(\mathbf{x}_1)$. When Ω is the unit sphere, $\mathcal{H}_1 = -1$ and $R_e = -\log(2)/(4\pi)$ for any $\mathbf{x}_1 \in \partial\Omega$ (see (B.30b) of Appendix B.1), so that (4.11) becomes

$$\frac{1}{C_T} \sim \frac{\pi}{\varepsilon} \left[1 + \frac{\varepsilon}{\pi} \log(2\varepsilon) - \frac{3\varepsilon}{2\pi} + \mathcal{O}(\varepsilon^2 \log \varepsilon) \right] , \tag{4.12}$$

which is in agreement with Eq. (3.39) of [44].

Based on our sign convention for $\mathcal{H}$, to apply (4.11) for a spheroidal geometry one needs only to replace $\mathcal{H}$ in (4.9) with $-\mathcal{H}$.

With this minor change, in Fig. 4.2(a) we plot both $\mathcal{H}_1$ and $R_e(\mathbf{x}_1)$ on the spheroid with semi-axes $(a_e, a_e, c_e) = (1, 1, \sqrt{2})$. The value of $R_e(\mathbf{x}_1)$ has been obtained numerically from a boundary integral method described [42]. We observe that both these quantities attain their global minimum at the poles of the spheroid indicating that a single patch placed at either $\mathbf{x} = (0, 0, \pm\sqrt{2})$ will generate the largest capacitance C_T.

Two Robin patches. As a further test of (1.5), we consider two circular patches of common radius ε and reactivity $b = 1$. We calculate that

$$C = 0.271628 , \qquad E_+ = 0.008360 , \qquad E_- = 0 . \tag{4.13a}$$

In this case, the formula (1.5) for C_T reduces to

$$\frac{1}{C_T} \sim \frac{2}{NC\varepsilon} \left[1 - \frac{C\bar{\mathcal{H}}}{2N} \varepsilon \log \varepsilon + \varepsilon \Big(2\pi C p_e(\mathbf{x}_1, \mathbf{x}_2) + \frac{\bar{\mathcal{H}} E_+}{NC} \Big) \right] , \tag{4.13b}$$

where $\bar{\mathcal{H}} = \mathcal{H}_1 + \mathcal{H}_2$ and the interaction term is given by

$$p_e(\mathbf{x}_1, \mathbf{x}_2) = 2G_e(\mathbf{x}_1; \mathbf{x}_2) + R_e(\mathbf{x}_1) + R_e(\mathbf{x}_2) . \tag{4.13c}$$

We consider patches that are aligned symmetrically about either the poles or the equator (see Figs. 4.2(a)-4.2(b)). For this case, we numerically calculate the regular parts and interaction terms to be

$$
\begin{aligned}
R_e(\mathbf{x}_{1,2}) &= -0.03232 \quad (\text{Polar case})\,, \qquad & R_e(\mathbf{x}_{1,2}) &= -0.05982 \quad (\text{Equatorial case})\,;\\
G_e(\mathbf{x}_1;\mathbf{x}_2) &= 0.01992 \quad (\text{Polar case})\,, \qquad & G_e(\mathbf{x}_1;\mathbf{x}_2) &= 0.02269 \quad (\text{Equatorial case})\,.
\end{aligned}
$$

As a function of ε, in Fig. 4.2(d) we observe clear agreement between our asymptotic formula (1.5) and numerical simulations. We observe as expected that patches centered at the polar regions provide a larger capacitance. As a further validation of our asymptotic result (1.5), we calculate the relative error between the numerically computed capacitance (C_T^{num}) and the asymptotic approximation (C_T) defined by

$$
\mathcal{E}_{\text{rel}} = \frac{|C_T - C_T^{\text{num}}|}{C_T^{\text{num}}}. \tag{4.14}
$$

In Fig. 4.2(e) we plot $\mathcal{E}_{\text{rel}}$ for a range of $\varepsilon \to 0$ and observe the predicted decay rate.

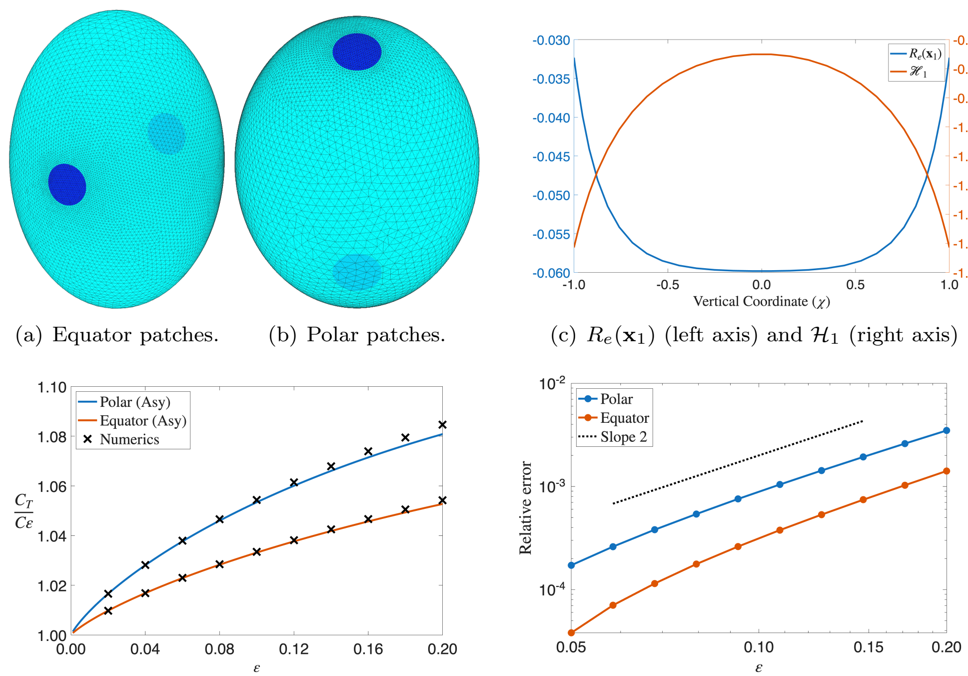

(a) Equator patches. (b) Polar patches. (c) $R_e(\mathbf{x}_1)$ (left axis) and $\mathcal{H}_1$ (right axis)

(d) Rescaled C_T against ε. (e) Relative error in C_T against ε.

FIG. 4.2. *Berg-Purcell problem for the spheroid with semi-axes* $(a_e, a_e, c_e) = (1, 1, \sqrt{2})$. *The capacitance of a configuration with two patches of common reactivity* $b = 1$ *and radius* ε *situated either on the equator (panel (a)) or on the poles (panel (b)) is calculated. Panel (c): regular part* $R_e(\mathbf{x}_1)$ *of the surface Neumann Green's function computed by the numerical method of [42]. Panel (d): comparison between our asymptotic result (1.5) and numerical computations for shrinking patch radius* ε*. The polar configuration provides the larger capacitance. Panel (e): the relative error* (4.14) *in* C_T *decays according to the rate predicted in* (1.5).

4.5. Comparison with points on the Fibonacci spiral. In this example, we consider the Berg-Purcell formula for the case of N identical patches arranged on

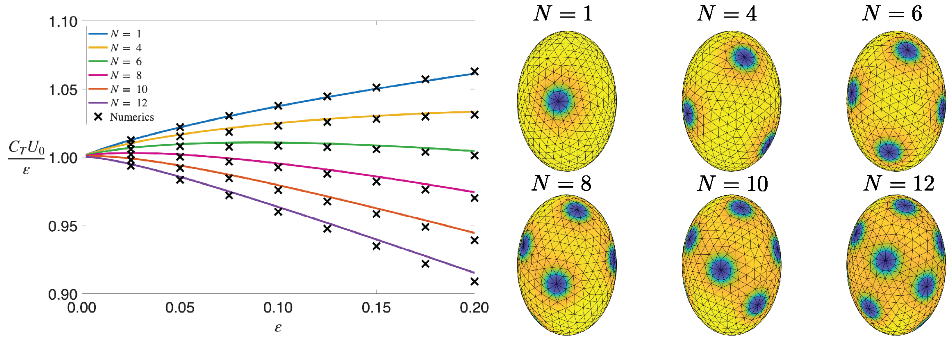

FIG. 4.3. *Solution of the Berg-Purcell problem (1.4) with N identical Robin patches of radius ε and reactivity $b = 1$ on the spheroid $(a_e, a_e, c_e) = (1, 1, \sqrt{2})$. For a range of patches centered at the Fibonacci spiral points (4.16), we plot the rescaled capacitance $C_T U_0/\varepsilon$ as $\varepsilon \to 0$ from asymptotic expansions (2.46) and full numerical solution (black crosses). The surface solution $u|_{\partial\Omega}$ of (1.4) obtained from the boundary integral method (cf. Sec. 4.1) is shown together with the mesh which resolves the solution near each patch.*

nodes of the Fibonacci spiral points. The Fibonacci spiral points are a simple and highly optimized set of points for generating near-uniform coverings of the sphere [23, 62].

The N patch centers are placed at the nodes of a Fibonacci (spherical) spiral, which gives a near-uniform, well-separated configuration for any N. With the golden angle $\gamma_g \equiv \pi\,(3 - \sqrt{5})$, define for $k = 0, 1, \ldots, N-1$

$$\chi_k = 1 - \frac{2k+1}{N} \in (-1, 1), \qquad \phi_k = k\,\gamma_g \pmod{2\pi}, \tag{4.15}$$

where χ_k is the elevation and ϕ_k the azimuth. The half-integer offset $(2k+1)/N$ spaces the nodes equally in χ (hence by equal area in latitude) and keeps them strictly off the poles, while the golden-angle increment γ_g distributes the azimuths quasi-uniformly. The corresponding centers on the spheroidal boundary $\partial\Omega$ with semi-axes $(a_e, a_e, c_e) = (1, 1, \sqrt{2})$ are

$$\mathbf{x}_k = \Big(a\sqrt{1-\chi_k^2}\,\cos\phi_k,\;\; a\sqrt{1-\chi_k^2}\,\sin\phi_k,\;\; c\,\chi_k \Big), \qquad k = 0, \ldots, N-1. \tag{4.16}$$

In Fig. 4.3, we plot the rescaled capacita nce $(C_T U_0)/\varepsilon$ against ε for various values of N. The solid lines are the asymptotic approximation (2.46) where the entries of the Green's matrix are constructed using the methods in [42]. The corresponding rescaled capacitance determined from the boundary integral method (see Sec. 4.1) are shown with black crosses. The close agreement between these curves in the case of many patch numbers serves as a highly non-trivial validation of our solution methodologies applied to the problem (1.4). This encompasses our high-order asymptotic expansions (Propositions 1 and 2), numerical computation of the path-dependent singular Green's function (2.18) and our boundary integral method (§4.1). In Fig. 4.3, we plot the solution $u|_{\partial\Omega}$ of (1.4) for $\varepsilon = 0.2$. We note that the surface is well resolved by the mesh which conforms to each of the N boundary patches.

4.6. Optimization of C_T for a perturbation of a sphere. For the Berg-Purcell problem, we now investigate how to optimize configurations of patches for domains that are small perturbations of the unit sphere. More specifically, we consider N partially reactive circular boundary patches of a common radius ε and reactivity b. Upon setting $C_i = C(b)$, $E_{i+} = E_+(b)$ and $E_{i-} = 0$ in (2.46), we obtain that

$$\frac{1}{C_{\mathrm{T}}} = \frac{2}{NC\varepsilon}\left[1 + \frac{\varepsilon C}{2N}\left(4\pi p_e - \overline{\mathcal{H}}\log\varepsilon + \overline{\mathcal{H}}\frac{2E_+}{C^2}\right) + \mathcal{O}(\varepsilon^2\log\varepsilon)\right], \tag{4.17}$$

where $p_e = p_e(\mathbf{x}_1, \ldots, \mathbf{x}_N)$ is the discrete inter-patch interaction energy defined in (1.5c), and $\overline{\mathcal{H}}$ is the sum of mean curvatures (see (1.5b)). By recalling (2.34) and (2.12) for E_+ and C, we write (4.17), after neglecting the $\mathcal{O}(\varepsilon^2\log\varepsilon)$ error term, as

$$\frac{1}{C_{\mathrm{T}}} \sim \frac{2}{NC\varepsilon} + \frac{1}{N^2}\mathcal{P}(\mathbf{x}_1, \ldots, \mathbf{x}_N; b)\,, \tag{4.18a}$$

where the objective function $\mathcal{P} = \mathcal{P}(\mathbf{x}_1, \ldots, \mathbf{x}_N; b)$ is defined by

$$\mathcal{P} \equiv (-\log\varepsilon + \gamma(b))\,\overline{\mathcal{H}} + 4\pi\sum_{i=1}^{N}\left[R_e(\mathbf{x}_i) + \sum_{\substack{j=1\\ j\neq i}}^{N} G_e(\mathbf{x}_j; \mathbf{x}_i)\right]. \tag{4.18b}$$

Here $\gamma(b)$, depending on the common patch reactivity b, is defined by

$$\gamma(b) \equiv \frac{2E_+}{C^2} = -\left(\frac{\int_{\mathbb{D}}\int_{\mathbb{D}} q(|\mathbf{y}|; b)q(|\mathbf{y}'|; b)\,\log|\mathbf{y}-\mathbf{y}'|\,d\mathbf{y}\,d\mathbf{y}'}{\left(\int_{\mathbb{D}} q(|\mathbf{y}|; b)\,d\mathbf{y}\right)^2}\right), \tag{4.18c}$$

where $\mathbb{D}$ is the unit disk centered at the origin. By recalling the limiting asymptotics for C and E_+ in (2.14) and (2.37), respectively, we have

$$\gamma(b) \sim \frac{1}{4}\,, \quad \text{as} \quad b \to 0\,; \qquad \gamma(b) \sim \frac{3}{2} - \log 4 \approx 0.114\,, \quad \text{as} \quad b \to \infty\,. \tag{4.19a}$$

The numerical evaluation of $\gamma(b)$ is discussed in §4.2. A heuristic approximation of $\gamma(b)$ for all $b > 0$ is given by the monotonically decreasing function [29]

$$\gamma(b) \approx \frac{3}{2} - \log 4 + \frac{2}{\frac{1}{\log 2 - 5/8} + 5.17\,b^{0.81}}\,. \tag{4.19b}$$

This leads to the formulation of a *discrete optimization problem.*
Optimization: For a given domain Ω with smooth and closed boundary $\partial\Omega$, let us fix the number $N > 1$ of circular boundary patches, their common radius $\varepsilon \ll 1$ and reactivity $b > 0$. We seek to determine the configuration $\{\mathbf{x}_1, \ldots, \mathbf{x}_N\} \subset \partial\Omega$ of the centers of the patches that minimizes $\mathcal{P}$ in (4.18b). Such an optimal patch arrangement maximizes the capacitance C_T.

From (4.18b), the optimal arrangement depends on ε, the patch reactivity through $\gamma(b)$, and the domain shape via the Green's function G_e and its regular part R_e. Since $\gamma(b) > 0$, but is monotone decreasing in b, partially reactive patches increase the influence of the mean curvature in the discrete energy, but to a lesser extent as b increases. The curvature term and the inter-patch interaction effect in (4.18b) will balance in an optimum arrangement since $G_e(\mathbf{x}_i; \mathbf{x}_j) \to +\infty$ as $\mathbf{x}_i \to \mathbf{x}_j$, which prevents the optimally located patches from concentrating too close to minima of the mean curvature.

We now apply (4.18b) to a domain Ω that is a perturbation of the unit sphere whose boundary is $r = 1 + \mu F(\phi, \theta)$, where $\mu \ll 1$, $r = |\mathbf{x}|$, and with $0 \leq \phi < 2\pi$ and $0 \leq \theta \leq \pi$ being the azimuthal and polar angles, respectively. For this geometry, the mean curvature of $\partial\Omega$ for $\mu \ll 1$ is (noting our sign convention)

$$\mathcal{H} \sim -1 + \frac{\mu}{2}\left(\Delta_{S^2} F + 2F\right) \quad \text{with} \quad \Delta_{S^2} F \equiv \frac{1}{\sin\theta}\left(\sin\theta\, \partial_\theta F\right)_\theta + \frac{1}{\sin^2\theta}\partial_{\phi\phi} F\,. \tag{4.20}$$

We will consider two cases. **Case I:** For a perturbed sphere bulging out at the poles, we take $F = \cos^2\theta$, which vanishes on the equator $\theta = \pi/2$. In **Case II** we take $F = \sin^2\theta$, so that the perturbed sphere instead bulges out on the equator. From (4.20) we calculate for these two cases that

$$\mathcal{H} = -1 + \mu\tilde{\mathcal{H}}(\theta)\,, \quad \text{where} \quad \tilde{\mathcal{H}}(\theta) \equiv \begin{cases} 1 - 2\cos^2\theta\,, & \text{Case I;} \\ 2\cos^2\theta\,, & \text{Case II.} \end{cases} \tag{4.21}$$

For our two choices of boundary deformations, the centers of the patches on the boundary of the perturbed sphere are labeled as $\mathbf{x}_j = (1 + \mu F(\theta_j))\mathbf{x}_{j0}$ where $\mathbf{x}_{j0} \equiv (\cos\phi_j \sin\theta_j, \sin\phi_j \sin\theta_j, \cos\theta_j)^T$ for $j = 1, \ldots, N$. We will choose the size of the boundary deformation to satisfy $\mu = \mathcal{O}(-1/\log\varepsilon)$ so that the curvature and inter-patch interaction terms in (4.18b) are of the same order. More specifically, we will set $\mu = -\beta/\log\varepsilon$, where $\beta > 0$ is independent of ε. Upon substituting (4.21) into (4.18b) we obtain with this choice of μ that

$$\begin{aligned} \mathcal{P} &\equiv N\left(-\log\varepsilon + \gamma(b)\right) \\ &\quad + \frac{\beta}{2}\sum_{j=1}^{N}\tilde{\mathcal{H}}(\theta_j) + 4\pi\sum_{i=1}^{N}\left[R_e(\mathbf{x}_{i0}) + \sum_{\substack{j=1\\ j\neq i}}^{N} G_e(\mathbf{x}_{j0};\mathbf{x}_{i0})\right] + \mathcal{O}\left(\frac{-1}{\log\varepsilon}\right). \end{aligned} \tag{4.22}$$

Finally, we explicitly evaluate the surface Neumann Green's function in (4.22) on the unit sphere using (B.30b) of Appendix B.1. In this way, we conclude that

$$\mathcal{P}(\mathbf{x}_1, \ldots, \mathbf{x}_N) \sim N\left(\log\left(\frac{\varepsilon}{2}\right) - \gamma(b)\right) + \mathcal{P}_0(\mathbf{x}_{10}, \ldots, \mathbf{x}_{N0})\,, \tag{4.23a}$$

where, with the two choices of $\tilde{\mathcal{H}}(\theta_j)$ given in (4.21), we have

$$\mathcal{P}_0 \equiv \frac{\beta}{2}\sum_{j=1}^{N}\tilde{\mathcal{H}}(\theta_j) + \sum_{i=1}^{N}\sum_{j=i+1}^{N}\left(\frac{4}{|\mathbf{x}_{i0} - \mathbf{x}_{j0}|} - 2\log\left(1 + \frac{2}{|\mathbf{x}_{i0} - \mathbf{x}_{j0}|}\right)\right). \tag{4.23b}$$

In Figs. 4.4-4.5 we present results obtained from the MATLAB optimization routine `fmincon` called with the `interior-point` algorithm. The objective function is given by $\mathcal{P}_0$ defined in (4.23b) with the two choices of $\tilde{\mathcal{H}}(\theta_j)$ described in (4.21). We consider $N = 1, \ldots, 12$ patches and initialize the algorithm at points with angular coordinates chosen with uniform random distribution in $(\phi, \theta) \in [0, 2\pi) \times [0, \pi)$.

In case I where the choice $F = \cos^2\theta$ yields an elongated domain, we see in Fig. 4.4 that the optimizing configurations have a tendency to cluster patches around the poles of the domain. In case II the choice $F = \sin^2\theta$ results in a domain which is more bulged in the equatorial region. In Fig. 4.5, we observe a trend for the optimizing patch locations to congregate around the equator. For $N = 1, 2, 3, 4$, we observe that the optimizers are coplanar on $z = 0$. For $N \geq 5$, the optimizing configurations occupy patch centers with $z \neq 0$. Similar geometric bifurcations have been observed in related optimization problems for narrow capture in two [18] and three dimensions [42].

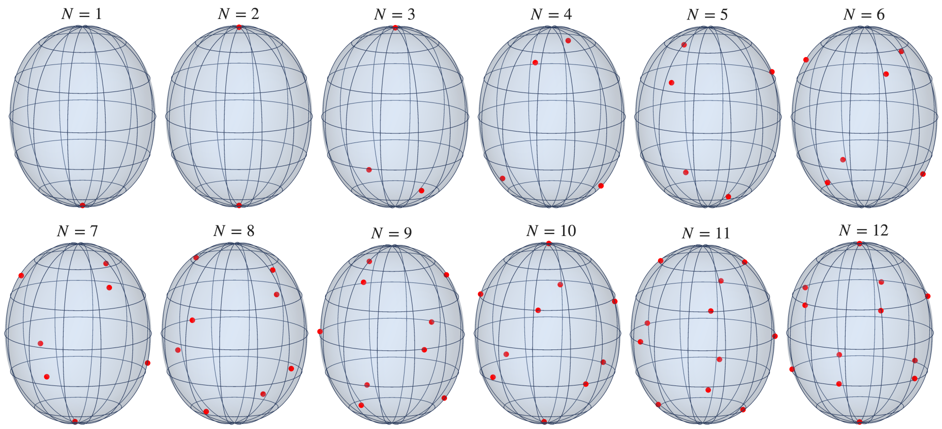

FIG. 4.4. *Optimization of the capacitance C_T for $N = 1, \ldots, 12$ surface patches in the Berg-Purcell problem, Case I. We consider a nearly spherical boundary defined by radial coordinate $r = 1 + \mu \cos^2\theta$ for $\mu = 0.25$. For $N = 1, \ldots, 12$ points, we numerically calculate the points $\{\mathbf{x}_j\}_{j=1}^N$ that minimize the discrete energy* (4.23).

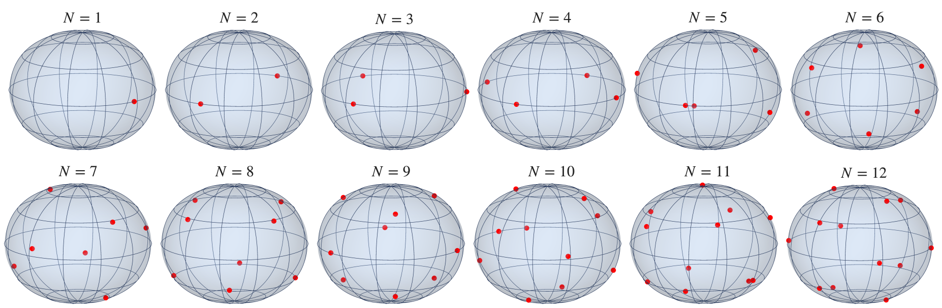

FIG. 4.5. *Optimization of the capacitance C_T for $N = 1, \ldots, 12$ surface patches in the Berg-Purcell problem, Case II. We consider a nearly spherical boundary defined by radial coordinate $r = 1 + \mu \sin^2\theta$ for $\mu = 0.25$. For $N = 1, \ldots, 12$ points, we numerically calculate the points $\{\mathbf{x}_j\}_{j=1}^N$ that minimize the discrete energy* (4.23).

5. Discussion. We have developed a unified asymptotic theory for two canonical diffusive capture problems in general smooth closed three-dimensional domains whose boundary consists of small non-overlapping partially reactive boundary patches of arbitrary shape on an otherwise reflecting surface. First, we considered the exterior Berg-Purcell problem of receptor-mediated absorption. Then, we adapted the analysis to treat the interior narrow escape problem for the mean first-reaction time for a diffusing particle to react on any of small boundary patches. Previous treatments were largely confined to the sphere, where the surface Neumann Green's function is known explicitly and the boundary is a surface of constant curvature. By performing a matched asymptotic analysis relying on a local orthogonal coordinate system, we have obtained three-term expansions (Propositions 1 and 2) for the capacitance C_T and the global (or volume-averaged) MFRT $\overline{u}$. The central outcome of our analysis consists in accurate closed-form expressions for the key quantities that are determined in terms of both local properties of each patch and those representing long-range interactions. In particular, the local geometry near each patch enters through the principal curvatures κ_{1i}, κ_{2i} and the patch reactivity b_i, as encoded in the reaction capacitance C_i and certain monopole coefficients $E_{i\pm}$. These latter quantities are determined up to various quadratures that involve the charge density on each patch. In contrast, the long-range interactions that encode the global domain geometry enter through a surface Neumann Green's matrix.

Resolving the weak, path-dependent singularity of the surface Neumann Green's function on a curved boundary was the key technical step that enabled our general-geometry analysis. For the special case of N identical circular patches, the results collapse to compact formulas where the curvature appears only through the mean curvature $\mathcal{H}_i = \frac{1}{2}(\kappa_{1i} + \kappa_{2i})$, and where they reduce to previously derived results for a spherical domain in the appropriate limit.

A natural application of these formulas that awaits to be explored is the optimization of capture over different surface geometries. More specifically, given a manifold where should a fixed number of receptors be placed, and how should their sizes and reactivities be apportioned, to maximize the absorption rate for capture of diffusing ligands. Our derived asymptotic results reduce this question to a finite-dimensional optimization problem in the patch locations, involving the Green's interaction energy

$$p(\mathbf{x}_1, \ldots, \mathbf{x}_N) = \sum_{i=1}^{N} \Big[R(\mathbf{x}_i) + \sum_{\substack{j=1 \\ i\neq j}}^{N} G(\mathbf{x}_j; \mathbf{x}_i) \Big] \,,$$

together with the local mean-curvature contributions $\mathcal{H}_i$. In practice, optimization will require coupling the asymptotic formulas to a numerical solver to build the Green's interaction matrix on the surface of interest, for instance through the boundary-integral methods [42]. We note one qualitative feature that distinguishes the three-dimensional setting from its two-dimensional counterpart [16, 30]: the spatially varying corrections enter at the $\mathcal{O}(\varepsilon \log \varepsilon)$ term due to local mean curvature effects while global effects are encoded in the $\mathcal{O}(\varepsilon)$ term. This differs from planar and spherical narrow-capture problems where the equivalent terms are independent of the trap configuration in the limit $\varepsilon \to 0$. We hypothesize that the set of optimizing locations will depend on the patch radius ε with smaller values being associated with clustered configurations around critical points of mean curvature.

A second direction for future work is to derive effective scaling laws in the dense-receptor limit $N \to \infty$ while keeping the receptor area $\mathcal{O}(N\varepsilon^2)$ fixed. On the sphere, the leading Berg-Purcell rate together with a packing correction can be captured by a homogenized effective reactivity to be imposed on the entire domain boundary (see [31, 44]). We conjecture that on a general surface the analogous law must involve some average of the local curvatures and an interaction energy whose growth with N reflects the geometry of optimal point configurations on the manifold. Establishing this law and identifying the effective conditions that summarize a densely patterned surface as a single homogenized boundary condition would connect the discrete asymptotics developed here to a continuum description of partially absorbing curved boundaries.

Finally, the asymptotic framework developed herein unlocks the potential for examining a broader class of geometry-dependent first-passage questions. The same inner/outer structure and the same curved-surface Green's function apply, with minor modification, to studying splitting probabilities among competing receptors [29, 40], to directional sensing [7] and source localization by a cell reading out the spatial pattern of capture events, and to the extreme-value statistics of the fastest few arrivals that govern the timing of many cellular decisions. We remark that the splitting probability is readily obtained from our analysis by calculating the local flux to a specific receptor and dividing by the total flux. Yet another application concerns the asymptotic analysis of mixed Steklov eigenvalue problems (see [29]). In each case the local curvature and the global Green's interactions are expected to play the organizing role they do here, and the methods of this paper provide a systematic route to quantifying how geometric effects shape stochastic processes.

Acknowledgments. AEL acknowledges support from the NSF under grant DMS-2052636. JGH was supported in part by a Sloan Research Fellowship. MJW is grateful for the support of the NSERC Discovery Grant Program (Canada). DSG acknowledges the Simons Foundation for supporting his sabbatical sojourn in 2024 at the CRM (CNRS – University of Montréal, Canada), and the Alexander von Humboldt Foundation for support within a Bessel Prize award. This research was supported in part by grants from the NSF (DMS-2235451) and Simons Foundation (MPS-NITMB-00005320) to the NSF-Simons National Institute for Theory and Mathematics in Biology (NITMB).

Appendix A. Boundary-fitted local orthogonal coordinates.

We introduce a local coordinate system defined near $\mathbf{x}_i$ using the intrinsic geometry of the surface as was done in [31]. We let t_1 and t_2 be the local orthogonal surface coordinates, centered at $\mathbf{x}_i$, that correspond to the two principal directions through $\mathbf{x}_i \in \partial\Omega$ with principal curvatures κ_1 and κ_2, respectively. Locally the surface is described by the quadratic form

$$z' = \mathcal{B}(t_1,t_2) \equiv \frac{1}{2}\kappa_1 t_1^2 + \frac{1}{2}\kappa_2 t_2^2 + o(t_1^2+t_2^2)\,. \tag{A.1}$$

In terms of a suitable orthogonal (rotation) matrix $\mathbf{Q}$, we introduce the local change of coordinates defined by

$$\mathbf{x}' \equiv \mathbf{Q}(\mathbf{x}-\mathbf{x}_i) = (t_1,t_2,\mathcal{B}(t_1,t_2))^T + d\hat{\mathbf{n}}\,, \tag{A.2a}$$

where $d \geq 0$ and $\hat{\mathbf{n}}$ is the inward pointing unit normal for the local parameterization $z' = \mathcal{B}(t_1,t_2)$ of the surface, which is given for $|t_1| \ll 1$ and $|t_2| \ll 1$ by

$$\hat{\mathbf{n}} = \frac{(-\mathcal{B}_{t_1}, -\mathcal{B}_{t_2}, 1)^T}{\sqrt{1+\mathcal{B}_{t_1}^2+\mathcal{B}_{t_2}^2}} = (-\kappa_1 t_1, -\kappa_2 t_2, 1)^T \left[1+\mathcal{O}(t_1^2+t_2^2)\right]\,. \tag{A.2b}$$

For the validity of this coordinate system locally we require that $d < 1/\max(0,\kappa_1,\kappa_2)$.

To transform the Laplacian of a generic function $V(\mathbf{x})$ from Cartesian to the local coordinates (t_1,t_2,d) of (A.2), we use the fact that $\mathbf{Q}$ preserves lengths, and so

$$\begin{aligned} \nu_{t_1} &\equiv |\partial \mathbf{x}/\partial t_1| = 1 - d\kappa_1 + \mathcal{O}(t_1^2+t_2^2+d^2)\,, \\ \nu_{t_2} &\equiv |\partial \mathbf{x}/\partial t_2| = 1 - d\kappa_2 + \mathcal{O}(t_1^2+t_2^2+d^2)\,, \\ \nu_{d} &\equiv |\partial \mathbf{x}/\partial d| = 1 + \mathcal{O}(t_1^2+t_2^2)\,. \end{aligned} \tag{A.3}$$

In terms of these scale factors, the Laplacian is transformed to

$$\begin{aligned} \Delta_{\mathbf{x}} V &= \frac{1}{\nu_{t_1}\nu_{t_2}\nu_d}\left[\frac{\partial}{\partial t_1}\left(\frac{\nu_{t_2}\nu_d}{\nu_{t_1}} V_{t_1}\right) + \frac{\partial}{\partial t_2}\left(\frac{\nu_{t_1}\nu_d}{\nu_{t_2}} V_{t_2}\right) + \frac{\partial}{\partial d}\left(\frac{\nu_{t_1}\nu_{t_2}}{\nu_d} V_d\right)\right]\,, \\ &= V_{dd} - \left(\frac{\kappa_1}{1-\kappa_1 d} + \frac{\kappa_2}{1-\kappa_2 d}\right) V_d \\ &\quad + \frac{1}{(1-d\kappa_1)(1-d\kappa_2)}\left[\frac{\partial}{\partial t_1}\left(\frac{1-d\kappa_2}{1-d\kappa_1} V_{t_1}\right) + \frac{\partial}{\partial t_2}\left(\frac{1-d\kappa_1}{1-d\kappa_2} V_{t_2}\right)\right]\,. \end{aligned} \tag{A.4}$$

Next, we introduce the ε-localized variables (ξ_1, ξ_2, η) defined by

$$\xi_1 \equiv t_1/\varepsilon\,, \quad \xi_2 \equiv t_2/\varepsilon\,, \quad \eta \equiv d/\varepsilon\,, \quad \Delta_{\mathbf{y}} \equiv \partial_{\xi_1\xi_1} + \partial_{\xi_2\xi_2} + \partial_{\eta\eta}\,. \tag{A.5}$$

In terms of these local variables, for $\varepsilon \to 0$ we find that the Laplacian (A.4) reduces to

$$\Delta_{\mathbf{x}} V = \frac{1}{\varepsilon^2}\Delta_{\mathbf{y}} V + \frac{1}{\varepsilon}\left[-2\mathcal{H}V_\eta + 2\mathcal{H}\eta\left(V_{\xi_1\xi_1} + V_{\xi_2\xi_2}\right) + 2\mathcal{Q}\eta\left(V_{\xi_1\xi_1} - V_{\xi_2\xi_2}\right)\right] + \mathcal{O}(1)\,, \tag{A.6}$$

where $\mathcal{H}$ is the mean curvature and $\mathcal{Q}$ is the curvature difference defined in terms of the two principal curvatures κ_1 and κ_2 of $\partial\Omega$ at $\mathbf{x} = \mathbf{x}_i$ by

$$\mathcal{H} = \frac{\kappa_1 + \kappa_2}{2}\,, \qquad \mathcal{Q} = \frac{\kappa_1 - \kappa_2}{2}\,. \tag{A.7}$$

Next, to derive a two-term approximation for the Euclidian distance $|\mathbf{x} - \mathbf{x}_i|$, we use (A.5) in (A.2) and collect powers of ε. Since $\mathbf{Q}$ is an orthogonal matrix, we obtain

$$\mathbf{Q}(\mathbf{x} - \mathbf{x}_i) = \varepsilon\mathbf{y} + \varepsilon^2\mathbf{a} + \mathcal{O}(\varepsilon^3)\,, \qquad |\mathbf{x} - \mathbf{x}_i|^2 = \varepsilon^2\mathbf{y}^T\mathbf{y} + 2\varepsilon^3\mathbf{y}^T\mathbf{a} + \mathcal{O}(\varepsilon^4)\,, \tag{A.8a}$$

where $\mathbf{y}$ and $\mathbf{a}$ are defined by

$$\mathbf{y} \equiv (\xi_1, \xi_2, \eta)^T\,, \qquad \mathbf{a} \equiv \left(-\kappa_1\xi_1\eta, -\kappa_2\xi_2\eta, \frac{1}{2}\kappa_1\xi_1^2 + \frac{1}{2}\kappa_2\xi_2^2\right)^T\,. \tag{A.8b}$$

By calculating $\mathbf{y}^T\mathbf{y} = \xi_1^2 + \xi_2^2 + \eta^2 \equiv \rho^2$ and $\mathbf{y}^T\mathbf{a} = -\eta\left(\kappa_1\xi_1^2 + \kappa_2\xi_2^2\right)/2$, we get

$$\begin{aligned}
|\mathbf{x} - \mathbf{x}_i| &\sim \varepsilon\rho\left(1 - \frac{\varepsilon\eta}{2\rho^2}\left[\mathcal{H}(\xi_1^2 + \xi_2^2) + \mathcal{Q}(\xi_1^2 - \xi_2^2)\right]\right) + \mathcal{O}(\varepsilon^3),\\
\frac{1}{|\mathbf{x} - \mathbf{x}_i|} &\sim \frac{1}{\varepsilon\rho}\left(1 + \frac{\varepsilon\eta}{2\rho^2}\left[\mathcal{H}(\xi_1^2 + \xi_2^2) + \mathcal{Q}(\xi_1^2 - \xi_2^2)\right]\right) + \mathcal{O}(\varepsilon)\,.
\end{aligned} \tag{A.9}$$

Finally, we observe from (A.9) that $|\mathbf{x} - \mathbf{x}_i| = \varepsilon\rho + \mathcal{O}(\varepsilon^3)$ and $\rho = (\xi_1^2 + \xi_2^2)^{1/2}$ when $\eta = 0$. As a result, if the orthogonal projection of the Robin patch $\partial\Omega_i^\varepsilon$ onto the tangent is a disk of radius εa_i, then the rescaled surface patch Γ_i is described by $\left(\xi_1^2 + \xi_2^2\right)^{1/2} \leq a_i + \mathcal{O}(\varepsilon^2)$. This small $\mathcal{O}(\varepsilon^2)$ difference between the the orthogonally-projected and on-surface patches does not influence our three-term asymptotic result in Propositions 1 and 2.

Appendix B. The surface Neumann Green's function.

We now derive (2.18b) and show that the unspecified $e(\mathbf{x}; \mathbf{x}_i)$ term in (2.18b), which is determined solely by the local behavior of $\partial\Omega$ near $\mathbf{x} = \mathbf{x}_i$, exhibits a mild singularity in that the value as $\mathbf{x} \to \mathbf{x}_i$ depends on the specific path of approach to $\mathbf{x}_i$. This detailed analysis below produces a result equivalent to that derived in [47] from microlocal analysis; here, we present an alternative approach based on a local coordinate system defined in Appendix A which is suited for the high-order asymptotic analysis of (1.4) and (1.9). In our analysis below, for ease of notation we omit the subscript e for this Green's function.

In terms of the ε-localized coordinates (A.5), we apply (A.6) to the problem (2.18a) for G. The boundary condition in (2.18a) on the surface $\eta = 0$ transforms locally to

$$\partial_n G = -\frac{1}{\varepsilon\nu_d}\partial_\eta G = \delta(\mathbf{x} - \mathbf{x}_i) = \delta(\mathbf{Q}^T\mathbf{x}') = \frac{1}{\varepsilon^2|\det\mathbf{Q}|}\delta(\xi_1)\delta(\xi_2)\,.$$

Since $\nu_d = 1 + \mathcal{O}(\varepsilon^2)$ and $|\det \mathbf{Q}| = 1$, we obtain that

$$G_\eta \sim -\frac{1}{\varepsilon}\delta(\xi_1)\delta(\xi_2)\,, \quad \text{on} \quad \eta = 0\,. \tag{B.1}$$

On the domain $\mathbb{R}^3_+$, as defined in (2.9), we substitute the expansion

$$G = \frac{G_0}{\varepsilon} + G_1 + \mathcal{O}(\varepsilon) \tag{B.2}$$

into both (A.6) applied to G and the boundary condition (B.1). By collecting powers of ε, we obtain the leading-order problem

$$\Delta_{\mathbf{y}} G_0 = 0\,, \quad \text{in } \mathbb{R}^3_+\,; \qquad \partial_\eta G_0 = -\delta(\xi_1)\delta(\xi_2)\,, \quad \text{on } \eta = 0\,, \tag{B.3}$$

where $\Delta_{\mathbf{y}} G_0 \equiv G_{0,\xi_1\xi_1} + G_{0,\xi_2\xi_2} + G_{0,\eta\eta}$. At next order we obtain that G_1 satisfies

$$\begin{aligned} &\Delta_{\mathbf{y}} G_1 = 2\mathcal{H}G_{0,\eta} - 2\mathcal{H}\eta\left(G_{0,\xi_1\xi_1} + G_{0,\xi_2\xi_2}\right) - 2\mathcal{Q}\eta\left(G_{0,\xi_1\xi_1} - G_{0,\xi_2\xi_2}\right)\,, \quad \text{in } \mathbb{R}^3_+\,, \\ &\partial_\eta G_1 = 0\,, \quad \text{on } \eta = 0\,. \end{aligned} \tag{B.4}$$

The solution to (B.3) is

$$G_0 = \frac{1}{2\pi\rho}\,, \quad \text{where} \quad \rho \equiv \left(s^2 + \eta^2\right)^{1/2}\,, \quad \text{and} \quad s^2 = \xi_1^2 + \xi_2^2\,, \tag{B.5}$$

and we conveniently decompose G_1 as

$$G_1 = 2\mathcal{H}G_+ - 2\mathcal{Q}G_-\,. \tag{B.6}$$

By using $G_{0,\xi_1\xi_1} + G_{0,\xi_2\xi_2} = -G_{0,\eta\eta}$ for $(\xi_1,\xi_2,\eta) \neq (0,0,0)$ in (B.4), the decomposition (B.6) yields that G_+ satisfies

$$\Delta_{\mathbf{y}} G_+ = G_{0,\eta} + \eta G_{0,\eta\eta} = \left[\eta G_{0,\eta}\right]_\eta\,, \quad \text{in} \quad \mathbb{R}^3_+\,; \qquad \partial_\eta G_+ = 0\,, \quad \text{on} \quad \eta = 0\,, \tag{B.7}$$

while G_- satisfies

$$\Delta_{\mathbf{y}} G_- = \eta\left(G_{0,\xi_1\xi_1} - G_{0,\xi_2\xi_2}\right)\,, \quad \text{in} \quad \mathbb{R}^3_+\,; \qquad \partial_\eta G_- = 0\,, \quad \text{on} \quad \eta = 0\,. \tag{B.8}$$

We can determine G_+ by simply using the PDE that G_0 solves. The result is as follows:

Lemma B.1. *For $\left(\xi_1,\xi_2,\eta\right) \neq (0,0,0)$, the solution to (B.7) that has no singularity in $\mathbb{R}^3_+$ has the form*

$$G_+ = \frac{\eta^2}{4}G_{0,\eta} + \frac{\eta}{4}G_0 - \frac{1}{4}\int^\eta G_0\,d\eta + \mathcal{F}(\xi_1,\xi_2)\,, \tag{B.9}$$

where $\mathcal{F}(\xi_1,\xi_2)$ is a 2-D harmonic solution satisfying $\Delta_\xi \mathcal{F} \equiv \mathcal{F}_{\xi_1\xi_1} + \mathcal{F}_{\xi_2\xi_2} = 0$.

Proof. For $(\xi_1,\xi_2,\eta) \neq (0,0,0)$ we readily calculate that

$$G_{+,\eta} = \frac{3}{4}\eta G_{0,\eta} + \frac{\eta^2}{4}G_{0,\eta\eta}\,, \qquad G_{+,\eta\eta} = \frac{\eta^2}{4}G_{0,\eta\eta\eta} + \frac{5}{4}\eta G_{0,\eta\eta} + \frac{3}{4}G_{0,\eta}\,. \tag{B.10}$$

Upon defining $\Delta_\xi \equiv \partial_{\xi_1\xi_1} + \partial_{\xi_2\xi_2}$, we use the PDE that G_0 solves to get

$$\begin{aligned}
\Delta_\xi G_+ &= \frac{\eta^2}{4}\left[\Delta_\xi G_0\right]_\eta + \frac{\eta}{4}\Delta_\xi G_0 - \frac{1}{4}\int^\eta \Delta_\xi G_0 \, d\eta + \Delta_\xi \mathcal{F}\,, \\
&= -\frac{\eta^2}{4}G_{0,\eta\eta\eta} - \frac{\eta}{4}G_{0,\eta\eta} + \frac{1}{4}\int^\eta G_{0,\eta\eta}\, d\eta + \Delta_\xi \mathcal{F}\,, \\
&= -\frac{\eta^2}{4}G_{0,\eta\eta\eta} - \frac{\eta}{4}G_{0,\eta\eta} + \frac{1}{4}G_{0,\eta} + \Delta_\xi \mathcal{F}\,.
\end{aligned} \tag{B.11}$$

Adding the last line in (B.11) to $G_{+,\eta\eta}$ from (B.10), and setting $\Delta_\xi \mathcal{F} = 0$ for $(\xi_1, \xi_2) \neq (0,0)$, we conclude that G_+ satisfies (B.7) on $\mathbb{R}^3_+$ as required. From (B.10) it follows that the boundary condition $G_{+\eta} = 0$ on $\eta = 0$ for $(\xi_1,\xi_2) \neq (0,0)$ holds. ∎

To determine G_+ explicitly, we use (B.5) for G_0 to obtain

$$G_{0,\eta} = -\frac{\eta}{2\pi\rho^3}\,, \qquad G_{0,\eta\eta} = -\frac{1}{2\pi\rho^3} + \frac{3\eta^2}{2\pi\rho^5}\,.$$

Replacing the integral in (B.9) with a definite integral, and recalling that $\int^x (a^2 + x^2)^{-1/2}\, dx = \log\left(x + \sqrt{x^2+a^2}\right)$, we get from (B.9) that

$$\begin{aligned}
G_+ &= \frac{\eta}{8\pi\rho}\left(1 - \frac{\eta^2}{\rho^2}\right) - \frac{1}{8\pi}\int_0^\eta \frac{dt}{\sqrt{\xi_1^2+\xi_2^2+t^2}} + \mathcal{F}(\xi_1,\xi_2)\,, \\
&= \frac{\eta}{8\pi\rho^3}\left(\xi_1^2+\xi_2^2\right) - \frac{1}{8\pi}\log\left(\eta+\rho\right) + \frac{1}{8\pi}\log\left(\sqrt{\xi_1^2+\xi_2^2}\right) + \mathcal{F}(\xi_1,\xi_2)\,.
\end{aligned}$$

To ensure that G_+ has no singularity in $\mathbb{R}^3_+$, we must choose, up to an additive constant K, that $\mathcal{F} = -(8\pi)^{-1}\log\left(\sqrt{\xi_1^2+\xi_2^2}\right)$. In this way, we conclude that

$$G_+ = \frac{\eta}{8\pi\rho^3}\left(\xi_1^2+\xi_2^2\right) - \frac{1}{8\pi}\log(\eta+\rho) + K\,. \tag{B.12}$$

Next, we solve (B.8) for G_-. By using (B.5) for G_0, (B.8) becomes

$$\Delta_{\mathbf{y}} G_- = \frac{3\eta\left(\xi_1^2-\xi_2^2\right)}{2\pi\rho^5}\,, \quad \text{in} \quad \mathbb{R}^3_+\,; \qquad \partial_\eta G_- = 0\,, \quad \text{on} \quad \eta = 0\,. \tag{B.13}$$

We first seek a particular solution G_{-p} to (B.13) by using the following simple lemma.

Lemma B.2. *Let $\mathbf{y} = (\xi_1,\xi_2,\eta)^T$, $\rho = |\mathbf{y}|$, and let $P_n(\mathbf{y})$ be a homogeneous polynomial in $\mathbf{y}$ of degree n, so that $P_n(t\mathbf{y}) = t^n P_n(\mathbf{y})$ for any scalar t. If $P_n(\mathbf{y})$ is also harmonic in 3-D, then*

$$\Delta_{\mathbf{y}}\left(\frac{P_n(\mathbf{y})}{\rho^3}\right) = \frac{6(1-n)P_n(\mathbf{y})}{\rho^5}\,. \tag{B.14}$$

Proof. We calculate

$$\Delta_{\mathbf{y}}\left(\frac{P_n}{\rho^3}\right) = \frac{\Delta_{\mathbf{y}} P_n}{\rho^3} + P_n \Delta_{\mathbf{y}}\left(\frac{1}{\rho^3}\right) + 2\nabla P_n \cdot \nabla\left(\frac{1}{\rho^3}\right)\,.$$

Since $\nabla\rho^{-3} = -3\mathbf{y}/\rho^5$ and $\Delta_{\mathbf{y}}\rho^{-3} = 6\rho^{-5}$ we get

$$\Delta_{\mathbf{y}}\left(\frac{P_n}{\rho^3}\right) = \frac{\Delta_{\mathbf{y}} P_n}{\rho^3} + \frac{6P_n}{\rho^5} - \frac{6}{\rho^5}\nabla P_n\cdot\mathbf{y}\,. \tag{B.15}$$

By using Euler's result $\mathbf{y}\cdot\nabla P_n = nP_n$ for homogeneous polynomials of degree n together with $\Delta_{\mathbf{y}} P_n = 0$, we observe that (B.15) reduces to (B.14). $\square$

To find a particular solution for (B.13) we simply choose the third-degree homogeneous polynomial $P_3(\mathbf{y}) = \alpha\eta\left(\xi_1^2 - \xi_2^2\right)$, where α is a parameter. By equating the right-hand sides of (B.14) and the PDE in (B.13), we identify that $\alpha = -1/(8\pi)$. This yields a particular solution for (B.13) given by

$$G_{-p} = -\frac{\eta}{8\pi}\frac{\left(\xi_1^2 - \xi_2^2\right)}{\rho^3}\,. \tag{B.16}$$

To satisfy the boundary condition on $\eta = 0$ in (B.13) we decompose G_- as

$$G_- = G_{-p} + G_{-c}\,, \tag{B.17}$$

where the complementary solution G_{-c} satisfies

$$\begin{aligned} &\Delta_{\mathbf{y}} G_{-c} = 0\,, \quad \text{in } \mathbb{R}^3_+\,, \\ &\partial_\eta G_{-c} = -\partial_\eta G_{-p} = \frac{1}{8\pi}\frac{\left(\xi_1^2 - \xi_2^2\right)}{\rho^3} = \frac{1}{8\pi s}\frac{\left(\xi_1^2 - \xi_2^2\right)}{s^2}\,, \quad \text{on } \eta = 0\,, \end{aligned} \tag{B.18}$$

with $\rho^2 = \eta^2 + s^2$ and $s^2 \equiv \xi_1^2 + \xi_2^2$.

To determine the solution to (B.18) that has no singularity in $\mathbb{R}^3_+$, it is convenient to use spherical coordinates (ρ, θ, ϕ), where θ and ϕ are the polar and azimuthal angles, respectively, so that

$$\eta = \rho\cos\theta\,, \quad s = \rho\sin\theta\,, \quad \frac{\xi_1^2 - \xi_2^2}{s^2} = \cos(2\phi)\,. \tag{B.19}$$

Since $\partial_\theta G_{-c}|_{\theta=\pi/2} = -s\partial_\eta G_{-c}|_{\eta=0}$, we write $\Delta_{\mathbf{y}}$ in spherical coordinates to obtain that (B.18) becomes

$$\begin{aligned} &\Delta_{\mathbf{y}} G_{-c} = 0\,, \quad \text{in } \rho > 0\,, \quad 0 \le \theta \le \pi/2\,, \quad 0 \le \phi < 2\pi\,, \\ &\partial_\theta G_{-c} = -\frac{1}{8\pi}\cos(2\phi)\,, \quad \text{on } \theta = \pi/2\,. \end{aligned} \tag{B.20}$$

By seeking a solution to (B.20) with no ρ dependence of the form

$$G_{-c} = v(\mu)\cos(2\phi)\,, \tag{B.21}$$

with $\mu = \cos\theta$, we conclude that $v(\mu)$ satisfies the ODE

$$\left[(1-\mu^2)v'\right]' - \frac{4}{1-\mu^2}v = 0\,, \quad \text{on} \quad 0 \le \mu < 1\,; \quad v'(0) = \frac{1}{8\pi}\,. \tag{B.22}$$

It is readily verified that the unique solution to (B.22) that has no singularity at $\mu = 1$ has the form $v = c(1-\mu)/(1+\mu)$, where c is a constant. By satisfying $v'(0) = 1/(8\pi)$ we determine this constant, and conclude that

$$v = -\frac{1}{16\pi}\left(\frac{1-\mu}{1+\mu}\right)\,. \tag{B.23}$$

Upon replacing $\mu = \cos\theta = \eta/\rho$, we obtain from (B.23) and (B.21) that

$$G_{-c} = -\frac{1}{16\pi}\left(\frac{\rho-\eta}{\rho+\eta}\right)\cos(2\phi)\,. \tag{B.24}$$

Then, upon substituting (B.24) and (B.16) into (B.17), the solution to (B.13) is

$$G_- = -\frac{1}{16\pi}\left[\frac{2\eta s^2}{\rho^3} + \left(\frac{\rho-\eta}{\rho+\eta}\right)\right]\cos(2\phi)\,. \tag{B.25a}$$

Equivalently, upon using $\cos(2\phi) = (\xi_1^2 - \xi_2^2)/s^2$ and $\rho^2 - \eta^2 = s^2$, we have

$$G_- = -\frac{1}{8\pi}\frac{\eta\left(\xi_1^2-\xi_2^2\right)}{\rho^3} - \frac{1}{16\pi}\frac{\left(\xi_1^2-\xi_2^2\right)}{(\rho+\eta)^2}\,, \quad \text{where} \quad \rho = |\mathbf{y}|\,. \tag{B.25b}$$

Finally, by substituting (B.25a) and (B.12) into (B.6), we obtain an explicit representation for the two-term asymptotic expansion (B.2). We emphasize that this truncated two-term expansion describes the local behavior of the solution to Laplace's equation with a Dirac singularity on the boundary. We summarize our result as follows:

PROPOSITION 3. *Let $\mathcal{H} = (\kappa_1+\kappa_2)/2$ and $\mathcal{Q} = (\kappa_1-\kappa_2)/2$, where κ_1 and κ_2 are the principal curvatures of $\partial\Omega$ at $\mathbf{x} = \mathbf{x}_i$. Then, in terms of the ε-local boundary-fitted coordinates (A.5) for the local coordinate transformation (A.2), and up to an arbitrary constant K, the local singularity behavior as $\mathbf{x}\to\mathbf{x}_i$ for the exterior surface Neumann Green's function satisfying (2.18a) is*

$$G_e \sim \frac{1}{2\pi\varepsilon\rho} + G_1 + \mathcal{O}(\varepsilon)\,, \tag{B.26a}$$

where

$$G_1 = \frac{\mathcal{H}}{4\pi}\left[\frac{\eta s^2}{\rho^3} - \log(\eta+\rho)\right] + K + \frac{\mathcal{Q}}{8\pi}\left[\frac{2\eta s^2}{\rho^3} + \left(\frac{\rho-\eta}{\rho+\eta}\right)\right]\frac{(\xi_1^2-\xi_2^2)}{s^2}\,. \tag{B.26b}$$

Equivalently, we can write (B.26) as

$$G_e \sim \frac{1}{2\pi\varepsilon\rho} + \frac{\mathcal{H}}{4\pi}\left(\frac{\eta(\xi_1^2+\xi_2^2)}{\rho^3} - \log(\eta+\rho)\right) + K + \frac{\mathcal{Q}}{4\pi}\frac{\eta(\xi_1^2-\xi_2^2)}{\rho^3} + \frac{\mathcal{Q}}{8\pi}\frac{(\xi_1^2-\xi_2^2)}{(\rho+\eta)^2} + \mathcal{O}(\varepsilon)\,. \tag{B.27}$$

Finally, we identify the constant $e(\mathbf{x};\mathbf{x}_i)$ in (2.18b) and the constant K in (B.27) by relating (B.27) to (2.18b). To do so, we substitute the two-term expansion for $|\mathbf{x}-\mathbf{x}_i|$, as given in (A.9), into (2.18b), while recalling $d = \eta\varepsilon$. Upon comparing the resulting expression with (B.27), we obtain that

$$G_e \sim \frac{1}{2\pi\varepsilon\rho} + \frac{\mathcal{H}}{4\pi}\left(\frac{\eta(\xi_1^2+\xi_2^2)}{\rho^3} - \log(\eta+\rho)\right) + R_e - \frac{\mathcal{H}}{4\pi}\log\varepsilon + \frac{\mathcal{Q}}{4\pi}\frac{\eta(\xi_1^2-\xi_2^2)}{\rho^3} + e + \mathcal{O}(\varepsilon)\,, \tag{B.28a}$$

which determines the constant K as $K = R_e - \frac{\mathcal{H}}{4\pi}\log\varepsilon$, and identifies $e(\mathbf{x};\mathbf{x}_i)$ as

$$e(\mathbf{x};\mathbf{x}_i) = \frac{\mathcal{Q}}{8\pi}\frac{(\xi_1^2-\xi_2^2)}{(\rho+\eta)^2}\,. \tag{B.28b}$$

We emphasize that the remaining terms in (B.28a) match identically, and these terms simply represent the effect of our chosen local parameterization (A.2a) of the surface.

We now write e in (B.28b) in terms of the Cartesian coordinate system. In (B.28b), we replace $\rho \sim |\mathbf{x}-\mathbf{x}_i|/\varepsilon$, $\eta = d/\varepsilon$, $\xi_1 = t_1/\varepsilon$, and $\xi_2 = t_2/\varepsilon$, and use (A.2a) to solve for t_1 and t_2. In this way, we calculate that

$$e(\mathbf{x};\mathbf{x}_i) = \frac{\mathcal{Q}}{8\pi(|\mathbf{x}-\mathbf{x}_i|+d)^2}\left(\frac{p_1^2}{(1-\kappa_1 d)^2} - \frac{p_2^2}{(1-\kappa_2 d)^2}\right) + o(1)\,, \tag{B.29}$$

where $d = \text{dist}(\mathbf{x}, \partial\Omega)$, $\mathcal{Q} = (\kappa_1 - \kappa_2)/2$, and p_1 and p_2 are the projections of $\mathbf{Q}(\mathbf{x}-\mathbf{x}_i)$ onto the two principal directions of $\partial\Omega$ at $\mathbf{x} = \mathbf{x}_i$, defined in terms of the components of $\mathbf{Q}(\mathbf{x} - \mathbf{x}_i)$ by $p_j = \left(\mathbf{Q}(\mathbf{x} - \mathbf{x}_i)\right)_j$ for $j = 1, 2$.

We remark that the singularity structure of the interior surface Neumann Green's function, satisfying (3.2), has exactly the same two-term asymptotic behavior as that given in (B.27) for the exterior problem. This is because the $1/|\Omega|$ term in (3.2) would only appear at at one higher-order. However, care is needed to determine the correct signs of κ_1 and κ_2 for the interior problem as they will be of opposite signs than that for the exterior problem.

B.1. Explicit results for the sphere. When Ω is the unit sphere, the surface Neumann Green's G_e satisfying (2.18a) for the *exterior problem* is (see [40, 44, 46])

$$G_e(\mathbf{x}; \mathbf{x}_i) = \frac{1}{2\pi\, |\mathbf{x} - \mathbf{x}_i|} - \frac{1}{4\pi} \log\left(1 + \frac{2}{|\mathbf{x} - \mathbf{x}_i| + |\mathbf{x}| - 1}\right), \tag{B.30a}$$

which has the following local behavior as $\mathbf{x} \to \mathbf{x}_i$:

$$G_e(\mathbf{x}; \mathbf{x}_i) \sim \frac{1}{2\pi|\mathbf{x} - \mathbf{x}_i|} + \frac{1}{4\pi} \log\big(|\mathbf{x}-\mathbf{x}_i| + |\mathbf{x}| - 1\big) + R_e + o(1)\,; \quad R_e \equiv -\frac{\log 2}{4\pi}\,. \tag{B.30b}$$

For this case, $\mathcal{H}_i = -1$ and $\mathcal{Q}_i = 0$ for any $\mathbf{x}_i \in \partial\Omega$.

The surface Neumann Green's function satisfying (3.2) for the *interior problem* is (see Appendix A of [19])

$$G_s(\mathbf{x}; \mathbf{x}_i) = \frac{1}{2\pi\, |\mathbf{x} - \mathbf{x}_i|} + \frac{|\mathbf{x}|^2 + 1}{8\pi} + \frac{1}{4\pi} \log\left(\frac{2}{1 - \mathbf{x}\cdot\mathbf{x}_i + |\mathbf{x} - \mathbf{x}_i|}\right) - \frac{7}{10\pi}\,, \tag{B.31a}$$

which has the following local behavior as $\mathbf{x} \to \mathbf{x}_i$:
(B.31b)

$$G_s(\mathbf{x}; \mathbf{x}_i) \sim \frac{1}{2\pi|\mathbf{x} - \mathbf{x}_i|} - \frac{1}{4\pi} \log\big(|\mathbf{x} - \mathbf{x}_i| + 1 - |\mathbf{x}|\big) + R_s + o(1)\,; \quad R_s \equiv \frac{\log 2}{4\pi} - \frac{9}{20\pi}\,.$$

For the unit sphere, $\mathcal{H}_i = 1$ and $\mathcal{Q}_i = 0$ for any $\mathbf{x}_i \in \partial\Omega$.

Appendix C. Monopole Coefficient E_{i+}.

Although the properties of E_{i+} were already reported in [29, 31], for completeness we outline the analysis of [31] (see also [29]) for the inner problem (2.31). This analysis identifies the monopole coefficient in the refined far-field behavior (2.33), whose properties were summarized in Lemma 2.2. For convenience we omit the subscript i below for the i-th patch.

We begin by decomposing the solution Φ_+ to (2.31) as

$$\Phi_+ = \Phi_{p+} + \Phi_{c+}\,, \tag{C.1}$$

where Φ_{p+} accounts for the inhomogeneous term in the PDE (2.31a) and satisfies the Neumann condition $\partial_\eta \Phi_{p+} = 0$ on the plane $\eta = 0$. The complementary part Φ_{c+} will satisfy the homogeneous PDE, but with an inhomogeneous Robin condition on the patch Γ. As similar to the derivation in Lemma B.1 for the analogous component of the surface Neumann Green's function, Φ_{p+} can be determined analytically in terms of w satisfying (2.11).

LEMMA C.1. *(Lemma C.1 of [31]) The solution to (2.31) satisfying $\partial_\eta \Phi_{p+} = 0$ on $\eta = 0$ is*

$$\Phi_{p+} = -\frac{\eta^2}{2} w_\eta - \frac{\eta}{2} w + \frac{1}{2}\int_0^\eta w(\xi_1,\xi_2,t)\, dt + \mathcal{F}_+(\xi_1,\xi_2;b)\,, \tag{C.2}$$

where $\mathcal{F}_+(\xi_1,\xi_2;b)$, with $\Delta_\xi \mathcal{F}_+ \equiv \mathcal{F}_{+,\xi_1\xi_1} + \mathcal{F}_{+,\xi_2\xi_2}$, is the unique solution to

$$\Delta_\xi \mathcal{F}_+ = q(\xi_1,\xi_2;b) I_\Gamma\,; \quad q \equiv -\left(\frac{1}{2} w_\eta|_{\eta=0}\right)\,, \quad I_\Gamma \equiv \begin{cases} 1\,, & (\xi_1,\xi_2) \in \Gamma \\ 0\,, & (\xi_1,\xi_2) \notin \Gamma\,, \end{cases} \tag{C.3a}$$

$$\mathcal{F}_+ \sim \frac{C}{2}\log s + o(1)\,, \quad \text{as} \quad s \equiv (\xi_1^2 + \xi_2^2)^{1/2} \to \infty\,. \tag{C.3b}$$

The $o(1)$ condition in the far-field (C.3b) specifies $\mathcal{F}_+$ uniquely. From the identity (2.12) relating C and q, an application of the divergence theorem shows that the logarithmic growth specified in (C.3b) is consistent with the PDE (C.3a). Finally, the far-field behavior for (C.2) is

$$\Phi_{p+} \sim \frac{C}{2}\left(\log(\eta+\rho) - \frac{\eta(\xi_1^2+\xi_2^2)}{\rho^3}\right) + o\left(1/\rho\right)\,, \quad \text{as} \quad \rho = (\xi_1^2+\xi_2^2+\eta^2)^{1/2} \to \infty\,. \tag{C.4}$$

Proof. We calculate that

$$\Phi_{p+,\eta} = -\frac{\eta^2}{2} w_{\eta\eta} - \frac{3}{2}\eta w_\eta\,, \quad \Phi_{p+,\eta\eta} = -\frac{\eta^2}{2} w_{\eta\eta\eta} - \frac{5}{2}\eta w_{\eta\eta} - \frac{3}{2} w_\eta\,, \tag{C.5}$$

with the first equation yielding $\Phi_{p+,\eta} = 0$ on $\eta = 0$. Next by calculating $\Delta_\xi \Phi_{p+} \equiv \Phi_{p+,\xi_1\xi_1} + \Phi_{p+,\xi_2\xi_2}$, and by using $w_{\eta\eta} = -\Delta_\xi w$ from (2.11a), we derive

$$\begin{aligned} \Delta_\xi \Phi_{p+} &= -\frac{\eta^2}{2}\partial_\eta\left[\Delta_\xi w\right] - \frac{\eta}{2}\Delta_\xi w + \frac{1}{2}\int_0^\eta \Delta_\xi w\, dt + \Delta_\xi \mathcal{F}_+ \\ &= \frac{\eta^2}{2} w_{\eta\eta\eta} + \frac{\eta}{2} w_{\eta\eta} - \frac{1}{2} w_\eta + \frac{1}{2} w_\eta|_{\eta=0} + \Delta_\xi \mathcal{F}_+\,. \end{aligned} \tag{C.6}$$

By adding (C.5) and (C.6), and by choosing $\mathcal{F}_+$ to satisfy the PDE in (C.3a), we get

$$\Delta_{\mathbf{y}} \Phi_{p+} \equiv \Phi_{p+,\eta\eta} + \Delta_\xi \Phi_{p+} = -2\left(\eta w_{\eta\eta} + w_\eta\right)\,. \tag{C.7}$$

Therefore, Φ_{p+} satisfies the inhomogeneous PDE (2.31a) subject to $\partial_\eta \Phi_{p+} = 0$ on $\eta = 0$.

Next, to establish (C.4), we use $w \sim C\rho^{-1}$ as $\rho \to \infty$ with $\rho = (\eta^2 + s^2)^{1/2}$ and $s \equiv (\xi_1^2 + \xi_2^2)^{1/2}$. We readily calculate for $\rho \to \infty$ that

$$-\frac{1}{2}\eta^2 w_\eta - \frac{1}{2}\eta w \sim -\frac{C}{2}\frac{\eta s^2}{\rho^3}\,, \tag{C.8a}$$

$$\frac{1}{2}\int_0^\eta w(\xi_1,\xi_2,t)\, dt \sim \frac{C}{2}\int_0^\eta \frac{1}{(s^2+t^2)^{1/2}}\, dt \sim \frac{C}{2}\left[\log\left(\eta+\rho\right) - \log s\right]\,. \tag{C.8b}$$

We conclude that Φ_{p+} in (C.2) has the divergent far-field behavior

$$\Phi_{p+} \sim \frac{C}{2}\left(\log\left(\eta+\rho\right) - \frac{\eta}{\rho^3}\left(\xi_1^2+\xi_2^2\right)\right) - \frac{C}{2}\log s + \mathcal{F}_+\,. \tag{C.9}$$ ∎

From (C.3b) we impose $\mathcal{F}_+ \sim (C/2)\log s + o(1)$ as $s \to \infty$ to obtain (C.4).

This lemma shows that the particular solution Φ_{p+} in (C.2) accounts for both the inhomogeneous term in the PDE (2.31a) as well as the two divergent terms in the required far-field behavior (2.31d). There is no monopole term associated with the far-field behavior of Φ_{p+}.

To determine the complementary solution Φ_{c+}, we substitute (C.1) into (2.31) to conclude that Φ_{c+} satisfies

$$\Delta_{\mathbf{y}}\Phi_{c+} = 0\,, \quad \mathbf{y} \in \mathbb{R}^3_+\,, \tag{C.10a}$$
$$-\partial_\eta \Phi_{c+} + b\Phi_{c+} = -b\mathcal{F}_+\,, \quad \eta = 0\,,\ (\xi_1, \xi_2) \in \Gamma\,, \tag{C.10b}$$
$$\partial_\eta \Phi_{c+} = 0\,, \quad \eta = 0\,,\ (\xi_1, \xi_2) \notin \Gamma\,, \tag{C.10c}$$
$$\Phi_{c+} \sim \frac{E_+}{\rho}\,, \quad \text{as} \quad \rho \to \infty\,, \tag{C.10d}$$

where $\mathcal{F}_+$ satisfies (C.3). To determine E_+ we apply Green's second identity to Φ_{c+} and $\hat{w} = -1 + w$, where w satisfies (2.11), over a hemisphere Ω_σ of radius $\sigma \gg 1$ in the upper half-space $\mathbb{R}^3_+$. By letting $\sigma \to \infty$ we get

$$\begin{aligned} 0 = \int_{\mathbb{R}^3_+} \left(\Phi_{c+}\Delta_{\mathbf{y}}\hat{w} - \hat{w}\Delta_{\mathbf{y}}\Phi_{c+}\right) d\mathbf{y} &= 2\pi \lim_{\sigma\to\infty} \sigma^2 \left(\Phi_{c+}\frac{\partial \hat{w}}{\partial |\mathbf{y}|} - \hat{w}\frac{\partial \Phi_{c+}}{\partial |\mathbf{y}|} \right) \Big|_{|\mathbf{y}|=\sigma} \\ &\quad + \int_\Gamma \left(b\hat{w}\mathcal{F}_+\right)|_{\eta=0}\, d\xi_1\xi_2\,. \end{aligned} \tag{C.11}$$

Then, by using $\hat{w} \sim -1 + C/|\mathbf{y}|$ and $\Phi_{c+} \sim E_+/|\mathbf{y}|$ as $|\mathbf{y}| \to \infty$, together with $b\hat{w} = \partial_\eta \hat{w} = \partial_\eta w$ on Γ when $\eta = 0$, we obtain from (C.11) that

$$E_+ = -\frac{1}{\pi}\int_\Gamma q(\xi_1, \xi_2; b)\, \mathcal{F}_+(\xi_1, \xi_2; b)\, d\xi_1\xi_2\,. \tag{C.12}$$

Finally, upon representing the solution $\mathcal{F}_+$ to (C.3) in terms of the 2-D free-space Green's function, we find that (C.12) yields (2.34) of Lemma 2.2. For $b \ll 1$, we have $q \sim b/2$ for an arbitrary patch shape Γ and so (2.34) reduces to (2.35).

When Γ is a disk of radius a, we observe that $\mathcal{F}_+ = \mathcal{F}_+(s; b)$ satisfies the radially symmetric ODE $\left(s\mathcal{F}_{+,s}\right)_s = q(s; b)\, s$. Upon integrating this ODE we determine E_+ in (C.12) as the quadrature

$$E_+ = -2\int_0^a q(s; b)\mathcal{F}_+(s; b)\, s\, ds\,; \qquad \mathcal{F}_{+,s} = \frac{1}{s}\int_0^s q(t; b)\, t\, dt\,, \quad 0 \le s \le a\,, \tag{C.13}$$

with $\mathcal{F}_+ = (C/2)\log a$ at $s = a$. Upon integrating (C.13) by parts, we readily obtain (2.36) of Lemma 2.2.

Finally, we obtain the asymptotic behavior for E_+ in (2.37). For $b \to \infty$, we use $C(\infty) \sim 2a/\pi$ and $q(t; \infty) = \pi^{-1}\left(a^2 - t^2\right)^{-1/2}$ from Lemma 2.1 directly in (2.36). By performing the integration, we obtain (2.37a). For $b \to 0$, we use $C \sim ba^2/2$ from (2.14b) and $q \sim b/2$ in (2.36). By integrating the resulting expression we get (2.37b).

Appendix D. Monopole coefficient E_{i-}.

In this appendix, we analyze the new problem (2.32) to identify the monopole coefficient in the refined far-field behavior (2.38), whose properties were summarized in Lemma 2.3. For clarity we again omit the subscript i below for the i-th patch.

For (2.32), we decompose Φ_- as

$$\Phi_- = \Phi_{p-} + \Phi_{c-}\,, \tag{D.1}$$

where Φ_{p-} is taken to satisfy

$$\Delta_{\mathbf{y}} \Phi_{p-} = \mathcal{N}_{-}(\mathbf{y}) \equiv 2\eta \left(w_{\xi_1 \xi_1} - w_{\xi_2 \xi_2} \right) \,, \quad \mathbf{y} \in \mathbb{R}_{+}^{3} \,, \tag{D.2a}$$

$$\partial_\eta \Phi_{p-} = 0 \,, \quad \text{on} \quad \eta = 0 \,. \tag{D.2b}$$

We now verify indirectly that Φ_{p-} satisfies the intricate far-field behavior given in (2.32d). To do so, we use $w \sim C/\rho$ as $\rho \to \infty$ from the far-field behavior in (2.11d) to estimate that

$$\mathcal{N}_{-} \sim 4\pi C \mathcal{N}_{-0} \,, \quad \text{where} \quad \mathcal{N}_{-0} \equiv \frac{3\eta}{2\pi\rho^5} \left(\xi_1^2 - \xi_2^2 \right) \,, \quad \text{as} \quad \rho = |\mathbf{y}| \to \infty \,. \tag{D.3}$$

We substitute (D.3) into the right-hand side of (D.2a) and compare the resulting limiting problem with the corresponding problem (B.13) for the term G_{-} in our analysis of the surface Neumann Green's function. In this way, we conclude that

$$\Phi_{p-} \sim 4\pi C G_{-} \,, \quad \text{as} \quad \rho = |\mathbf{y}| \to \infty \,. \tag{D.4}$$

By substituting the exact solution in (B.25b) for G_{-} into (D.4) we conclude that the limiting behavior of Φ_{p-} as $\rho = |\mathbf{y}| \to \infty$ agrees precisely with that required in (2.32d). As a result, Φ_{p-} has no monopole behavior as $|\mathbf{y}| \to \infty$.

Next, we use the method of images to represent the solution Φ_{p-} of (D.2) in terms of the Green's function $g(\mathbf{y}'; \mathbf{y})$, with $\mathbf{y}' = \left(\xi_1', \xi_2', \eta' \right)^T$, satisfying

$$\Delta_{\mathbf{y}'} g = \delta(\mathbf{y}' - \mathbf{y}) \,, \quad \mathbf{y}' \in \mathbb{R}_{+}^{3} \,; \qquad \partial_{\eta'} g = 0 \,, \quad \text{on} \quad \eta' = 0 \,, \tag{D.5}$$

which has the solution

$$g(\mathbf{y}'; \mathbf{y}) = -\frac{1}{4\pi |\mathbf{y}' - \mathbf{y}|} - \frac{1}{4\pi |\mathbf{y}' - \bar{\mathbf{y}}|} \,, \quad \text{with} \quad \bar{\mathbf{y}} \equiv (\xi_1, \xi_2, -\eta)^T . \tag{D.6}$$

In deriving an integral representation for Φ_{p-} from Green's second identity we must take into account that the far-field behavior for Φ_{p-} is non-vanishing as $\rho' = |\mathbf{y}'| \to \infty$. To do so, we write the far-field behavior (2.32d) with no additional monopole in terms of spherical coordinates (ρ', θ', ϕ'), with $0 \le \theta' \le \pi/2$ and $0 \le \phi' < 2\pi$. We readily conclude that $\Phi_{p-} \sim \Phi_{p\infty} + o\left(1/\rho'\right)$ as $\rho' \to \infty$, where

$$\Phi_{p\infty}(\theta', \phi') \equiv -\frac{C}{4} \left(2\cos\theta' + \frac{1}{\left(1 + \cos\theta'\right)^2} \right) \sin^2(\theta') \, \cos(2\phi') \,. \tag{D.7}$$

By applying Green's second identity to g and Φ_{p-} over a large hemisphere Ω_σ in the upper half-space, and using $g \sim -1/\left(2\pi\rho'\right)$ for $\rho' \to \infty$ together with (D.7), we obtain for $\sigma \to \infty$ that

$$\Phi_{p-}(\mathbf{y}) = \int_{\mathbb{R}_{+}^{3}} g(\mathbf{y}'; \mathbf{y}) \mathcal{N}_{-}(\mathbf{y}') \, d\mathbf{y}' + \frac{1}{2\pi} \int_0^{\pi/2} \sin(\theta') \left(\int_0^{2\pi} \Phi_{p\infty}(\theta', \phi') \, d\phi' \right) d\theta' \,. \tag{D.8}$$

By using (D.7), we calculate $\int_0^{2\pi} \Phi_{p\infty} \, d\phi' = 0$, so that (D.8) reduces to

$$\Phi_{p-}(\mathbf{y}) = -\frac{1}{4\pi} \int_{\mathbb{R}_{+}^{3}} \mathcal{N}_{-}(\mathbf{y}') \left(\frac{1}{|\mathbf{y}' - \mathbf{y}|} + \frac{1}{|\mathbf{y}' - \bar{\mathbf{y}}|} \right) d\mathbf{y}' \,. \tag{D.9}$$

To determine the complementary solution we substitute (D.1) into (2.32) to obtain

$$\Delta_{\mathbf{y}} \Phi_{c-} = 0\,, \quad \mathbf{y} \in \mathbb{R}^3_+\,, \tag{D.10a}$$
$$-\partial_\eta \Phi_{c-} + b\Phi_{c-} = -b\mathcal{F}_-\,, \quad \eta = 0\,,\, (\xi_1, \xi_2) \in \Gamma\,, \tag{D.10b}$$
$$\partial_\eta \Phi_{c-} = 0\,, \quad \eta = 0\,,\, (\xi_1, \xi_2) \notin \Gamma\,, \tag{D.10c}$$
$$\Phi_{c-} \sim \frac{E_-}{\rho}\,, \quad \text{as} \quad \rho \to \infty\,, \tag{D.10d}$$

where $\mathcal{F}_- = \mathcal{F}_-(\xi_1, \xi_2)$ is given by

$$\mathcal{F}_- = \Phi_{p-}|_{\eta=0} = -\frac{1}{2\pi} \int_{\mathbb{R}^3_+} \frac{\mathcal{N}_-(\mathbf{y}')}{|\mathbf{y}' - \mathbf{y}|}\, d\mathbf{y}'\,, \quad \text{where} \quad \mathbf{y} = (\xi_1, \xi_2, 0)^T\,. \tag{D.11}$$

To determine our first expression for E_- we apply Green's identity to Φ_{c-} and $\hat{w} = -1 + w$, in a similar way as was done to find E_+ in (C.11) and (C.12). This yields that

$$E_-(b) = -\frac{1}{\pi} \int_\Gamma q(\xi_1, \xi_2)\, \mathcal{F}_-(\xi_1, \xi_2)\, d\xi_1 d\xi_2\,, \qquad \text{with} \quad q = -\frac{1}{2} w_\eta|_{\eta=0}\,. \tag{D.12}$$

Upon using (D.11) for $\mathcal{F}_-(\xi_1, \xi_2)$, with $\mathcal{N}_-$ as defined in (D.2a), (D.12) reduces to

$$E_-(b) = \frac{1}{\pi^2} \int_\Gamma q(\xi_1, \xi_2) \mathcal{I}(\xi_1, \xi_2)\, d\xi_1 d\xi_2\,, \quad \text{with} \quad \mathcal{I} \equiv \int_{\mathbb{R}^3_+} \frac{\eta' \left(w_{\xi_1'\xi_1'} - w_{\xi_2'\xi_2'} \right)}{|\mathbf{y}' - \mathbf{y}|}\, d\mathbf{y}'\,, \tag{D.13}$$

where $\mathbf{y}' = (\xi_1', \xi_2', \eta')^T$ and $\mathbf{y} = (\xi_1, \xi_2, 0)^T$.

Next, we derive an alternative expression to (D.13) that, more conveniently, determines the integral $\mathcal{I}$ not from a 3-D integration, but from an integration only over the patch Γ. To do so, we introduce an auxiliary function $\Psi(\mathbf{y}')$ satisfying

$$\begin{aligned} &\Delta_{\mathbf{y}'} \Psi = \frac{3\eta'}{(r')^5} \left[(\xi_1' - \xi_1)^2 - (\xi_2' - \xi_2)^2 \right]\,, \quad \mathbf{y}' \in \mathbb{R}^3_+\,, \\ &\Psi_{\eta'} = 0\,, \quad \text{on} \quad \eta' = 0\,, \end{aligned} \tag{D.14}$$

where we have defined $r' \equiv |\mathbf{y}' - \mathbf{y}|$. In our analysis below we will use the equivalent representation that

$$\Delta_{\mathbf{y}'} \Psi = \eta' \left(\partial_{\xi_1'\xi_1'} \left(\frac{1}{r'} \right) - \partial_{\xi_2'\xi_2'} \left(\frac{1}{r'} \right) \right)\,, \quad \mathbf{y}' \in \mathbb{R}^3_+\,. \tag{D.15}$$

The explicit solution to (D.14) is readily obtained from a translation and a scaling of the Green's function G_- in (B.25b), which solved the closely related problem (B.13). In this way, we conclude that

$$\Psi = -\left(\frac{\eta'}{4(r')^3} + \frac{1}{8\,(r' + \eta')^2} \right) \left[(\xi_1' - \xi_1)^2 - (\xi_2' - \xi_2)^2 \right]\,, \tag{D.16}$$

so that on the plane $\eta' = 0$, we have

$$\Psi|_{\eta'=0} = -\frac{1}{8} \left(\frac{(\xi_1' - \xi_1)^2 - (\xi_2' - \xi_2)^2}{(\xi_1' - \xi_1)^2 + (\xi_2' - \xi_2)^2} \right)\,. \tag{D.17}$$

Next, we apply Green's second identity to Ψ and w over a large hemisphere of radius $\rho' \equiv |\mathbf{y}'| = \sigma \gg 1$ in the upper half-space $\eta' \geq 0$, and use the fact that w is harmonic, that $\Psi_{\eta'} = 0$ on $\eta' = 0$, and that $w_{\eta'}$ is non-vanishing on $\eta' = 0$ only on the patch Γ. In this way, we obtain that

(D.18)
$$\int_{\mathbb{R}^3_+} w \Delta_{\mathbf{y}'} \Psi \, d\mathbf{y}' = \int_\Gamma \left(\Psi \partial_{\eta'} w\right)_{\eta'=0} \, d\xi_1' \, d\xi_2' + \lim_{\sigma\to\infty} \left(\sigma^2 \int_0^{\pi/2} \int_0^{2\pi} \left(w\partial_{\rho'}\Psi - \Psi \partial_{\rho'} w\right)\Big|_{\rho'=\sigma} \sin\theta' d\theta' \, d\phi' \right),$$

where $0 \leq \theta' \leq \pi/2$ and $0 \leq \phi' < 2\pi$ are the angular spherical coordinates. Then, by using (D.15) for $\Delta_{\mathbf{y}'}\Psi$ on the left-hand side of (D.18), we integrate by parts and use decay at infinity. Upon recalling the definition (D.13) for $\mathcal{I}$, we conclude that

(D.19)
$$\mathcal{I} = \int_{\mathbb{R}^3_+} \frac{\eta' \left(w_{\xi_1'\xi_1'} - w_{\xi_2'\xi_2'}\right)}{|\mathbf{y}' - \mathbf{y}|} \, d\mathbf{y}' = \int_\Gamma \left(\Psi \partial_{\eta'} w\right)_{\eta'=0} \, d\xi_1' \, d\xi_2' \,, + \lim_{\sigma\to\infty} \left(\sigma^2 \int_0^{\pi/2} \int_0^{2\pi} \left(w\partial_{\rho'}\Psi - \Psi \partial_{\rho'} w\right)\Big|_{\rho'=\sigma} \sin\theta' \, d\theta' \, d\phi' \right).$$

To estimate the integral over the hemisphere, we use $w \sim C/\rho'$ and $\partial_{\rho'} w \sim -C/(\rho')^2$ as $\rho' \to \infty$. In addition, in terms of spherical coordinates, we calculate that the far-field behavior of Ψ given in (D.16) has the form

(D.20a)
$$\Psi \sim g(\theta')\cos(2\phi') + \mathcal{O}\left(1/\rho'\right), \quad \partial_{\rho'}\Psi = \mathcal{O}\left(1/(\rho')^2\right), \quad \text{as} \quad \rho' = |\mathbf{y}'| \to \infty \,,$$

where $g(\theta')$ is defined by

(D.20b)
$$g(\theta') \equiv -\frac{1}{4}\cos\theta' \sin^2(\theta') - \frac{1}{8}\left(\frac{1-\cos\theta'}{1+\cos\theta'}\right).$$

Upon using these far-field estimates of w and Ψ we conclude that

(D.21)
$$\begin{aligned} &\lim_{\sigma\to\infty} \left(\sigma^2 \int_0^{\pi/2} \int_0^{2\pi} \left(w\partial_{\rho'}\Psi - \Psi \partial_{\rho'} w\right)\Big|_{\rho'=\sigma} \sin\theta' \, d\theta' \, d\phi' \right) \\ &= \lim_{\sigma\to\infty} \left(C \int_0^{\pi/2} g(\theta') \, d\theta' \left(\int_0^{2\pi} \cos(2\phi') \, d\phi' \right) + \mathcal{O}(1/\sigma) \right) = 0 \,. \end{aligned}$$

As a result, since the limit over the hemisphere in (D.19) vanishes, we obtain upon using (D.17) in (D.19) that

(D.22)
$$\mathcal{I} = -\frac{1}{8} \int_\Gamma \left(\frac{\left(\xi_1' - \xi_1\right)^2 - \left(\xi_2' - \xi_2\right)^2}{\left(\xi_1' - \xi_1\right)^2 + \left(\xi_2' - \xi_2\right)^2} \right) \partial_{\eta'} w|_{\eta'=0} \, d\xi_1' \, d\xi_2' \,.$$

Finally, by setting $\partial_{\eta'} w|_{\eta'=0} = -2q$ in (D.22) we combine (D.22) and (D.13) to obtain our main result for E_- given in (2.39) of Lemma 2.3.

Appendix E. Perfectly reactive elliptically-shaped patches.

For a perfectly reactive elliptically-shaped patch of semi-axes εa_{i1} and εa_{i2}, we now adapt the approach in [61] to calculate the reactive capacitance $C_i(\infty)$ in (2.12) as well as the monopole coefficients $E_{i+}(\infty)$ and $E_{i-}(\infty)$ in (2.34) and (2.39), respectively. This is done by calculating the charge density q_i from an exact solution w_i of (2.11). In our derivation below, for clarity we omit the subscript i patch index.

To solve (2.11) with $b_i = \infty$ when Γ is an ellipse of semi axes a_1 and a_2, with $a_1 \geq a_2$, we first introduce ellipsoidal coordinates in the form

$$\frac{\xi_1^2}{a_1^2+\theta} + \frac{\xi_2^2}{a_2^2+\theta} + \frac{\eta^2}{\theta} = 1\,. \tag{E.1}$$

For a given (ξ_1, ξ_2, η) the three roots θ of (E.1), labeled by λ, μ, and ν, satisfy $\lambda \geq 0 \geq \mu \geq -a_2^2 \geq \nu \geq -a_1^2$. Level sets of constant $\lambda > 0$ are ellipsoids that have the limiting behavior $\xi_1^2/a_1^2 + \xi_2^2/a_2^2 \to 1$ and $\eta \to 0$ as $\lambda \to 0^+$, while for $\lambda \to \infty$ the ellipsoid becomes a large sphere $\xi_1^2 + \xi_2^2 + \eta^2 \to \lambda$ of radius $\sqrt{\lambda}$.

As a result, we look for a solution to (2.11) in the form $w(\xi_1, \xi_2, \eta) = \mathcal{W}(\lambda)$. From separating variables in the Laplacian written in terms of ellipsoidal coordinates, we find that $\mathcal{W}(\lambda)$ satisfies the boundary value problem

$$\begin{gathered}\frac{d}{d\lambda}\left[\sqrt{\lambda(a_1^2+\lambda)(a_2^2+\lambda)}\frac{d\mathcal{W}}{d\lambda}\right] = 0\,, \quad 0 < \lambda < \infty\,, \\ \mathcal{W}(0^+) = 1\,, \quad \text{(on elliptical patch)}\,; \qquad \mathcal{W} \to 0 \quad \text{as} \quad \lambda \to \infty\,.\end{gathered} \tag{E.2}$$

The solution is

$$\mathcal{W}(\lambda) = \frac{1}{A}\int_\lambda^\infty \frac{d\zeta}{\sqrt{\zeta(a_1^2+\zeta)(a_2^2+\zeta)}}\,, \quad A \equiv \int_0^\infty \frac{d\zeta}{\sqrt{\zeta(a_1^2+\zeta)(a_2^2+\zeta)}}\,. \tag{E.3}$$

When $a_1 > a_2$, A can be written in terms of the complete elliptic integral $K(m)$ as

$$A = \frac{2}{a_1}K(m)\,, \quad \text{with} \quad m \equiv \sqrt{1-\frac{a_2^2}{a_1^2}}\,, \quad \text{where} \quad K(m) \equiv \int_0^{\pi/2} \frac{1}{\sqrt{1-m^2\sin^2\theta}}d\theta\,, \tag{E.4}$$

so that (E.3) becomes

$$\mathcal{W}(\lambda) = \frac{a_1}{2K(m)}\int_\lambda^\infty \frac{d\zeta}{\sqrt{\zeta(a_1^2+\zeta)(a_2^2+\zeta)}}\,. \tag{E.5}$$

To determine the reactive capacitance $C(\infty)$ we let $\lambda \to \infty$ in (E.5) and use that $|\mathbf{y}| = \xi_1^2 + \xi_2^2 + \eta^2 \approx \lambda$ as $\lambda \to \infty$, so that $|\mathbf{y}| \sim \sqrt{\lambda}$. This yields for $|\mathbf{y}| \to \infty$ that

$$\mathcal{W} \sim \frac{a_1}{2K(m)}\int_\lambda^\infty \zeta^{-3/2}\,d\zeta \sim \frac{a_1}{K(m)\sqrt{\lambda}} \sim \frac{a_1}{K(m)|\mathbf{y}|}\,, \quad \text{as} \quad |\mathbf{y}| \to \infty\,,$$

which identifies that $C(\infty) = a_1/K(m)$. In this way, we recover the classical result for the capacitance of an elliptic patch (see, e.g., [61]). If $a_1 < a_2$, we simply swap a_1 and a_2 in the formula for $C(\infty)$.

Next, we determine the charge density $q(\mathbf{y};\infty)$ by first calculating $\partial_\eta \lambda$. From an implicit differentiation of (E.1) we get

$$\frac{\partial\lambda}{\partial\eta} = 2\eta\left[\frac{\eta^2}{\lambda} + \lambda\left(\frac{\xi_1^2}{(a_1^2+\lambda)^2} + \frac{\xi_2^2}{(a_2^2+\lambda)^2}\right)\right]^{-1}\,. \tag{E.6}$$

To evaluate (E.6) on the elliptical patch we let $\lambda \to 0$ in (E.6) while using $\eta^2/\lambda \to 1 - \xi_1^2/a_1^2 - \xi_2^2/a_2^2$ as $\lambda \to 0$. This yields that

(E.7) $$\frac{\partial\lambda}{\partial\eta} \to \frac{2\eta}{\eta^2/\lambda} = \frac{2\lambda}{\eta} = 2\sqrt{\lambda}\left(1 - \frac{\xi_1^2}{a_1^2} - \frac{\xi_2^2}{a_2^2}\right)^{-1/2}, \quad \text{as} \quad \eta \to 0\,, \quad \frac{\xi_1^2}{a_1^2} + \frac{\xi_2^2}{a_2^2} \leq 1.$$

Then, we calculate $\mathcal{W}'(\lambda)$ from (E.5) and estimate it as $\lambda \to 0$ to obtain

(E.8) $$\mathcal{W}'(\lambda) = -\frac{a_1}{2K(m)} \frac{1}{\sqrt{\lambda(\lambda + a_1^2)(\lambda + a_2^2)}} \sim -\frac{\lambda^{-1/2}}{2a_2 K(m)}\,, \quad \text{as} \quad \lambda \to 0\,.$$

From using (E.7) and (E.8) to evaluate the chain rule $w_\eta = \mathcal{W}'(\lambda)\partial_\eta \lambda$ as $\lambda \to 0$, we calculate the charge density on the patch as

(E.9)
$$q(\mathbf{y};\infty) = -\tfrac{1}{2} w_\eta|_{\eta=0} = \frac{1}{2a_2 K(m)}\left(1 - \frac{\xi_1^2}{a_1^2} - \frac{\xi_2^2}{a_2^2}\right)^{-1/2} = \frac{C}{2a_1 a_2}\left(1 - \frac{\xi_1^2}{a_1^2} - \frac{\xi_2^2}{a_2^2}\right)^{-1/2},$$

where $C = C(\infty)$ is the reactive capacitance. Therefore, we have recovered the result presented in [61].

Finally, to determine the monopole coefficients $E_+(\infty)$ and $E_-(\infty)$ we substitute the second expression in (E.9) for q into (2.34) and (2.39), respectively, to yield iterated double integrals over the elliptical patch Γ. Upon replacing $\tilde{\xi_1} = \xi_1/a_1$ and $\tilde{\xi_2} = \xi_2/a_2$ in these formulae (and dropping the tilde) the integrations can be expressed in terms of the unit disk $\mathbb{D}$ centered at the origin. In this way, we obtain from (2.34) that

(E.10)
$$\frac{E_+}{C^2} = -\frac{1}{8\pi^2}\int_{\mathbb{D}} \frac{1}{\sqrt{1-|\mathbf{y}'|^2}}\left(\int_{\mathbb{D}} \frac{\log\left[a_1^2(\xi_1 - \xi_1')^2 + a_2^2(\xi_2 - \xi_2')^2\right]^{1/2}}{\sqrt{1-|\mathbf{y}|^2}}\, d\mathbf{y}\right) d\mathbf{y}'\,,$$

while from (2.39) we derive

(E.11)
$$\frac{E_-}{C^2} = \frac{1}{16\pi^2}\int_{\mathbb{D}} \frac{1}{\sqrt{1-|\mathbf{y}'|^2}}\left(\int_{\mathbb{D}} \left(\frac{a_1^2(\xi_1' - \xi_1)^2 - a_2^2(\xi_2' - \xi_2)^2}{a_1^2(\xi_1' - \xi_1)^2 + a_2^2(\xi_2' - \xi_2)^2}\right)\frac{1}{\sqrt{1-|\mathbf{y}|^2}}\, d\mathbf{y}\right) d\mathbf{y}'\,.$$

Here $|\mathbf{y}|^2 = \xi_1^2 + \xi_2^2$ and $|\mathbf{y}'|^2 = (\xi_1')^2 + (\xi_2')^2$. Remarkably, these two iterated double integrals can be evaluated analytically in closed form. We summarize our results as follows:

LEMMA E.1. *Let Γ be a perfectly absorbing elliptical-shaped patch $\xi_1^2/a_1^2 + \xi_2^2/a_2^2 \leq 1$ with semi-axes $a_1 > 0$ and $a_2 > 0$ that are aligned with the two principal directions of curvature. Then, the reactive capacitance $C = C(\infty)$ and the charge density $q = q(\mathbf{y};\infty)$ defined in (2.12) are by*

(E.12) $$C = \frac{a_>}{K(m)}\,, \quad q = \frac{C}{2a_2 a_1}\frac{1}{\sqrt{1 - \xi_1^2/a_1^2 - \xi_2^2/a_2^2}}\,, \quad m \equiv \sqrt{1 - \frac{a_<^2}{a_>^2}}\,,$$

where $a_< = \min(a_1, a_2)$, $a_> = \max(a_1, a_2)$, and $K(m)$ is the complete elliptic integral of the first kind. Finally, the integrals in (E.10) and (E.11) for the two ratios $E_\pm/C^2$ are given explicitly by

(E.13) $$\frac{E_+}{C^2} = -\frac{1}{2}\log\left(\frac{a_1 + a_2}{2}\right) - \log 2 + \frac{3}{4}\,, \qquad \frac{E_-}{C^2} = \frac{a_1 - a_2}{4(a_1 + a_2)}\,.$$

We need only derive the explicit results in (E.13). Our derivation relies on two elementary results from complex analysis.

LEMMA E.2. *Suppose that* $\mathsf{P}(z)$ *is a polynomial of degree* $M > 1$ *of the form* $\mathsf{P}(z) = d\prod_{j=1}^{M}(z - z_j)$, *with* $d \neq 0$, *for which* $P(0) \neq 0$ *and* $P(z)$ *is non-vanishing on the boundary* $|z| = 1$. *Suppose that* $|z_j| > 1$ *for* $j = 1, \ldots, k$, *while* $|z_j| < 1$ *for* $j = k+1, \ldots, M$ *for some* $k \in \{0, \ldots, M\}$. *Then,*

$$\frac{1}{2\pi}\int_0^{2\pi} \log\left|\mathsf{P}\left(e^{i\theta}\right)\right| d\theta = \log|d| + \sum_{j=1}^{k}\log|z_j|\,. \tag{E.14}$$

Proof. By applying Jensen's formula (see [59]) to the polynomial $\mathsf{P}(z)$, we obtain in terms of its roots inside the unit disk that

$$\frac{1}{2\pi}\int_0^{2\pi} \log\left|\mathsf{P}\left(e^{i\theta}\right)\right| d\theta = \log|\mathsf{P}(0)| - \sum_{j=k+1}^{M}\log|z_j|\,. \tag{E.15}$$

We readily obtain (E.14) by substituting $|\mathsf{P}(0)| = |d|\prod_{j=1}^{M}|z_j|$ into (E.15). When there is no root outside the unit disk, the second term on the right side of (E.15) vanishes. $\square$

The second result that we need from complex analysis is the following:

LEMMA E.3. *Consider the quadratic polynomial* $\mathsf{A}(z) = z^2 + \zeta z + \beta$, *where* β *is real with* $-1 < \beta < 1$ *and* ζ *is complex-valued. Then, the two roots of* $\mathsf{A}(z)$ *are inside the unit disk* $|z| < 1$ *if and only if* $\zeta = \zeta_R + i\zeta_I$ *satisfies*

$$\frac{\zeta_R^2}{(1+\beta)^2} + \frac{\zeta_I^2}{(1-\beta)^2} < 1\,. \tag{E.16}$$

Proof. We prove this result by calculating the winding number of A, labeled by $N_w(\mathsf{A})$, as z traverses the unit disk $|z| = 1$ once counterclockwise, with parameterization $z = e^{i\theta}$ for $0 \leq \theta \leq 2\pi$. We write $\mathsf{A}(e^{i\theta}) = e^{i\theta}h(\theta)$, with $h(\theta) \equiv e^{i\theta} + \zeta + \beta e^{-i\theta}$, so that

$$N_w\left(\mathsf{A}(e^{i\theta})\right) = N_w\left(e^{i\theta}\right) + N_w\left(h(\theta)\right)\,.$$

Since $N_w\left(e^{i\theta}\right) = 1$, we conclude that $\mathsf{A}(z)$ has its two roots inside the unit disk if and only if $N_w\left(h(\theta)\right) = 1$. By separating $h(\theta)$ into real and imaginary parts as $h(\theta) = h_R + ih_I$, we calculate that

$$h_R = \zeta_R + (1+\beta)\cos\theta\,, \quad h_I \equiv \zeta_I + (1-\beta)\sin\theta\,, \tag{E.17}$$

where $\zeta = \zeta_R + i\zeta_I$. Since $-1 < \beta < 1$, it follows that the image of the unit disk is

$$\frac{(h_R - \zeta_R)^2}{(1+\beta)^2} + \frac{(h_I - \zeta_I)^2}{(1-\beta)^2} = 1\,. \tag{E.18}$$

The necessary and sufficient condition for $N_w(h) = 1$ is that the origin $(h_R, h_I) = (0,0)$ lies strictly within the ellipse (E.18), which yields (E.16). $\square$

With these two elementary results, we now derive the explicit formulas in (E.13).

Proof. (Proof of (E.13) of Lemma E.1) We will first prove (E.13) for E_+/C^2. We begin by introducing

$$\xi_1 = \rho\cos\theta\,, \quad \xi_2 = \rho\sin\theta\,, \quad \xi_1' = \rho'\cos\psi\,, \quad \xi_2' = \rho'\sin\psi\,,$$

so that the argument of the logarithm in (E.10) becomes

$$\mathsf{F}(\theta,\psi) \equiv a_1^2(\xi_1-\xi_1')^2 + a_2^2(\xi_2-\xi_2')^2 = \mathsf{X}^2+\mathsf{Y}^2 = (\mathsf{X}+i\mathsf{Y})\,(\mathsf{X}-i\mathsf{Y})\,,$$

where $\mathsf{X} \equiv a_1\,(\rho\cos\theta - \rho'\cos\psi)$, $\mathsf{Y} \equiv a_2\,(\rho\sin\theta-\rho'\sin\psi)$, and $i=\sqrt{-1}$. By defining $\mathsf{U}\equiv \mathsf{X}+i\mathsf{Y}$, this leads to the factorization

$$\mathsf{F}(\theta,\psi) = \mathsf{U}(\theta,\psi)\mathsf{U}(-\theta,-\psi)\,, \tag{E.19a}$$

where $\mathsf{U}=\mathsf{U}(\theta,\phi)$ is defined by

$$\mathsf{U}(\theta,\phi) = \rho\,(a_1\cos\theta + ia_2\sin\theta) - \rho'\,(a_1\cos\psi+ia_2\sin\psi)\ . \tag{E.19b}$$

By performing the angular integrations we observe from symmetry that

(E.20)
$$\begin{aligned}\int_0^{2\pi}\int_0^{2\pi}\log\left[\mathsf{F}(\theta,\psi)\right]d\theta\,d\psi &= \int_0^{2\pi}\int_0^{2\pi}\left(\log|\mathsf{U}(\theta,\psi)| + \log|\mathsf{U}(-\theta,-\psi)|\right)\,d\theta\,d\psi\\ &= 2\int_0^{2\pi}\int_0^{2\pi}\log|\mathsf{U}(\theta,\psi)|\,d\theta\,d\psi\,.\end{aligned}$$

Upon substituting (E.20) into (E.10) and converting to polar coordinates we obtain
(E.21)
$$\frac{E_+}{C^2} = -\frac{1}{8\pi^2}\int_0^1\int_0^1 \frac{\mathcal{J}\rho\rho'}{\sqrt{1-\rho^2}\sqrt{1-(\rho')^2}}\,d\rho\,d\rho'\,, \quad \mathcal{J}\equiv\int_0^{2\pi}\int_0^{2\pi}\log|\mathsf{U}(\theta,\psi)|\,d\theta\,d\psi\,.$$

Next, we will calculate $\mathcal{J}=\mathcal{J}(\rho,\rho')$ explicitly. To do so, we first introduce the complex variables $z=e^{i\theta}$ and $w=e^{i\psi}$, so that after some algebra we write (E.19b) as

$$\mathsf{U} = d_1\left(z+\frac{\beta}{z}\right) + d_2\left(w+\frac{\beta}{w}\right)\,, \tag{E.22}$$

where d_1, d_2 and β, satisfying $-1<\beta<1$ are defined by

$$d_1\equiv\frac{\rho}{2}(a_1+a_2)\,,\quad d_2\equiv -\frac{\rho'}{2}(a_1+a_2)\,,\quad \beta\equiv\frac{a_1-a_2}{a_1+a_2}\,. \tag{E.23}$$

Case I: Suppose that $|d_1|>|d_2|$, so that $\rho>\rho'$. For this case we write U in (E.22) in terms of a polynomial in z as

$$\mathsf{U} = \frac{\mathsf{P}(z)}{z}\,, \quad \text{with} \quad \mathsf{P}(z) = d_1\mathsf{A}(z)\,, \tag{E.24a}$$

where

$$\mathsf{A}(z) = z^2+\zeta z+\beta\,, \quad \text{with} \quad \zeta\equiv -\rho_\star\left(w+\frac{\beta}{w}\right)\,, \tag{E.24b}$$

and $\rho_\star \equiv \rho'/\rho < 1$. We set $z = e^{i\theta}$ and integrate $\log|\mathsf{U}|$ first with respect to θ, for each fixed $w = e^{i\psi}$ with $0 < \psi < 2\pi$. On the unit disk we have from (E.24a) that $\log|\mathsf{U}| = \log|\mathsf{P}(e^{i\theta})|$, and so since $\mathsf{P}(z) = d_1\mathsf{A}(z)$, we must first determine the location of the zeroes of $\mathsf{A}(z)$ to apply Lemma E.2.

To do so, we use Lemma E.3. By setting $w = e^{i\psi}$ in ζ in (E.24b) we decompose $\zeta = \zeta_R + i\zeta_I$ to get $\zeta_R = -\rho_\star(1+\beta)\cos\psi$ and $\zeta_I = -\rho_\star(1-\beta)\sin\psi$. The criterion (E.16) becomes

$$\frac{\rho_\star^2(1+\beta)^2}{(1+\beta)^2}\cos^2\psi + \frac{\rho_\star^2(1-\beta)^2}{(1-\beta)^2}\sin^2\psi = \rho_\star^2 < 1\,,$$

which holds since $|\rho_\star| < 1$. As a result, $\mathsf{A}(z)$ and $\mathsf{P}(z)$ have no roots outside the unit disk. Therefore, by (E.14) of Lemma E.2 we have

$$\text{(E.25)}\qquad \frac{1}{2\pi}\int_0^{2\pi}\log|\mathsf{U}|\,d\theta = \frac{1}{2\pi}\int_0^{2\pi}\log|\mathsf{P}(e^{i\theta})|\,d\theta = \log|d_1|\,.$$

Upon trivially performing the second integration over ψ, we conclude that $\mathcal{J}$ in (E.21) in **Case I** is

$$\text{(E.26)}\qquad \mathcal{J} = 4\pi^2\log|d_1|\,,\quad \text{with}\quad d_1 = \frac{\rho}{2}(a_1+a_2)\,.$$

For **Case II** where $|d_1| < |d_2|$, so that $\rho < \rho'$, we we write U in (E.22) in terms of a polynomial in w as

$$\text{(E.27a)}\qquad \mathsf{U} = \frac{\mathsf{P}(w)}{w}\,,\quad \text{with}\quad \mathsf{P}(w) = d_2\mathsf{A}(w)\,,$$

where $\mathsf{A}(w)$ is now defined by

$$\text{(E.27b)}\qquad \mathsf{A}(w) = w^2 + \zeta w + \beta\,,\quad \text{with}\quad \zeta \equiv \rho_\star\left(z + \frac{\beta}{z}\right)\,,$$

and $\rho_\star \equiv \rho/\rho' < 1$. By repeating the analysis as in Case I, it follows by Lemma E.3 that $\mathsf{A}(w)$ has no roots in $|w| > 1$. From Lemma E.2 we get $\mathcal{J} = 4\pi^2\log|d_2|$.

By combining these two cases, and by recalling (E.23) for d_1 and d_2, we have derived the key result

(E.28)
$$\mathcal{J} = 4\pi^2\log\left(\max(|d_1|,|d_2|)\right) = 4\pi^2\log\left(\overline{a}\rho_>\right)\,;\quad \rho_> \equiv \max(\rho,\rho')\,,\quad \overline{a} \equiv \frac{(a_1+a_2)}{2},$$

so that we need only to perform the radial integrations. Upon substituting (E.28) into (E.21), and using $\int_0^1\left(1-\rho^2\right)^{-1/2}\,d\rho = 1$, we obtain that

$$\text{(E.29)}\qquad \frac{E_+}{C^2} = -\frac{1}{2}\log\overline{a} - \frac{1}{2}\int_0^1\int_0^1\mathsf{K}(\rho,\rho')\,d\rho\,d\rho'\,;\qquad \mathsf{K} \equiv \frac{\rho\rho'\log\rho_>}{\sqrt{1-\rho^2}\sqrt{1-(\rho')^2}}\,.$$

Since K is symmetric about the diagonal, i.e. $\mathsf{K}(\rho,\rho') = \mathsf{K}(\rho',\rho)$, (E.29) becomes

$$\text{(E.30)}\qquad \frac{E_+}{C^2} = -\frac{1}{2}\log\overline{a} - \int_0^1\frac{\rho\log\rho}{\sqrt{1-\rho^2}}\left(\int_0^\rho\frac{\rho'}{\sqrt{1-(\rho')^2}}\,d\rho'\right)d\rho\,.$$

The inner integral in (E.30) is simply $1-\sqrt{1-\rho^2}$, so that (E.30) reduces to

$$\frac{E_+}{C^2} = -\frac{1}{2}\log\overline{a} + \int_0^1 \rho\log\rho\,d\rho - \int_0^1 \frac{\rho\log\rho}{\sqrt{1-\rho^2}}\,d\rho\,. \tag{E.31}$$

Integration by parts yields $\int_0^1 \rho\log\rho\,d\rho = -1/4$. To evaluate the second integral we set $t=\sqrt{1-\rho^2}$, and then integrate by parts to get

$$\int_0^1 \frac{\rho\log\rho}{\sqrt{1-\rho^2}}\,d\rho = \frac{1}{2}\int_0^1 \log\left(1-t^2\right)\,dt = \log 2 - 1\,.$$

In this way, we obtain $E_+/C^2 = -\frac{1}{2}\log\overline{a} - 1/4 - \log 2 + 1$, with $\overline{a}=(a_1+a_2)/2$, which confirms the first result in (E.13).

To calculate E_-/C^2 from (E.11), we simply observe that

$$\frac{E_-}{C^2} = -\frac{a_1}{2}\frac{\partial}{\partial a_1}\left(\frac{E_+(a_1,a_2)}{C^2(a_1,a_2)}\right) + \frac{a_2}{2}\frac{\partial}{\partial a_2}\left(\frac{E_+(a_1,a_2)}{C^2(a_1,a_2)}\right)\,.$$

Therefore, by using our formula for E_+/C^2 we get $E_-/C^2 = (a_1-a_2)/(4[a_1+a_2])$, which confirms the second result in (E.13). ∎

Finally, we remark that since C, q, and E_+ are invariant under rotations, these quantities are independent of the orientation of the elliptical patch with respect to the principal directions of curvature. However, in our derivation of E_- we assumed that the semi-axes of the small elliptical patch were aligned with the principal directions of curvature on the boundary through the center of the patch. The more general case of an oblique elliptical patch is readily treated through a rotation matrix.

References.

[1] A. Alonso, R. G. Endres, and J. B. Kirkegaard. Local clustering and global spreading of receptors for optimal spatial gradient sensing. *Phys. Rev. Lett.*, 134:158401, 2025.

[2] W. Arendt and ter Elst A. F. M. The Dirichlet-to-Neumann operator on exterior domains. *Poten. Anal.*, 43:313–340, 2015.

[3] T. Askham, L. Greengard, J. Hoskins, L. Lu, M. O'Neil, M. Rachh, F. Vico, and V. Rokhlin. fmm3dbie: FMM-accelerated boundary integral equation solvers.

[4] J. W. S. Baron Rayleigh. *The Theory of Sound*, volume 2. Dover, New York, 2nd edition, 1945.

[5] O. Bénichou and R. Voituriez. From first-passage times of random walks in confinement to geometry-controlled kinetics. *Phys. Rep.*, 539(4):225–284, 2014.

[6] H. C. Berg and E. M. Purcell. Physics of chemoreception. *Biophys J.*, 20(2):193–219, 1977.

[7] A. J. Bernoff, A. Jilkine, A. Navarro Hernández, and A. E. Lindsay. Single-cell directional sensing from just a few receptor binding events. *Biophys. J.*, 122:3108–3116, 2023.

[8] A. J. Bernoff and A. E. Lindsay. Numerical approximation of diffusive capture rates by planar and spherical surfaces with absorbing pores. *SIAM J. Appl. Math.*, 78(1):266–290, 2018.

[9] A. J. Bernoff and A. E. Lindsay. Kinetic Monte Carlo methods for three-dimensional diffusive capture problems in exterior domains. *Royal Soc. Open Sci.*, 12(2):241033, 2025.

[10] A. J. Bernoff, A. E. Lindsay, and D. D. Schmidt. Boundary homogenization and capture time distributions of semipermeable membranes with periodic patterns of reactive sites. *Multiscale Model. & Simul.*, 16(3):1411–1447, 2018.

[11] P. C. Bressloff. Asymptotic analysis of particle cluster formation in the presence of anchoring sites. *Eur. Phys. J. E*, 47(5):30, 2024.

[12] P. C. Bressloff and J. M. Newby. Stochastic models of intracellular transport. *Rev. Mod. Phys.*, 85:135–196, 2013.

[13] L. Bundrock, A. Girouard, D. S. Grebenkov, M. Levitin, and I. Polterovich. The exterior Steklov problem for Euclidean domains. *J. Spect. Th., accepted; preprint is available arXiv:2511.09490*, 2025.

[14] Louis Carillo, Tony Lelièvre, Thomas Normand, Gabriel Stoltz, and Urbain Vaes. The narrow escape problem in arbitrary dimension, 2026.

[15] H. Cavanagh, D. Kempe, J. K. Mazalo, M. Biro, and R. G. Endres. T cell morphodynamics reveal periodic shape oscillations in three-dimensional migration. *J. Royal Soc. Interface*, 19(190):20220081, 2022.

[16] S. Chakraborty, J. G. Hoskins, and A. E. Lindsay. Fast integral methods for the Neumann Green's function: applications to capture and signaling problems in two dimensions, 2025.

[17] X. Chen and A. Friedman. Asymptotic analysis for the narrow escape problem. *SIAM J. Math. Anal.*, 43(6):2542–2563, 2011.

[18] A. Cheviakov and M. Ward. Optimization of trap locations for narrow capture problems. In D. S. Grebenkov, R. Metzler, and G. Oshanin (Eds.), editors, *Target Search Problems*, pages 225–246. Springer Nature Switzerland, Cham, 2024.

[19] A. Cheviakov and M. J. Ward. Optimizing the principal eigenvalue of the Laplacian in a sphere with interior traps. *Math. Comp. Model.*, 53(7-8):1394–1409, 2011.

[20] A. F. Cheviakov, M. J. Ward, and R. Straube. An asymptotic analysis of the mean first passage time for narrow escape problems: Part II: The sphere. *Multiscale Model. Simul.*, 8(3):836–870, 2010.

[21] U. Dobramysl and D. Holcman. Mixed analytical-stochastic simulation method for the recovery of a Brownian gradient source from probability fluxes to small windows. *J. Comput. Phys.*, 355:22–36, 2018.

[22] D. Gomez and A. F. Cheviakov. Asymptotic analysis of narrow escape problems in nonspherical three-dimensional domains. *Phys. Rev. E*, 91(1):012137, 2015.

[23] Á. González. Measurement of areas on a sphere using Fibonacci and latitude–longitude lattices. *Math. Geosci.*, 42(1):49–64, 2009.

[24] D. S. Grebenkov. Spectral theory of imperfect diffusion-controlled reactions on heterogeneous catalytic surfaces. *J. Chem. Phys.*, 151:104108, 2019.

[25] D. S. Grebenkov. Paradigm shift in diffusion-mediated surface phenomena. *Phys. Rev. Lett.*, 125:078102, 2020.

[26] D. S. Grebenkov. Diffusion-controlled reactions: An overview. *Molecules*, 28(22):7570, 2023.

[27] D. S. Grebenkov. Spectral properties of the Dirichlet-to-Neumann operator for spheroids. *Phys. Rev. E*, 109:055306, 2024.

[28] D. S. Grebenkov and R. Maurette. Reactive capacitance of flat patches of arbitrary shape. *Phys. Rev. E.*, 113:034112, 2026.

[29] D. S. Grebenkov and M. J. Ward. The asymptotic analysis of some PDE and Steklov eigenvalue problems with partially reactive patches in 3-D. *under revision, SIAM Review, ArXiv: 2509.17394 [math.AP]*, 2026.

[30] D. S. Grebenkov and M. J. Ward. Competition of small targets in planar domains:

from Dirichlet to Robin and Steklov boundary condition. *Eur. J. Appl. Math.*, 5:1–48, 2026.

[31] D. S. Grebenkov and M. J. Ward. The effective reactivity for capturing Brownian motion by partially reactive patches on a spherical surface. *Multiscale Model. Simul.*, 24(2):660–692, 2026.

[32] L. Greengard, M. O'Neil, M. Rachh, and F. Vico. Fast multipole methods for the evaluation of layer potentials with locally-corrected quadratures. *J. Comput. Phys. X*, 10:100092, 2021.

[33] G. Handy and S. D. Lawley. Revising Berg-Purcell for finite receptor kinetics. *Biophys. J.*, 120(11):2237–2248, 2021.

[34] D. Holcman and Z. Schuss. The narrow escape problem. *SIAM Rev.*, 56(2):213–257, 2014.

[35] J. Kaye and L. Greengard. A fast solver for the narrow capture and narrow escape problems in the sphere. *J. Comput. Phys. X*, 5:100047, 2020.

[36] H. Kersten. Grenz- und sprungrelationen für potentiale mit quadrat- summierbarer f1ächenbelegung. *Resultate der Mathematik*, 3:17–24, 1980.

[37] R. Kress. *Linear Integral Equations*. Applied Mathematical Sciences, Springer, 2014.

[38] T. Lagache and D. Holcman. Extended narrow escape with many windows for analyzing viral entry into the cell nucleus. *J. Stat. Phys.*, 166(2):244–266, 2017.

[39] P. Lagerstrom and D. Reinelt. Note on logarithmic switchback terms in regular and singular perturbation problems. *SIAM J. Appl. Math.*, 44(3):451–462, 1984.

[40] S. D. Lawley, A. E. Lindsay, and C. E. Miles. Receptor organization determines the limits of single-cell source location detection. *Phys. Rev. Lett.*, 125(1):018102, 2020.

[41] A. E. Lindsay and A. J. Bernoff. Numerical approximation of diffusive capture rates by planar and spherical surfaces with absorbing pores. *SIAM J. Appl. Math.*, 78(1):266–290, 2018.

[42] A. E. Lindsay, A. J. Bernoff, T. Goodwill, and J. G. Hoskins. The three dimensional Neumann Green's function for general surfaces: singular asymptotics and boundary integral methods, 2026.

[43] A. E. Lindsay, A. J. Bernoff, and A. Navarro Hernández. Short-time diffusive fluxes over membrane receptors yields the direction of a signalling source. *Royal Soc. Open Sci.*, 10(4):221619, 2023.

[44] A. E. Lindsay, A. J. Bernoff, and M. J. Ward. First passage statistics for the capture of a Brownian particle by a structured spherical target with multiple surface traps. *Multiscale Model. Simul.*, 15(1):74–109, 2017.

[45] R. Metzler, G. Oshanin, and S. Redner, editors. *First-Passage Phenomena and Their Applications*. World Scientific, 2014.

[46] I. M. Nemenman and A. S. Silbergleit. Explicit Green's function of a boundary value problem for a sphere and trapped flux analysis in Gravity Probe B experiment. *J. Appl. Phys.*, 86(1):614–624, 1999.

[47] M. Nursultanov, J. C. Tzou, and L. Tzou. On the mean first arrival time of Brownian particles on Riemannian manifolds. *J. Math. Pures et Appl.*, 150:202–240, 2021.

[48] P. O. Persson and G. Strang. A simple mesh generator in matlab. *SIAM Rev.*, 46(2):329–345, 2004.

[49] C. E. Plunkett and S. D. Lawley. Boundary homogenization for partially reactive patches. *Multi. Model. & Simul.*, 22(2):784–810, 2024.

[50] I. Y. Popov. Extension theory and localization of resonances for domains of trap

type. *Mathematics of the USSR-Sbornik*, 71(1):209, feb 1992.
[51] S. Redner. *A Guide to First-Passage Processes.* Cambridge University Press, 2001.
[52] J. Reingruber and D. Holcman. Gated narrow escape time for molecular signaling. *Phys. Rev. Lett.*, 103:148102, 2009.
[53] B. Schamberger, A. Roschger, R. Ziege, K. Anselme, M. B. Amar, M. Bykowski, A. P. G. Castro, A. Cipitria, R. Coles, R. Dimova, M. Eder, S. Ehrig, L. M. Escudero, M. E. Evans, P. R. Fernandes, P. Fratzl, L. Geris, N. Gierlinger, E. Hannezo, A. Iglič, J. J. K. Kirkensgaard, P. Kollmannsberger, Ł . Kowalewska, N. A. Kurniawan, I. Papantoniou, L. Pieuchot, T. H. V. Pires, L. Renner, A. Sageman-Furnas, G. E. Schröder-Turk, A. Sengupta, V. R. Sharma, A. Tagua, C. Tomba, X. Trepat, S. L. Waters, E. Yeo, C. M. Bidan, and J. W. C. Dunlop. Curvature in biological systems: Its quantification, emergence, and implications across the scales. *Adv. Mater.*, 35(13):2206110, 2023.
[54] Z. Schuss. The narrow escape problem: A short review of recent results. *J. Sci. Comput.*, 53(1):194–210, 2012.
[55] Z. Schuss. *Brownian Dynamics at Boundaries and Interfaces.* Springer, 2013.
[56] Z. Schuss, A. Singer, and D. Holcman. The narrow escape problem for diffusion in cellular microdomains. *Proc. Nat. Acad. Sci. USA*, 104(41):16098–16103, 2007.
[57] A. Silbergleit, I. Mandel, and I. Nemenman. Potential and field singularity at a surface point charge. *J. Math. Phys.*, 44(10):4460–4466, 2003.
[58] A. Singer, Z. Schuss, D. Holcman, and R. S. Eisenberg. Narrow escape, Part I. *J. Stat. Phys.*, 122(3):437–463, 2006.
[59] E. M. Stein and R. Shakarchi. *Complex Analysis*, volume 2. Princeton University Press, Princeton, NJ, 2003.
[60] T. L. Stepien, C. Zmurchok, J. B. Hengenius, R. M. Caja Rivera, M. R. D'Orsogna, and A. E. Lindsay. Moth mating: Modeling female pheromone calling and male navigational strategies to optimize reproductive success. *Appl. Sci.*, 10(18), 2020.
[61] W. Strieder. Diffusion-controlled reaction on an elliptic site. *J. Chem. Phys.*, 130(17):176103, 2009.
[62] R. Swinbank and R. J. Purser. Fibonacci grids: A novel approach to global modelling. *Quart. J. Royal Meteorol. Soc.*, 132(619):1769–1793, 2006.
[63] B. Vioreanu and V. Rokhlin. Spectra of multiplication operators as a numerical tool. *SIAM J. Scient. Comput.*, 36(1):A267–A288, 2014.
[64] F. Wei, D. Yang, R. Straube, and J. Shuai. Brownian diffusion of ion channels in different membrane patch geometries. *Phys. Rev. E*, 83:021919, 2011.
[65] H. Xiao and Z. Gimbutas. A numerical algorithm for the construction of efficient quadrature rules in two and higher dimensions. *Comput. Math. Appl.*, 59:663–676, 2010.